A Comprehensive Investigation of Retrodirective Cross-Eye Jamming

by

Warren Paul du Plessis

Submitted in partial fulfilment of the requirements for the degree
Philosophiae Doctor (Electronic Engineering)

in the
Department of Electrical, Electronic and Computer Engineering
Faculty of Engineering, Built Environment and Information Technology
University of Pretoria

25 February 2010

SUMMARY

A Comprehensive Investigation of Retrodirective Cross-Eye Jamming

Author: Warren Paul du Plessis
Supervisor: Professor J. W. Odendaal
Co-Supervisor: Professor J. Joubert
Department: Department of Electrical, Electronic and Computer Engineering
Faculty Engineering, Built Environment and Information Technology
University: University of Pretoria
Degree: Philosophiae Doctor (Electronic)

Keywords: Electronic warfare, electronic countermeasures, radar countermeasures, monopulse radar, radar tracking, radar measurements, radar antennas, radar position measurement, jamming, and radar.

Cross-eye jamming is an Electronic Attack (EA) technique that induces an angular error in the radar being jammed. The main benefit of cross-eye jamming is that it is effective against monopulse tracking radars, which are largely immune to other forms of jamming. The objective of this research is to gain a complete understanding of cross-eye jamming so that systems that might be developed in future can be properly specified.

The main contribution of this work is a comprehensive mathematical and experimental study of retrodirective cross-eye jamming. The mathematical analysis considers all aspects of an isolated, single-loop, retrodirective cross-eye jamming engagement, thereby avoiding the approximations inherent in other cross-eye jamming analyses. Laboratory experiments that accurately represent reality by using the radar for both transmission and reception, and simulating a true retrodirective cross-eye jammer were performed to validate the theoretical analysis. Lastly, the relationship between the angular error induced in the radar being jammed and the matching required from a cross-eye jammer system is explored.

The most important conclusion of this work is that the traditional analyses of cross-eye jamming are inaccurate for the conditions under which cross-eye jammers operate. These inaccuracies mean that the traditional analyses are overly conservative, particularly at short ranges and for high cross-eye gains, suggesting that practical cross-eye jammers can be realised more easily than is generally believed.

ACKNOWLEDGEMENTS

I would like to acknowledge the support of the following organisations:

The Armaments Corporation of South Africa (Armscor): For supporting this research and granting permission to publish the results.

The Council for Scientific and Industrial Research (CSIR): For supporting my studies.

I would further like to sincerely thank the following people for their help and support, without which this thesis would not have been possible:

My beloved wife, Helen: My inspiration and strength. Without your support I could never have completed anything as substantial and challenging as this thesis.

Wimpie Odendaal and Johan Joubert: For patience during my registration saga and valuable guidance throughout my studies.

Christo Cloete: For asking me to "take a quick look" at cross-eye jamming three years ago.

My family: For never giving up on me, no matter what.

My Lord Jesus Christ: Without whom I would not even be alive, let alone able to complete this work.

Table of Contents

1 Introduction **1**
1.1 Introductory Remarks . . . 1
1.2 Background and Motivation . . . 1
1.3 Scope and Objectives . . . 2
1.3.1 Scope . . . 2
1.3.2 Objectives . . . 3
1.4 Original Contributions . . . 3
1.5 Overview of the Thesis . . . 4

2 Background **6**
2.1 Introductory Remarks . . . 7
2.2 Electronic Warfare . . . 7
2.3 Tracking Radar . . . 10
2.4 Glint Analysis . . . 11
2.4.1 Glint Analyses . . . 11
2.4.2 Limitations of Glint Analyses . . . 18
2.5 Cross-Eye Jammer Implementation . . . 19
2.5.1 Non-Retrodirective Implementation . . . 20
2.5.2 Retrodirective Implementation . . . 22
2.6 Concluding Remarks . . . 24

3 Monopulse Model **26**
3.1 Introductory Remarks . . . 27
3.2 Mathematical Analysis . . . 28
3.2.1 General Case . . . 28
3.2.2 Phase-Comparison Case . . . 29
3.2.3 Equivalence . . . 30
3.3 Results and Discussion . . . 32
3.4 Concluding Remarks . . . 36

4 Mathematical Analysis **37**
4.1 Introductory Remarks . . . 37
4.2 Mathematical Analysis . . . 37
4.2.1 Extended Analysis of Cross-Eye Jamming . . . 37
4.2.2 Equivalence to Other Results . . . 43
4.3 Results and Discussion . . . 49
4.4 Concluding Remarks . . . 57

5 Experiments **58**
5.1 Introductory Remarks . . . 59
5.2 Experimental Setup . . . 59
5.2.1 Overall Layout . . . 59
5.2.2 Radar System . . . 61
5.2.3 Jammer System . . . 63
5.3 Data Processing . . . 64
5.3.1 Time Gating . . . 65
5.3.2 Determining System Parameters . . . 70
5.3.3 Measurement System Compensation . . . 74
5.4 Results and Discussion . . . 74
5.5 Concluding Remarks . . . 83

6 Tolerance Analysis **84**
6.1 Introductory Remarks . . . 85
6.2 Mathematical Analysis . . . 85
6.2.1 Phase-Front Analysis . . . 86
6.2.2 Extended Analysis . . . 88
6.3 Results and Comparison . . . 91
6.4 Concluding Remarks . . . 95

7 Conclusions and Future Research **96**
7.1 General Conclusions . . . 97
7.2 Future Research . . . 99

References **100**

A Terminology **106**

B Approximations **109**

C Derivatives of Monopulse Pattern **112**

CHAPTER 1

INTRODUCTION

1.1 Introductory Remarks

This chapter provides a brief introduction to the current study. A short introduction to cross-eye jamming and the motivation for the current study are given in Section 1.2. The scope and objectives of this study are presented in Section 1.3, and the original contributions made during the pursuit of these objectives are summarised in Section 1.4. The chapter concludes with an overview of the layout of the thesis in Section 1.5.

1.2 Background and Motivation

Cross-eye jamming is an Electronic Attack (EA) technique that seeks to deceive a radar as to the true position of a target. This capability is typically required during the final stages of a missile engagement when a platform is attempting to protect itself against incoming radar-guided missiles. While the concept of cross-eye jamming has existed since the 1950s, it is only recently that practical systems have been developed.

Monopulse tracking radars represent a significant threat to modern military systems because they are largely immune to traditional jamming techniques. The proliferation of missiles with monopulse seekers has made the development of countermeasures against monopulse radars essential. Cross-eye jamming is one of the few jamming techniques that is effective against monopulse radars.

The main drawback of cross-eye jamming is that it is very difficult to obtain the amplitude and phase matching required for a cross-eye jammer to work in practice. The advent of operational Digital Radio-Frequency Memory (DRFM) jammers has meant that it is now possible to achieve the required matching under operational conditions.

The principle behind cross-eye jamming is extremely simple and was developed based on early glint research. Glint affects all radars and is a naturally-occurring phenomenon that only depends on the characteristics of a radar target. However, the analyses of glint used to motivate cross-eye jamming are based on approximations that are invalid for the conditions under which cross-eye jammers operate.

No comprehensive, rigorous analysis of cross-eye jamming has ever been published, so it is likely that the principles behind cross-eye jamming are incompletely understood. The main reasons for this lack of a comprehensive analysis are the mathematical difficulties associated with analysing glint, the challenges related to implementing a practical cross-eye jammer, and the fact that glint analyses were believed to give an adequate representation of cross-eye jamming.

Experimental results considering cross-eye jamming are almost unheard of in the open literature. This is because such experiments will generally involve military radars,

so the results are classified. The measurements that do exist in the open literature are not representative of a cross-eye jamming scenario.

There is thus a need for a comprehensive, rigorous mathematical analysis of retrodirective cross-eye jamming supported by measurements that adequately simulate a cross-eye jamming scenario. This study seeks to address this requirement.

1.3 Scope and Objectives

This work seeks to gain an understanding of cross-eye jamming as a prelude to implementing practical systems.[1] This study makes no attempt to address all aspects of cross-eye jamming, and the scope of this study is outlined in Section 1.3.1. The objectives of this study are summarised in Section 1.3.2.

1.3.1 Scope

A complete consideration of all aspects of cross-eye jamming will not be undertaken as this would excessively expand the scope of this study. The following limitations will thus be imposed on this work:

Retrodirective implementation: A number of possible cross-eye jammer implementations exist, but the most promising and widely-considered is the retrodirective implementation.

Isolated case: The current study will be limited to the case where the return from a cross-eye jammer is isolated and does not compete with any other returns. This could occur when some kind of pull off is initiated before commencing cross-eye jamming. Analyses of the case where the jammer return competes with the skin return of the platform mounting the jammer are extremely rare in the literature, and either require a number of limiting assumptions or are extremely complex.

Single jammer loop: A single retrodirective cross-eye jammer loop allows one signal to pass through the jammer in each direction. This implies that there is only one receiving antenna element and one transmitting antenna element (possibly the same physical antenna) on each side of the jammer, and that the circuitry comprising the jammer can only process two signals, one in each direction through the jammer. While systems comprising a number of jammer loops have been considered in the literature, the overwhelming majority of cross-eye jamming literature only considers the single-loop case.

While each of these restrictions limits the applicability of this work, the limitations are clearly understood from the outset and follow the majority of the cross-eye literature. The possibility of removing these restrictions is considered when future work is contemplated in Section 7.2 .

[1] Note that the construction of a practical cross-eye jammer will not be undertaken as part of this work because military secrecy issues would prohibit publication of the results.

1.3.2 Objectives

As stated previously, the main objective of this study is to gain an understanding of cross-eye jamming as a prelude to developing practical systems. This overall objective is broken down into the following detailed objectives:

Mathematical analysis: The current analyses of cross-eye jamming are borrowed from the analysis of glint and suffer from a number of limitations.

The first important limitation is that the mathematics has been simplified by ignoring the averaging due to the finite size of the radar antenna aperture. This leads to inaccurate results when the relative phase shift of the two directions through a cross-eye jammer approaches 180°. This is a particularly large problem as cross-eye jammers are designed for precisely this condition.

The other important limitation of existing cross-eye jammer analyses is that they ignore the retrodirective implementation of cross-eye jammers. This ommission is problematic because it is widely acknowledged that the tolerances placed on a cross-eye jammer system are impossible to achieve in practical systems unless the retrodirective implementation is used.

This study thus seeks to develop a comprehensive, rigorous mathematical analysis of retrodirective cross-eye jamming. It is anticipated that such an analysis will lead to new insights into cross-eye jamming.

Experimental validation: Very few references to experiments involving cross-eye jamming are available in the literature. Those references that do exist are generally vague because they deal with systems of military importance. The remaining experimental results do not properly consider the retrodirective implementation of a cross-eye jammer, and usually use the jammer for transmission and the radar only as a receiver.

This study aims to perform experiments that properly simulate reality. The main objectives of these experiments are to use the radar for both transmission and reception and to consider a retrodirective cross-eye jammer.

1.4 Original Contributions

The original contributions of this work are summarised below.

Generic monopulse antenna model: A generalised phase-comparison monopulse antenna is an accurate model of any monopulse antenna near boresight. The only restriction is that the monopulse antenna being modelled should be symmetrical. The main implication of this result for the current study is that the mathematical results derived are applicable to any monopulse radar, but this result is likely to find wider application in the modelling of monopulse antennas in other contexts. The only comparable result in the literature uses linear fits to the sum- and difference-channel antenna patterns on boresight, but this linear model is only accurate over a very small range of angles.

Sum-channel error: A retrodirective cross-eye jammer does not induce an angular error in the sum channel of a monopulse radar. Given that a monopulse radar uses the sum-channel antenna beam for both transmission and reception, this result applies to any radar that uses the same antenna beam for both transmission and reception (e.g. some types of conical-scan radar). This significant result shows that the assumption that retrodirective cross-eye jamming affects all radars because glint affects all radars is incorrect.

Phase-front error estimates: The error predicted by the conventional phase-front analysis of cross-eye jamming is shown to be accurate at long ranges, but to underestimate the angular error induced in the radar being jammed at shorter ranges. This result means that retrodirective cross-eye jamming is more effective than universally assumed based on conventional glint analyses.

Existence of settling angle: The settling angle (the angle where the monopulse error has a stable zero) does not exist under certain circumstances. This result suggests that a suitably designed retrodirective cross-eye jammer can be used to break a monopulse radar's lock on a target. The widely-held view that a retrodirective cross-eye jammer is only able to induce an angular error smaller than a radar's antenna beamwidth is thus shown to be incorrect.

Sensitivity to tolerances: A retrodirective cross-eye jammer will achieve a specified minimum angular error with optimum tolerance to system parameter variations when the two directions through the jammer are designed for a surprisingly large amplitude mismatch and a relative phase shift of 180°. While this result has been known for some time, a full qualitative and quantitative analysis, and a closed-form solution for the optimum design point are presented here.

Four papers summarising the work described in this thesis have been submitted for publication [1–4].

1.5 Overview of the Thesis

The content of the chapters in this thesis are outlined below.

Chapter 1: This chapter provides a brief introduction to cross-eye jamming, emphasising why cross-eye jamming is important and highlighting the limitations of existing work as motivations for this study.

Chapter 2: A more detailed background study of cross-eye jamming is presented. An introduction to monopulse radar is given to show why monopulse radars are challenging to jam. An overview of the analyses of glint that are reused for cross-eye jamming is presented with the emphasis on the limitations of these analyses when applied to cross-eye jamming. A number of possible implementations of cross-eye jamming are critically evaluated to demonstrate the importance of the retrodirective implementation.

Chapter 3: The use of a generalised phase-comparison monopulse antenna as an accurate approximation to any monopulse antenna is developed. The use of this result is demonstrated by modelling the measured patterns of two monopulse antennas. This chapter forms the basis of a submitted journal paper [1].

Chapter 4: An extended analysis of the effect of an isolated, single-loop, retrodirective cross-eye jammer on a monopulse radar is described. A number of significant conclusions that arise from this analysis are considered, and the disagreement between this extended analysis and the phase-front analysis of cross-eye jamming is investigated. This chapter forms the basis of a published journal paper [2].

Chapter 5: Experiments conducted to validate the theoretical analysis of cross-eye jamming are described and results are presented. Comparisons between the measurements and the phase-front and extended analyses are presented. The results validate the conclusions reached in Chapter 4. This chapter forms the basis of a submitted journal paper [3].

Chapter 6: The tolerance requirements on retrodirective cross-eye jammer systems are evaluated. Both the phase-front theory and the theory developed in Chapter 4 are considered, and qualitative and quantitative comparisons are provided. This chapter forms the basis of a submitted journal paper [4].

Chapter 7: A brief conclusion and some suggestions for future research are given.

Three appendices are provided to summarise important information, and an overview of their content is given below.

Appendix A: The terminology used in this thesis is summarised. Definitions of new terms and the specific meanings of common terms like “antenna” are provided.

Appendix B: The accuracy of approximations used in the analysis of cross-eye jamming is evaluated. Approximations to the range and angular separation of the jammer antenna elements are considered.

Appendix C: The fact that the even-order derivatives of a general monopulse error are all zero is proved. This result is used in Chapter 3 to derive a general monopulse antenna model.

CHAPTER 2

BACKGROUND

2.1 Introductory Remarks

The main goal of this chapter is to provide sufficient background information to motivate the need for this work. The field of Electronic Warfare (EW) is briefly described in Section 2.2 with the aim of placing cross-eye jamming in context. An introduction to tracking radars is provided in Section 2.3 to introduce monopulse radars and their inherent resistance to many types of jamming. Cross-eye jamming is based on artificially recreating the worst-case glint angular error, so the deterministic analyses of glint are summarised in Section 2.4, where the limitations of these analyses when applied to cross-eye jamming are highlighted. The importance of the retrodirective implementation of cross-eye jamming is motivated in Section 2.5 by comparing a number of possible implementations of cross-eye jamming. The main points considered in this chapter are summarised in Section 2.6.

2.2 Electronic Warfare

The Electromagnetic (EM) spectrum has considerable potential for application in military environments to the point that there are even proposals for considering the EM spectrum as a warfighting domain on par with land, sea, air and space [5]. EW is the term given to the techniques used to ensure that maximum benefit is obtained from the EM spectrum.

EW is normally divided into three broad categories which are summarised below [6–11].

Electronic Support (ES): ES is that portion of EW that is devoted to extracting as much information as possible from the EM spectrum. ES aims to determine the presence, parameters (including frequency, modulation, position, etc.) and identity of emitters, and to determine the intent of their users. Signal detection, emitter identification, Direction-Finding (DF) and geolocation are examples of technologies that fall under ES. ES was historically known as Electronic warfare Support Measures (ESM).

Electronic Attack (EA): EA aims to deny, or at least disrupt, an adversary's use of the EM spectrum. This can range from simply transmitting high-power signals that overwhelm all an adversary's receivers to more complex deception techniques like cross-eye jamming. EA includes technologies such as jamming and deception techniques. EA was historically know as Electronic Countermeasures (ECM).

Electronic Protection (EP): The aim of EP is to protect friendly forces' use of the EM spectrum in the presence of intentional (usually jamming by an adversary) and unintentional (usually electromagnetic compatability issues) interference. Issues like low-sidelobe antennas, wideband systems, and even frequency planning fall under EP. EP was historically know as Electronic Counter-Countermeasures (ECCM)

Historically, EA techniques sought to exploit some vulnerability of the implementation of a system, but this approach has become increasingly difficult with the wide proliferation of both military and civilian systems that have few inherent vulnerabilities. Examples of this trend include low-sidelobe antennas and wideband systems including spread-spectrum communications. The need for advanced EA techniques is thus increasing.

Cross-eye jamming is a technique that aims to deceive a missile's radar seeker as to the true position of a target [6–24]. The main application of cross-eye jamming is as a self-protection technique during the final stages of an engagement when radar-guided missiles are approaching a platform that must be protected.[1] Other possibilities that can achieve the same effect are briefly considered below.

Offboard decoys: This very general heading includes passive decoys like chaff, and active systems like towed decoys and expendable decoys. Chaff is a cloud of small dipoles designed to give a large radar return that, in this context, is used to draw a radar off its target [6,9–11,22,25]. Chaff is a relatively simple countermeasure, and modern radar seekers are able to distinguish chaff from the true target. Towed and expendable decoys are based on the same concept as chaff, but use more advanced decoys that are much more difficult to distinguish from the true target [18, 22].

Despite their current popularity, offboard decoys suffer from a number of disadvantages including high life-cycle cost when expendable elements are used, limited availability when only a finite number of decoys can be carried, significant delay while the decoy moves away from the host platform, and a limited ability to cater for multiple targets due to geometric considerations.

Cross-polarisation jamming: This jamming technique returns signals to a radar using the opposite polarisation to the radar's intended polarisation, and works on the principle that an antenna's cross-polarisation pattern tends to differ significantly from its co-polarisation pattern [6, 8–11, 18, 22, 25].

This is an example of a jamming technique that takes advantage of deficiencies in the design and realisation of radar systems, and as such, is becoming less useful as modern radar antennas are designed to have low cross-polarisation characteristics. In addition, the depolarising effect of multipath limits the potential applicability of this technique.

Terrain bounce: This technique attempts to create a strong target on the surface by transmitting a strong signal towards the surface that is then reflected to the missile [6, 9–11, 22].

[1] Cross-eye jamming is not considered EP despite the fact that it is used for self protection because it attacks a missile's radar seeker.

While this technique is feasible, a very high jammer signal power is required to ensure that the target created on the surface is strong enough to compete with a platform's skin return. The jammer antenna must also have a narrow elevation antenna beamwidth and low sidelobes to ensure that this technique does not simply act as a beacon by transmitting a strong signal towards the missile.

Co-operative jamming: A number of platforms that cannot be resolved by a radar co-operate to deceive a radar as to their true number and positions in this technique [6, 9–11, 22, 25]. For example, versions of cross-eye jamming based on transceivers on multiple platforms [26, 27] can be considered co-operative jamming.

The major drawback of co-operative jamming is that the radar being jammed must not be able to resolve the platforms, but modern radars have high-resolution capabilities in range, Doppler, azimuth and elevation making this condition difficult to achieve. Additionally, correctly synchronising transceivers on a number of platforms is challenging.

Note that techniques that do not cause an angular error are not suitable for self-protection against radar-guided missiles because, for example, a missile that has been deceived as to the true range to its target will still hit the target on its way to the apparent target position.

Cross-eye jamming is able to overcome the disadvantages of the techniques listed above, and has the following advantages [18]:

- cross-eye jamming is based on glint which affects all radars, so cross-eye jamming will affect all radars,[2]
- a cross-eye jammer is always available because it does not utilise expendable elements,
- the nature of a retrodirective cross-eye jammer means that it will transmit a jamming signal in the direction of any incoming signal, so multiple threats can be dealt with simultaneously, and
- a cross-eye jammer can be constructed from two jammer systems that are connected together, so these jammers are available for other applications when cross-eye jamming is not required.

However, cross-eye jamming does suffer from the following drawbacks [18]:

- a cross-eye jammer's signals tend to cancel at the radar being jammed so high-gain, high-power systems are required, and
- achieving the system matching required to implement a successful cross-eye jammer is challenging, particularly under operational conditions.

Despite these drawbacks, a number of authors have recently described the successful demonstration of cross-eye jammers against tracking radars [18, 19, 21, 28, 29].

[2]This widely-held belief is refuted later in this thesis where it is shown that retrodirective cross-eye jammers have no effect on radars that use the same antenna beam for both transmission and reception including some conical-scan radars. However, radars with this characteristic are unlikely to be employed as seekers because, as mentioned in Section 2.3, they are relatively simple to jam, so cross-eye jamming will be effective against all radars likely to be encountered.

2.3 Tracking Radar

A monopulse radar is a type of tracking radar that is able to determine the direction to a target with a single measurement (or pulse – hence the name) [13,15,17,22,30,31]. Types of tracking radar are introduced below as motivation for the development of monopulse radars. The difficulties associated with jamming monopulse radars are highlighted.

A tracking radar is a radar that is designed to track a target as accurately as possible. Tracking a target in angle requires some way of determining whether the radar is pointing towards the target, and determining the direction and magnitude of any angular error encountered.

Early tracking radars worked by switching between two antenna beams which were squinted relative to the radar's axis (boresight). When a target is perfectly on boresight, the returns from the two antenna beams will have equal amplitude. The difference between the amplitudes of the signals received by the two beams gives an indication of the angular tracking error when the target is not on boresight.

A simple extension to this sequential lobing utilises a single squinted antenna beam which is rotated around the boresight direction giving a configuration known as conical-scan radar. This means that a target that is exactly on boresight produces no variation as the beam is rotated, but that there will be a variation when the target is not on boresight. The magnitude of the tracking error can be found from the amplitude of the variation of the received signal over time, and the direction to the target can be determined from the received signal's phase variation over time [31].

The greatest drawback of sequential-lobing and conical-scan radars is that the measured angular error will be influenced by any variations in the received signal over time. These signals can either be due to the natural variations in target amplitude (scintillation) or due to jamming [6–9, 11, 12, 16, 25, 32]. Sequential-lobing and conical-scan radars are so vulnerable to jamming that alternative techniques that transmit using a fixed antenna beam and only scan on receive, Lobing on Receive Only (LORO) and Conical Scan on Receive Only (COSRO), have been developed solely to reduce this vulnerability [6–9, 11, 16, 25, 33].

This led to the development of monopulse radar, where multiple beams are formed simultaneously, thereby removing errors due to variations of the received signal over time [6–8, 10, 11, 13, 15, 17, 22, 30, 31]. Generally four antenna beams are formed to allow tracking in both azimuth and elevation. These beams are combined into a sum-channel beam (generated by summing all the beams) and two difference-channel beams, one for azimuth and the other for elevation (formed by taking the differences of the relevant sets of beams). The sum channel is used for signal transmission and normalisation of the received signal, while the normalised difference-channel returns are used to determine the angular error.

There are two main classes of monopulse radar, namely amplitude- and phase-comparison monopulse, though phased-array and hybrid implementations are also possible. Differences relate mainly to the implementation of the squinted beams rather than to any fundamental difference in approach [30].

The main challenge associated with jamming monopulse radars arises from the fact that amplitude variations over time have no effect on the tracking accuracy. This is mainly as a result of the fact that the antenna beams are formed simultaneously rather

than sequentially.

An additional complication is that a monopulse radar that encounters jamming can switch to a home-on-jam mode where the radar stops transmitting and only uses its receivers [6, 8, 9, 11, 16, 22, 25, 32]. The fact that the antenna beams are formed simultaneously means that even a noisy signal can be tracked extremely accurately in home-on-jam mode.

The difficulties associated with jamming monopulse radars have led to the consideration of other jamming techniques including cross-eye jamming [6, 8, 10, 12, 13, 16, 18, 19, 21, 25, 26, 34, 35], which works by attempting to recreate the worst-case glint angular error.

2.4 Glint Analysis

Glint is a naturally-occurring phenomenon that causes angular errors in all types of radar. Glint is caused by the interactions of reflections from a number of points on a target that cannot be resolved by a radar and is solely dependent on the characteristics of the target [17, 30, 31, 36]. This section provides a review of the main deterministic approaches to analysing glint with the emphasis on their relevance to cross-eye jamming. A number of different analyses of glint are presented in Section 2.4.1 and their limitations when applied to cross-eye jamming are considered in Section 2.4.2.

2.4.1 Glint Analyses

In 1953, Delano [37] published the first paper in the open literature on glint. Even at this early stage using relatively simple statistical models, glint's potential to produce apparent targets outside the physical extent of the true target was established. Delano found that, under certain simplifying assumptions, the apparent target is outside the real target 13.4% of the time [37]. While the exact figure is open to debate, the result is not, and the importance of understanding and compensating for glint was clearly demonstrated.

Glint analyses can be loosely classified as statistical and deterministic analyses. While a number of valuable papers considering statistical analyses of glint have been published (including Delano's paper cited above), they will not be considered further here because they are of limited relevance to cross-eye jamming.

Glint analyses are derived by assuming that the scatterers are all at the same range, and that the scatterers transmit and that the radar only receives. While this is clearly not what happens in reality, it does provide an accurate model of glint. The different ranges to each of the scatterers are accounted for by adjusting the relative phases of the scatterers. Similarly, differences in the signals the scatterers receive from the radar due to angular variations in the sum-channel antenna pattern are accommodated by changing the relative amplitudes and phases of the scatterers. This approach allows accurate results to be achieved with surprisingly simple mathematical analyses.

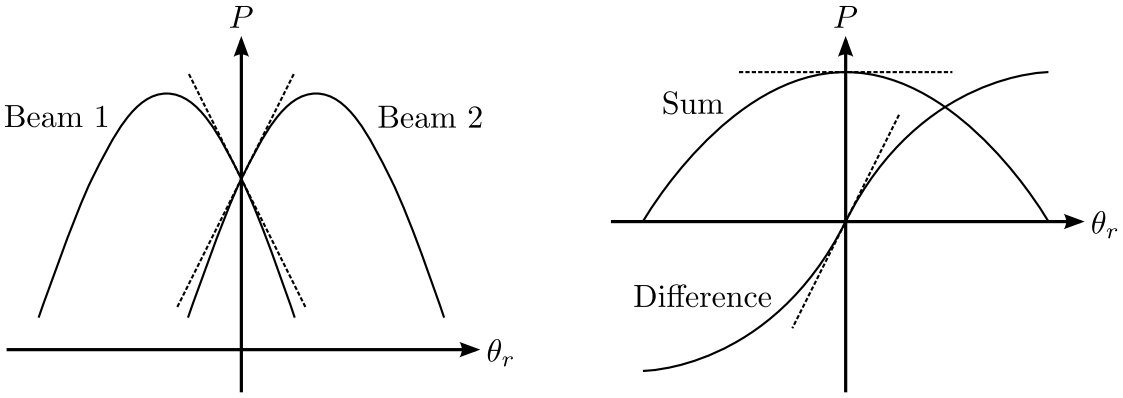

(a) Amplitude-comparison squinted beams.

(b) Monopulse sum- and difference-channel antenna patterns.

Figure 2.1: Linear fits to monopulse antenna patterns. The solid and dashed lines indicate the true patterns and linear fits to the true patterns on boresight respectively. The horizonal axis the radar rotation and the vertical axis is the antenna pattern.

Linear-Fit Analysis

The first deterministic analysis of glint was published by Meade in 1955 [38] and made use of linear fits to the antenna patterns of a lobing radar system near boresight as shown in Figure 2.1(a). The same approach has been applied to amplitude-comparison monopulse radars by Leonov and Fomichev [13], Vakin and Shustov [12], and Stratakos *et al.* [39], though both Leonov and Fomichev [13], and Vakin and Shustov [12] also consider other analyses. Sherman [30, 40], and later Schleher [10], used essentially the same approach, but formed linear approximations to the sum- and difference-channel antenna patterns of a monopulse antenna on boresight as shown in Figure 2.1(b). This approach is equivalent to the approach shown in Figure 2.1(a) because the sum- and difference-channel antenna patterns formed using the linear approximations to the squinted antenna patterns shown in Figure 2.1(a) are identical to the linear approximations shown in Figure 2.1(b). Sherman's approach has the benefit that its applicability to any type of monopulse radar is obvious, while this is not necessarily true when linear fits to squinted antenna patterns are used. This is clearly demonstrated by the fact that Leonov and Fomichev [13] only apply the linear-fit analysis to amplitude-comparison monopulse systems and derive a completely different analysis for phase-comparison monopulse systems (described below), despite the fact that the linear-fit analysis can be applied to any monopulse radar.

The use of the linear-fit analysis by Vakin and Shustov [12] is extremely significant as this is the most widely-referenced analysis of cross-eye jamming (either directly or via Van Brunt [25] who references this work). For this reason, a brief summary of the mathematical derivation of the linear-fit analysis of glint is given below. Sherman's approach of using a linear fit to the monopulse sum- and difference-channel antenna patterns is used [30, 40] here because it is simpler, it gives identical results, and its applicability to all types of monopulse radars is clear.

The relationship between the monopulse error (the ratio of the difference-channel

return to the sum-channel return) to the monopulse indicated angle is assumed to be

$$\theta_i = k_m \frac{d}{s} \tag{2.1}$$

where θ_i is the monopulse indicated angle, k_m is a constant, and s and d are the signals received in the sum and difference channels respectively. From (2.1), the difference-channel return can be written as

$$d = \frac{s\theta_i}{k_m}. \tag{2.2}$$

Assume two sources are present at angles θ_1 and θ_2 measured from the radar's boresight direction, and that the amplitude and phase of the second source relative to the first source are a and ϕ respectively. The total sum-channel return is given by

$$s_t = 1 + ae^{j\phi} \tag{2.3}$$

and the total difference-channel return is given by

$$d_t = \frac{\theta_1}{k_m} + ae^{j\phi}\frac{\theta_2}{k_m} \tag{2.4}$$

where (2.2) was used. From (2.1), the indicated angle is given by

$$\theta_i = \frac{\theta_1 + ae^{j\phi}\theta_2}{1 + ae^{j\phi}} \tag{2.5}$$

which can be simplified by setting

$$\theta_{1,2} = \theta_r \pm \theta_e \tag{2.6}$$

where θ_r is the angle from boresight to the point between the two scatterers and θ_e is half the angular separation of the scatterers as seen by the radar to give

$$\theta_i = \theta_r + \theta_e \frac{1 - ae^{j\phi}}{1 + ae^{j\phi}}. \tag{2.7}$$

Only the real part[3] of this complex indicated angle is used to form the final indicated angle in an exact monopulse processor [15, 30] giving

$$\Re\{\theta_i\} = \theta_r + \theta_e \frac{1 - a^2}{1 + a^2 + 2a\cos(\phi)} \tag{2.8}$$

which can be simplified to

$$\Re\{\theta_i\} = \theta_r + \theta_e G_C \tag{2.9}$$

[3]Either the real or the imaginary part of the complex indicated angle should be used depending on which portion of the complex indicated angle contains information about the position of a single point target. The real part of the indicated angle is used for the linearised monopulse system considered here, but the imaginary part of the complex indicated angle is used for the phase-comparison monopulse systems considered in the rest of this document.

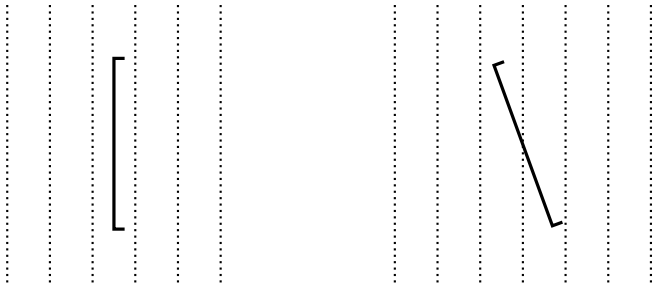

(a) Aligned. (b) Not aligned.

Figure 2.2: Graphical representation of why an antenna will receive maximum power from an incoming signal when it is aligned with incoming phase fronts. The antenna aperture and phase fronts are denoted with solid and dotted lines respectively.

when the cross-eye gain is defined as [9]

$$G_C = \frac{1 - a^2}{1 + a^2 + 2a\cos(\phi)}. \tag{2.10}$$

The largest indicated angle will thus be achieved when $a \to 1$ and $\phi \to 180°$ because this makes the cross-eye gain large. Equation (B.12) on page 110 shows that the angular separation of the scatterers can be written as

$$\theta_e \approx \frac{d_c}{2r}\cos(\theta_c) \tag{2.11}$$

where d_c is the linear separation of the scatterers, r is the range from the radar to the scatterers, and θ_c is the angle between the scatterers' broadside direction and the direction to the radar. Substituting (2.11) into (2.9) gives

$$\Re\{\theta_i\} = \theta_r + \frac{d_c}{2r}\cos(\theta_c)\, G_C \tag{2.12}$$

which is the form provided in the literature.

An important observation arising from (2.11) and (2.12) is that a cross-eye jammer will produce a constant linear offset rather than a constant angular error [9,18,34]. The importance of this observation is based on the fact that a constant angular error will not cause a missile to miss its target, while a constant linear offset will [24,34].

Phase-Front Analysis

Arguably the most important contribution to the understanding of glint was the development of the phase-front analysis of glint which was published by Howard [41].[4] This analysis is based on the fact that any antenna will receive maximum power from an incoming signal when it is aligned with the signal's phase fronts [34, 41, 42]. The antenna in Figure 2.2(a) is aligned with the phase fronts, so the signals over the entire

[4]Interestingly, Howard credits B. L. Lewis, listed as co-inventor with Howard on the original cross-eye jamming patent [14], as the originator of the phase-front analysis of glint.

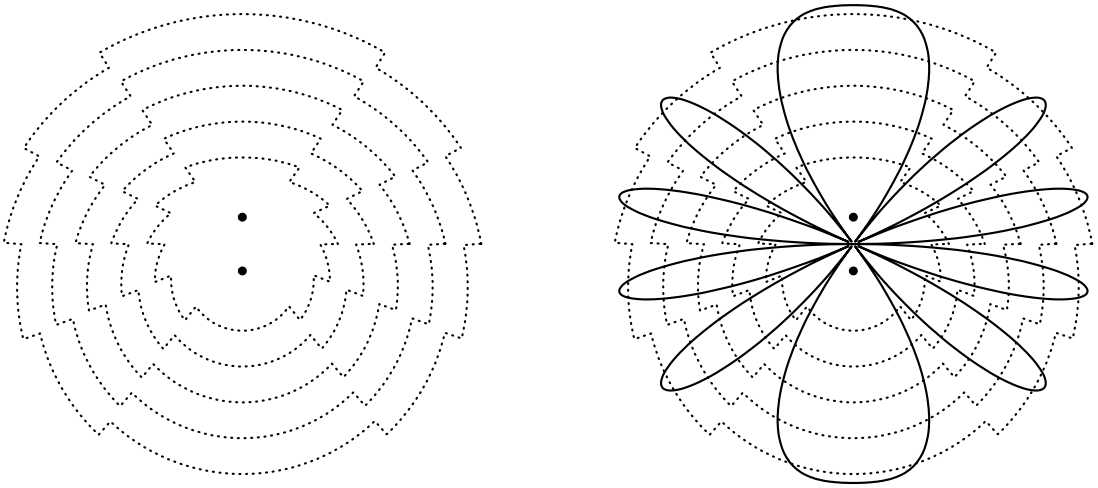

(a) Phase fronts.

(b) Phase fronts (dotted lines) and signal amplitude (solid lines).

Figure 2.3: Fields resulting from two sources of equal amplitude and 180° relative phase shift spaced 2.5 wavelengths apart. The positions of the sources are shown by circles.

antenna aperture will add in phase giving the highest possible received power. However, the antenna in Figure 2.2(b) is not aligned with the phase fronts, so the signals over the antenna aperture are not in phase and will thus partially cancel, thereby reducing the power received compared to the antenna in Figure 2.2(a). The direction an antenna will point to receive maximum power can thus be determined from the slope of the phase fronts of the incoming signal.

The phase fronts created by two sources 2.5 wavelengths apart with equal amplitudes and 180° relative phase are shown in Figure 2.3. Figure 2.3(a) only shows the phase fronts, and similar plots can be found in the literature (e.g. [13, 31, 41, 43]). The amplitude of the signal is plotted with the phase-fronts in Figure 2.3(b), showing that the amplitude of the signal has its minimum values in the directions where the phase-front distortion is greatest [34]. This is because phase-front distortions are maximised in those directions where the phase difference between the two scatterers is 180°, causing maximum cancellation of the signals from the scatterers.

Lindsay [42] built on the phase-front analysis of glint by using the derivative of the phase in space (the normal to the phase front) to determine the direction an antenna will point. The main benefit of this approach is that it allows the angular error, amplitude scintillation and Doppler shift due to multiple scatterers to be explained in terms of phase-front distortion. Dunn and Howard [43] reached a similar conclusion in a paper published a mere five months after Lindsay's paper. The main difference between these results is that Dunn and Howard only consider the derivative of phase with respect to target aspect angle, while Lindsay finds the normal to the phase front by determining the vector gradient.

Given the importance of the phase-front analysis, an abbreviated derivation is given below. The form of this analysis is slightly different to that provided in the literature, but it follows Lindsay's approach of using the direction of the phase gradient to determine

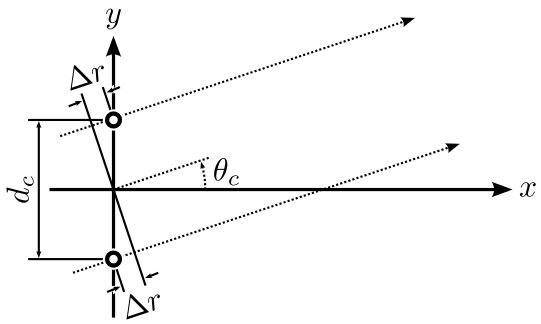

Figure 2.4: The configuration of two scatterers used to derive the phase-front analysis of glint.

the direction a radar will point [42] using

$$\nabla\Phi = \hat{r}\frac{\partial\Phi}{\partial r} + \hat{\theta}_c\frac{1}{r}\frac{\partial\Phi}{\partial\theta_c} \tag{2.13}$$

and

$$\delta = \arctan\left[\frac{\frac{1}{r}\frac{\partial\Phi}{\partial\theta_c}}{\frac{\partial\Phi}{\partial r}}\right] \tag{2.14}$$

where $\nabla\Phi$ is the gradient of the phase, $\hat{r}$ and $\hat{\theta}_c$ are the unit vectors in the radial direction and perpendicular to the radial direction respectively, and δ is the angular error. Consider two scatterers on the y axis as shown in Figure 2.4, where the rays from the scatterers are assumed to be parallel under the far-field assumption [44, 45]. The total signal received at a point far from the scatterers is given by

$$E = e^{j\beta r}\left[ae^{j\phi_0}e^{j\beta\frac{d_c}{2}\sin(\theta_c)} + e^{-j\beta\frac{d_c}{2}\sin(\theta_c)}\right] \tag{2.15}$$

where β is the free-space phase constant, r is the range to the point where the fields are being determined, a and ϕ_0 are the amplitude and phase of the top scatterer relative to the bottom scatterer, and the rest of the parameters are defined in Figure 2.4. The phase of the signal in (2.15) is given by

$$\Phi = \arctan\left[\frac{\Im\{E\}}{\Re\{E\}}\right] \tag{2.16}$$

$$\approx \frac{\cos(\beta r)\left(a\sin\left[\beta\frac{d_c}{2}\sin(\theta_c)+\phi_0\right] - \sin\left[\beta\frac{d_c}{2}\sin(\theta_c)\right]\right) + \cdots}{\cos(\beta r)\left(a\cos\left[\beta\frac{d_c}{2}\sin(\theta_c)+\phi_0\right] + \cos\left[\beta\frac{d_c}{2}\sin(\theta_c)\right]\right) - \cdots}$$
$$\frac{\sin(\beta r)\left(a\cos\left[\beta\frac{d_c}{2}\sin(\theta_c)+\phi_0\right] + \cos\left[\beta\frac{d_c}{2}\sin(\theta_c)\right]\right)}{\sin(\beta r)\left(a\sin\left[\beta\frac{d_c}{2}\sin(\theta_c)+\phi_0\right] - \sin\left[\beta\frac{d_c}{2}\sin(\theta_c)\right]\right)} \tag{2.17}$$

where Φ is the phase of the total signal, and the approximation is due to the assumption that the arctangent function can be approximated by its argument because its argument is small. This assumption is reasonable because the calculations above can be assumed to be performed at angles where $\Phi \approx 0$. The derivatives of the total field phase are given by

$$\frac{\partial\Phi}{\partial r} = 2\beta\frac{1+a^2+2a\cos\left[\phi_0+d_c\sin(\theta_c)\right]}{\left[\Re\{E\}\right]^2} \tag{2.18}$$

and

$$\frac{\partial \Phi}{\partial \theta_c} = \beta d_c \cos(\theta_c) \frac{1 - a^2}{[\Re\{E\}]^2}. \tag{2.19}$$

From (2.14), this means that the angular error is given by

$$\delta \approx \frac{d_c}{2r} \cos(\theta_c) \frac{1 - a^2}{1 + a^2 + 2a \cos[\phi_0 + d_c \sin(\theta_c)]} \tag{2.20}$$

where δ is the angular error, and the approximation was again formed under the assumption that the arctangent can be replaced by its argument. Comparing (2.12) to (2.20) shows that the arguments of the cosine in the denominator are different, but this apparent discrepancy is easily resolved by setting

$$\phi = \phi_0 + d_c \sin(\theta_c) \tag{2.21}$$

on the basis that the linear-fit analysis accounts for phase variations due to range offsets in the value of ϕ.

Poynting-Vector Analysis

Dunn and Howard [43] analysed glint by determining the direction of the Poynting vector that arises due to multiple scatterers. This result clearly showed that the direction of power flow can deviate from the radial direction and is normal to the phase front. Concerns over the validity of the phase-front analysis based on the assumption that power flow must be radial were thus addressed.

Phase-Comparison Monopulse Analysis

Leonov and Fomichev [13] give an analysis of glint for phase-comparison monopulse systems that they also apply to cross-eye jamming. This analysis gives the same results as the linear-fit analysis showing that cross-eye jamming affects both amplitude- and phase-comparison monopulse radars.

This analysis is similar to the extended analysis described in Section 4.2.1, but the results differ, mainly because Leonov and Fomichev do not consider the retrodirective implementation of cross-eye jamming. Furthermore, Leonov and Fomichev introduce a number of assumptions that limit the accuracy of their models in order to obtain agreement with other results. Finally, Leonov and Fomichev also make no attempt to generalise these results to other types of monopulse radar, instead opting to use the linear-fit analysis for amplitude-comparison monopulse systems.

Equivalence of Glint Analyses

Yin and Huang [46] have shown that the phase-front and Poynting-vector analyses of glint are equivalent under the geometric optics approximation (the wavelength is negligibly small). Kajenski [47] extended this result to show that the equivalence also holds when polarisation is considered.

Vakin and Shustov [12] have shown that the phase-front analysis gives the same results as the linear-fit analysis. Leonov and Fomichev [13] show that the result for

their phase-comparison analysis also gives results that are identical to the linear-fit and phase-front analyses. While neither of these works gives a formal mathematical proof of the equivalences implied, the fact that the results are identical suggests that such an equivalence exists.

Graphical Analysis

Falk *et al.* [19, 21] have published a graphical analysis of cross-eye jamming that can also be used to understand glint. The analysis compares the signals received by the two antenna elements of a phase-comparison monopulse radar tracking two scatterers. The error induced by a cross-eye jammer (and glint) is determined by examining the vector diagrams of the signals received by each of the antenna elements as the radar antenna is rotated. The angular error is determined by the direction where the phase difference between the signals received by the two antenna elements is minimised.

Pattern Analysis

Cross-eye jamming can also be analysed by assuming particular amplitude-comparison monopulse antenna patterns, and then numerically evaluating the effect of cross-eye jamming [8, 12, 16, 24, 34]. Vakin and Shustov's results based on this analysis appear to be the source of the oft-quoted assertion that even a perfect cross-eye jammer will only create an error that is 60% of the radar's 3-dB beamwidth [12, 16, 25], though Redmill [34], Lothes *et al.* [8] and Tucker and Vidger [24] have independently reproduced this result. Furthermore, Vakin and Shustov state that the results in (2.12) and (2.20) are only valid as long as $a \leq 0.9$ or $a \geq 1.1$, and the jammer antenna element spacing is less than 10% of the radar's 3-dB beamwidth, again based on pattern analysis [12, 16].

2.4.2 Limitations of Glint Analyses

All analyses of glint suffer from limitations based on their mathematical formulation, and when cross-eye jamming is considered, by the fact that they do not consider the retrodirective implementation of cross-eye jammers.[5]

The mathematical simplifications for each of the analyses described above are slightly different. As shown in (2.1), the linear-fit analysis linearises the antenna patterns near boresight, while both the phase-front and Poynting-vector approaches assume that the radar antenna is infinitesimally small and only responds to the fields at a point. Furthermore, as seen by comparing (2.14) and (2.20), the highly nonlinear arctangent function is linearised to simplify the results. This simplification is the reason that infinite errors are predicted whereas the largest error physically possible is 90° [48]. The error due to these simplifications is generally small near boresight and when the phase-fronts are not strongly distorted. However, a cross-eye jammer violates these conditions by seeking to strongly distort the phase-fronts to rotate the radar's boresight away from the jammer. Errors caused by these assumptions are the motivation for Vakin and Shustov's bound considered above.

[5]The fact that glint analyses have limited accuracy when applied to cross-eye jamming is one of the main topics of this thesis and are considered throughout this document from various perspectives.

(a) Ideal case. (b) Realistic case.

Figure 2.5: Graphical explanation of why the assumption that an antenna is infinitesimally small leads to errors. The antenna aperture and phase fronts are denoted with solid and dotted lines respectively.

The effect of the linearisation of antenna patterns is seen in Figure 2.1, where the error inherent in linearisation is seen to increase as the target moves away from boresight. Using a linear fit to the monopulse antenna patterns implicitly assumes that the radar antenna is infinitesimally small (see Sections 3.2.1 and 4.2.2), so all glint analyses thus assume that the radar antenna responds to the fields at a point.

The assumption of an infinitesimally small antenna is explored in Figure 2.5. The finite aperture of the antenna is ignored in Figure 2.5(a), and the antenna is assumed to align itself with the fields at the centre of the antenna. A more realistic representation of what is likely to happen is shown in Figure 2.5(b) where the entire antenna aperture is considered [12,34]. The true situation is actually worse than a consideration of only the phase fronts suggests because, as shown in Figure 2.3(b), the amplitude of the signal is lowest at the largest phase distortions. This means the signals at edges of the antennas in Figure 2.5 will be stronger than at the centre of the antenna effectively distorting the antenna patterns [14, 43].

The pattern analysis used as the basis of a number of widely-held assumptions about cross-eye jamming is limited by the fact that, strictly speaking, the results are only valid for the exact amplitude-comparison monopulse system simulated [8]. While this statement is perhaps overly conservative, it is clear that pattern analysis cannot lead to a completely general understanding of glint or cross-eye jamming because of this limitation. For example, Vakin and Shustov's bound considered above is based on comparisons between the linear-fit and pattern analyses [12], and mathematical and experimental results in Section 4.3 and 5.4 show that this bound is incomplete.

The practical implementation of cross-eye jammers is considered in Section 2.5, where it is shown that realising a cross-eye jammer without using the retrodirective implementation is probably not practically feasible. As mentioned previously, glint analyses assume that any scenario can be modelled by transmitting from a number of collinear sources with varying amplitudes and phases, and that the radar is only a receiver. This approach is clearly demonstrated in the mathematical derivations of the linear-fit and phase-front analyses above. However, this model does not adequately consider retrodirective cross-eye jammers (or even retrodirective arrays) because the fact that the signal received at one antenna is transmitted from another antenna is ignored.

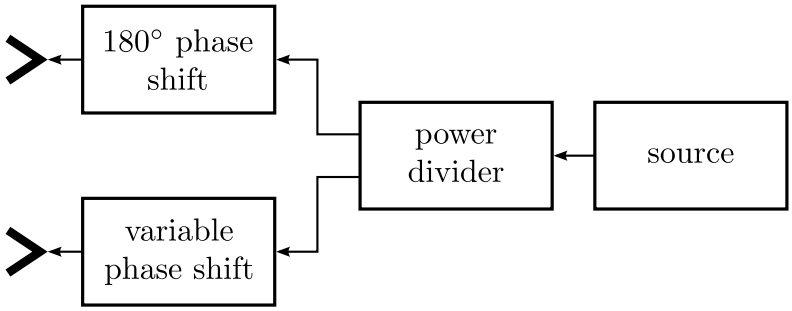

Figure 2.6: The configuration of a transmit-only cross-eye jammer.

2.5 Cross-Eye Jammer Implementation

A cross-eye jammer attempts to artificially recreate the worst-case glint angular error. This is done by using two antennas to transmit signals that ideally have a phase difference of 180° from the perspective of the radar being jammed. The analyses of glint show that the resulting error is proportional to the spacing of the scatterers, so antennas used for cross-eye jamming are widely separated.

Despite the fact that much of the literature only considers the retrodirective implementation of cross-eye jamming (e.g. [6–11, 14, 16, 18–24, 49–54]), other alternatives do exist [25]. However, the non-retrodirective implementations of cross-eye jamming place extreme tolerance requirements on a cross-eye jammer system making them impractical [6, 10, 17, 25, 34].

A retrodirective system is a system that receives signals on one side of the system and retransmits those signals on the other side of the system. Only systems that receive on both sides of the system and retransmit the received signals on the opposite sides of the system are considered, but multi-loop retrodirective beacons that only allow signals in each loop to propagate in one direction also exist.

A number of non-retrodirective cross-eye jammer implementations are considered in Section 2.5.1, and the difficulties associated with practical realisation of these implementations are outlined. The retrodirective implementation of cross-eye jamming and its benefits are described in Section 2.5.2.

2.5.1 Non-Retrodirective Implementation

A number of cross-eye jammer implementations that are not retrodirective are possible [25]. These are outlined below and their practical limitations highlighted.

Transmit Only

The simplest implementation of a cross-eye jammer does not utilise a receiver and is shown in Figure 2.6. The 180° phase shift to the one antenna is inherent in the operation of a cross-eye jammer, while the variable phase shift to the other antenna allows the jammer to be steered in the direction of the radar being jammed.

The source in Figure 2.6 is typically a noise source, and the system seeks to exploit the home-on-jam mode in modern missiles mentioned in Section 2.3. The application of

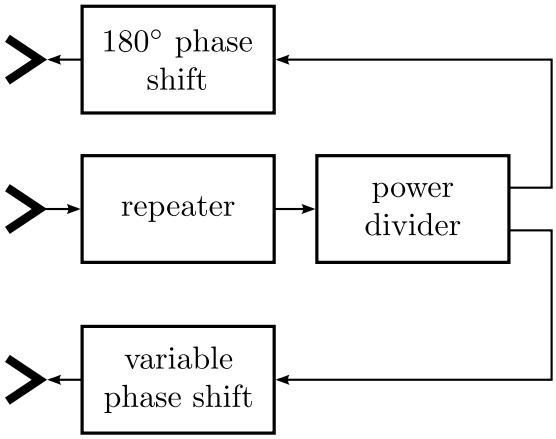

Figure 2.7: The configuration of a cross-eye jammer based on a single repeater.

the cross-eye approach means that the jamming signal appears to come from a position removed from the true jammer position, ensuring that a missile will miss the target.

The biggest drawback of the transmit-only approach to cross-eye jamming is that no feedback is received from a missile because the missile's transmitter is not active. This is a particularly large problem for a cross-eye jammer where the range of angles over which the jammer is effective is very small. For example, an angular error of 1.5 mrad is enough to turn an ideal cross-eye jammer into a perfect beacon for a jammer antenna element spacing of 10 m at 10 GHz.

Single Repeater

The addition of a single receiver leads to the cross-eye implementation shown in Figure 2.7. The incoming signal is sampled by a single antenna and then retransmitted from two antennas. The receiver block in Figure 2.7 is assumed to include all the equipment required to receive, process and retransmit the received radar signal.

The main benefit of this approach is that the missile's transmitter remains active, so any variations in the missile's position or mode can be determined. An additional benefit of retransmitting the signal received from the missile is that the missile will hopefully be unaware that it is being jammed and not activate countermeasures.

Limitations

The first problem with the implementations of cross-eye jamming described above is that the jammer needs to be able to control the relative phase of the signals transmitted from the two antennas to ensure that the jammer signal is directed towards the radar being jammed [6, 10]. This problem is greatly complicated by the fact that environmental effects (including temperature, humidity, pressure, vibration and platform flexing) have to be compensated for to prevent the jammer becoming a beacon. For example, a change in antenna position of only 1.5 cm due to the wings of an aircraft flexing during flight can turn an ideal cross-eye jammer into a perfect beacon, with similar results being given in the literature [6, 8, 10, 11, 17, 25, 34].

The second problem with the implementations of cross-eye jamming described above

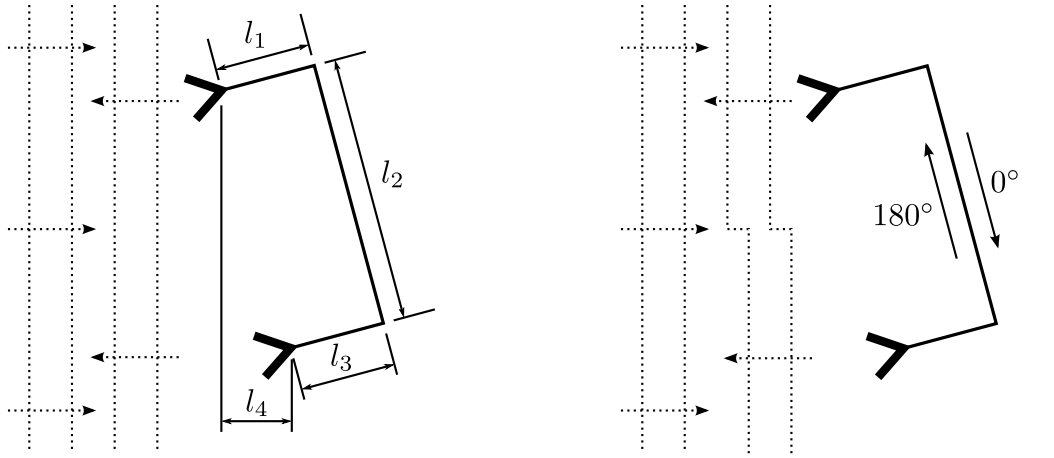

(a) Retrodirective array. (b) Retrodirective cross-eye jammer.

Figure 2.8: Graphical description of the retrodirective concept.

is that the jammer is only effective over a very narrow range of angles. As mentioned previously, an angular error of less than 1.5 mrad is enough to turn an ideal cross-eye jammer into a perfect beacon for a jammer antenna element spacing of 10 m at 10 GHz. It is extremely unlikely that a DF system will be able to achieve the required angular accuracy unless it uses a baseline comparable to the jammer antenna element spacing.

One possibility for overcoming these limitations is to sweep the relative phase shift of the two signals transmitted by the cross-eye jammer. The main drawback of this approach is that the angular error induced in the radar being jammed will be too small for the apparent target to be outside the physical extent of the platform the majority of the time [34]. It might be possible to reduce the dynamic stability of a missile as a whole causing it to miss its target [55], but this would rely on a detailed knowledge of the missile's characteristics.

Combining the functions of the DF system required to determine the direction to the radar being jammed and the cross-eye jammer system leads to an approach that overcomes most of the difficulties listed above. This approach is the retrodirective implementation of cross-eye jamming considered in Section 2.5.2.

2.5.2 Retrodirective Implementation

The retrodirective implementation of cross-eye jamming is based on the retrodirective array. This section thus starts with a brief description of retrodirective arrays and then moves on to retrodirective cross-eye jammers.

Retrodirective Arrays

Retrodirective arrays are often called Van Atta arrays after their inventor [56] and have been extensively considered in the literature (e.g. [22, 57–61]). A retrodirective array consists of a number of pairs of antennas connected by paths along which signals can travel, usually in both directions.

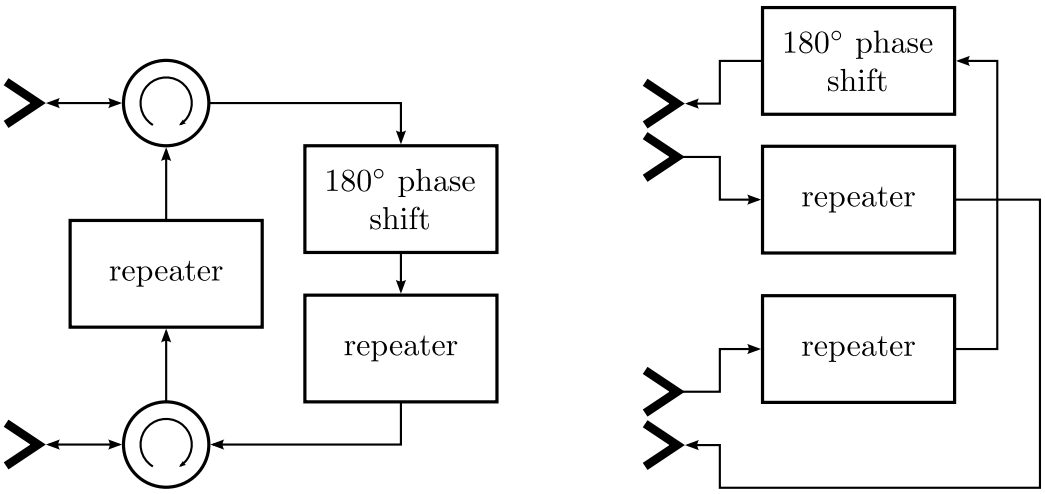

(a) Single antennas used for both transmission and reception.

(b) Separate antennas for transmission and reception.

Figure 2.9: Two possibilities for implementing a retrodirective cross-eye jammer.

The principle behind a retrodirective array is extremely simple and is illustrated in Figure 2.8(a). When a plane wave is incident on the array, the signals passing through the array in the two directions will travel identical distances and emerge in phase in the direction of the incoming signal. For the direction of the incoming plane wave in Figure 2.8(a), the path length for the signal received by the top antenna is $l_1+l_2+l_3+l_4$ and the path length for the signal received by the bottom antenna is $l_4+l_3+l_2+l_1$. While Figure 2.8(a) only considers one pair of antennas, the concept can be extended to any number of antennas as long as the lengths of the cables connecting each pair of antennas are identical and the points between all the pairs of antennas are coincident. It is also possible to build a retrodirective array where signals can only travel between each pair of antennas in one direction (e.g. if an amplifier is used), with the retrodirective effect being caused by the interaction between the signals from a number of pairs of antennas.

Retrodirective Cross-Eye Jammers

The operation of a retrodirective cross-eye jammer is identical to that of a retrodirective array except that one of the directions through the cross-eye jammer has a phase shift of 180° relative to the other direction through the array. This is illustrated in Figure 2.8(a) by showing that a phase-front distortion will be retransmitted in the direction of the incoming signal. The main advantage of the retrodirective cross-eye jammer implementation is thus that the jamming signal is reradiated in the direction of the radar being jammed without requiring a knowledge of that direction or any control of the cross-eye jammer phases. Only the matching between the two directions through the cross-eye jammer needs to be controlled (see Chapter 6). The practical realisation of a retrodirective cross-eye jammer is considered in Figure 2.9.

Figure 2.9(a) expands Figure 2.8(b) to show how the signals in the two directions through the cross-eye jammer can be split and the necessary 180° phase shift realised.

Note that circulators are used in Figure 2.9(a) for illustration purposes only and that other possibilities (e.g. switches) are also possible [25, 50]. The transmission lines between the antennas and the circulators are short in Figure 2.9 only to save space here and can be any length. The main benefit of this approach is that only the circuit elements that are not common to both directions through the cross-eye jammer have to be matched. This is because the common circuit elements (antennas and cables) affect both directions through the cross-eye jammer identically, so the effects of these common circuit elements cancel out. The greatest drawback of this retrodirective implementation is that it is very difficult to obtain high isolation between the two directions through the cross-eye jammer.

The Radar Cross Section (RCS) of a retrodirective beacon is given by [62]

$$\sigma_b = \frac{[n\lambda G_a]^2 G_R}{4\pi} \tag{2.22}$$

where σ_b is the beacon RCS, n is the number of receive-transmit antenna pairs, λ is the wavelength, G_a is the gain of the beacon/jammer antenna elements and G_R is the gain of the repeaters. A repeater gain of 31.4 dB ($G_R \approx 1400$) is required to obtain a 10 m^2 target ($\sigma_b = 10$ m^2) with a single repeater ($n = 1$) connected to two antennas each of which has a gain of 10 dBi ($G_a \approx 10$) at X-Band ($\lambda = 0.03$ m). The only isolation between the two high-gain repeaters in Figure 2.9(a) is provided by the two circuit elements denoted by circulators. If the isolation of each of these two circuit elements is less than the gain of the repeaters plus some safety margin, it is extremely likely that the system will oscillate. Obtaining isolations of 35 dB or more to avoid oscillation is possible, but extremely challenging as evidenced by the large number of patents describing cross-eye jammer implementations [49–54].

The implementation in Figure 2.9(b) overcomes the isolation problem by using separate antennas for transmission and reception on each side of the cross-eye jammer. The biggest drawback of this retrodirective cross-eye jammer implementation is that none of the circuit elements are common to the two directions through the cross-eye jammer, dramatically increasing the difficulties associated with matching the cross-eye jammer system.

Another disadvantage of the configuration shown in Figure 2.9(b) is that the cross-eye jammer is not reciprocal, while the configuration shown in Figure 2.9(a) is. Falk *et al.* [19, 21] have shown that reciprocal scattering effects such as multipath reflections do not influence the performance of a cross-eye jammer as long as the jammer itself is reciprocal.

As with retrodirective arrays, a number of cross-eye jammer loops of the form shown in Figure 2.8(b) can be used [20, 63]. The main benefit of using multiple cross-eye jammer loops is that additional degrees of freedom are introduced, allowing the angular range over which a cross-eye jammer is effective to be increased and the sensitivity to system tolerances to be reduced. As mentioned in Section 1.3.1, a detailed investigation of multi-loop cross-eye jamming falls outside the scope of this study.

Even though the retrodirective implementation of cross-eye jamming greatly simplifies the realisation of a practical system, the challenges remaining are still significant. This is shown by the large number of proposed cross-eye jammer implementations [14,27,34,49–54,64,65], and the fact that only recently has the existence of practical

cross-eye jammers been acknowledged [18, 19, 21, 28, 29] and speculated on [66–68].

2.6 Concluding Remarks

Cross-eye jamming is placed within the greater field of EW, and the benefits of cross-eye jamming over comparable self-protection techniques are highlighted. Tracking radars are then introduced and the fact that modern monopulse radars are extremely difficult to jam is highlighted. However, all radars are affected by glint, so cross-eye jamming attempts to recreate the worst-case glint angular error. The analyses of glint are briefly summarised and their limitations when applied to cross-eye jamming are highlighted. The importance of the retrodirective implementation of cross-eye jamming is demonstrated by considering a number of other possible implementations of cross-eye jamming and noting their drawbacks.

With the background to and motivation for the current study clearly established, the development now moves to a consideration of the monopulse model that will be used to analyse cross-eye jamming in Chapter 3.

CHAPTER 3

MONOPULSE MODEL

3.1 Introductory Remarks

The use of a generalised phase-comparison monopulse antenna as a model for any monopulse antenna is considered in this chapter. This is done as a prelude to analysing a cross-eye jamming scenario in Chapter 4 to demonstrate the wide validity of that analysis. The work described in this chapter forms the basis of a submitted journal paper [1].[1]

A monopulse radar uses two antenna beams, the sum- and difference-channel beams. The sum-channel beam has a peak in the radar's boresight direction and is used for transmission, target detection and angle-error normalisation. The difference-channel beam has a null in the radar's boresight direction and is used to form an error signal determined by the angular tracking error [13, 15, 17, 22, 30, 31]. The sum- and difference-channel beams can be formed in a number of ways, including:

- amplitude-comparison monopulse systems using the sum and difference of two squinted beams [13, 15, 17, 22, 30, 31],
- phase-comparison monopulse systems using the sum and difference of two beams with offset phase centres [13, 15, 17, 22, 30, 31],
- phased arrays which form the sum- and difference-channel beams directly [13, 17, 30, 69], and
- combinations of these approaches (e.g. the five-horn feed forms the sum-channel beam directly while forming the difference-channel beams using the amplitude-comparison approach) [30, 31].

Of these, phase-comparison is the most common [26]. While there are significant differences in the design and practical implementation of each of these monopulse systems, they all form a sum-channel beam (peak on boresight) and a difference-channel beam (null on boresight), so all monopulse systems work in the same way.

Sherman [30] has shown the equivalence of the antenna patterns in the amplitude- and phase-comparison cases, but acknowledges that his analysis considers antenna patterns that "have a peculiar, asymmetrical shape and are not likely to have practical application" and "are likely to have unusual shapes" [30].

The equivalence of a general monopulse antenna and a generalised phase-comparison monopulse antenna near boresight is proved in Section 3.2. The use of a generalised phase-comparison monopulse antenna to approximate measured monopulse antenna patterns is considered in Section 3.3. Concluding remarks are provided in Section 3.4.

[1] Portions of this chapter are reprinted, with permission, from [1].

3.2 Mathematical Analysis

The use of an antenna array to model any antenna is the basis of the analysis in this section. The sum- and difference-channel antenna patterns and monopulse errors for a general monopulse antenna model and a generalised phase-comparison monopulse antenna are then outlined. Finally, the equivalence of these two cases is demonstrated.

The pattern of an antenna array can be related to its excitation by

$$AF = \sum_{n=-\frac{N-1}{2}}^{\frac{N-1}{2}} a_n e^{j\beta dn\sin(\theta)} \tag{3.1}$$

$$= \sum_{n=1}^{\frac{N-1}{2}} a_n e^{j\beta dn\sin(\theta)} + a_0 + \sum_{n=-\frac{N-1}{2}}^{-1} a_n e^{j\beta dn\sin(\theta)} \tag{3.2}$$

$$= a_0 + \sum_{n=1}^{\frac{N-1}{2}} \left[a_n e^{j\beta dn\sin(\theta)} + a_{-n} e^{-j\beta dn\sin(\theta)}\right] \tag{3.3}$$

$$= \sum_{n=0}^{\frac{N-1}{2}} \left[\alpha_n e^{j\beta dn\sin(\theta)} + \alpha_{-n} e^{-j\beta dn\sin(\theta)}\right] \tag{3.4}$$

where AF is the antenna pattern, a_n is the excitation of each antenna element (can be complex), $\alpha_n = a_n$ except $\alpha_0 = a_0/2$, N is the number of antenna elements, β is the free-space phase constant, d is the antenna element spacing, and θ is the angle measured from broadside [44, 45, 69]. Adjusting the excitation values a_n, the element spacing d, and the number of elements N allows any antenna pattern to be modelled by (3.1).

The form of AF provided in (3.4) will be used extensively below and is obtained from (3.1) by splitting the summation and substituting $n \rightarrow -n$ into the negative portion of the summation.

Note that (3.1) assumes an odd number of elements and is limited to a single plane only to simplify the results below. The results are equally applicable to more general arrays with odd or even numbers of elements in more than one plane.

3.2.1 General Case

The patterns and excitations of the sum- and difference-channel antenna beams are assumed to be symmetric and antisymmetric respectively. This is a reasonable assumption because any relaxation of this condition will mean that the radar's tracking performance will differ depending on which side of boresight the target is on. No assumptions are made about the relationship between the sum- and difference-channel antenna patterns.

The sum-channel antenna beam can thus be determined from (3.4) by noting that symmetry requires $\alpha_{-n} = \alpha_n$ giving

$$S_G = 2\sum_{n=0}^{\frac{N_S-1}{2}} b_n \cos\left[\beta d_1 n\sin\left(\theta\right)\right] \tag{3.5}$$

where S_G is the general sum-channel antenna pattern. The difference-channel antenna beam can be determined from (3.4) by noting that antisymmetry requires $\alpha_{-n} = -\alpha_n$ giving

$$D_G = 2j \sum_{n=0}^{\frac{N_D-1}{2}} c_n \sin\left[\beta d_2 n \sin\left(\theta\right)\right] \tag{3.6}$$

where D_G is the general difference-channel antenna pattern. The values of N, α_n and d in (3.4) have been replaced by N_S, b_n and d_1 in (3.5), and N_D, c_n and d_2 in (3.6) to ensure that the above formulation does not include any assumptions about the relationship between the sum- and difference-channel antenna patterns.

The monopulse error is now formed by dividing (3.6) by (3.5) and taking the imaginary part of the result to give

$$M_G = \Im\left\{\frac{D_G}{S_G}\right\} \tag{3.7}$$

$$= \frac{\sum_{n=0}^{\frac{N_D-1}{2}} c_n \sin\left[\beta d_2 n \sin\left(\theta\right)\right]}{\sum_{n=0}^{\frac{N_S-1}{2}} b_n \cos\left[\beta d_1 n \sin\left(\theta\right)\right]} \tag{3.8}$$

when an exact monopulse processor is used [15,30]. This error is then processed to form the monopulse indicated angle used for tracking.

As an aside, the sum- and difference-channel antenna patterns in (3.5) and (3.6) respectively, and the monopulse error in (3.8) become linear when d_1 and d_2 tend to zero. This shows that the linear-fit analysis implicitly assumes that the antenna aperture is infinitesimally small as mentioned in Section 2.4.2.

3.2.2 Phase-Comparison Case

A phase-comparison monopulse radar forms its antenna beams by using two antenna elements whose phase centres are separated along the axis of the radar. In the analysis below, a different spacing is used for the sum- and difference-channel antenna elements to make the result more general, but a practical phase-comparison monopulse antenna will have a single spacing for both the sum and difference channels.

As before, the sum- and difference-channel antenna patterns will be assumed to be symmetrical and antisymmetrical around boresight respectively. The implications of this assumption are that the two antenna elements for each channel are symmetrically positioned around the centre of the antenna and the two portions of the phased-array antenna are symmetrical.

The symmetry requirement on the antenna elements means that the two portions of the phase-comparison antenna have the same form as the general, symmetrical sum-channel pattern given in (3.5). The generalised phase-comparison sum-channel antenna

pattern is thus given by

$$S_P = \left[e^{j\beta\frac{d_s}{2}\sin(\theta)} + e^{-j\beta\frac{d_s}{2}\sin(\theta)}\right] 2\sum_{n=0}^{\frac{N_P-1}{2}} e_n \cos\left[\beta d_3 n \sin(\theta)\right]$$

$$= 4\cos\left[\beta\frac{d_s}{2}\sin(\theta)\right]\sum_{n=0}^{\frac{N_P-1}{2}} e_n \cos\left[\beta d_3 n \sin(\theta)\right] \tag{3.9}$$

where d_s is the spacing of the sum-channel antenna elements. The generalised phase-comparison difference-channel antenna pattern is given by

$$D_P = \left[e^{j\beta\frac{d_s}{2}\sin(\theta)} - e^{-j\beta\frac{d_s}{2}\sin(\theta)}\right] 2\sum_{n=0}^{\frac{N_P-1}{2}} e_n \cos\left[\beta d_3 n \sin(\theta)\right]$$

$$= 4j\sin\left[\beta\frac{d_d}{2}\sin(\theta)\right]\sum_{n=0}^{\frac{N_P-1}{2}} e_n \cos\left[\beta d_3 n \sin(\theta)\right] \tag{3.10}$$

where d_d is the spacing of the difference-channel antenna elements. The values of N_s, b_n and d_1 in (3.5) have been replaced by N_P, e_n and d_3 above to emphasise that these values are unique to the phase-comparison antenna elements.

The monopulse error is calculated by taking the imaginary part of (3.10) divided by (3.9) giving

$$M_P = \frac{\sin\left[\beta\frac{d_d}{2}\sin(\theta)\right]}{\cos\left[\beta\frac{d_s}{2}\sin(\theta)\right]} \tag{3.11}$$

where M_P is the monopulse error, and an exact monopulse processor was again assumed [15,30]. In a practical phase-comparison monopulse antenna the antenna-element spacings for the sum and difference channels are the same, so (3.11) reduces to

$$M_P = \tan\left[\beta\frac{d_p}{2}\sin(\theta)\right] \tag{3.12}$$

where $d_p = d_s = d_d$.

3.2.3 Equivalence

It can be seen that the sum-channel antenna patterns in (3.5) and (3.9) both have a sum-of-cosines form by noting that

$$2\cos(x)\cos(y) = \cos(x+y) + \cos(x-y). \tag{3.13}$$

The odd-order derivatives of the sum-channel antenna patterns on boresight are always zero for both the general and phase-comparison cases. The differences between the remaining non-zero derivatives can now be minimised through an appropriate choice of d_s, N_P, d_3 and e_n in (3.9) to give good agreement between the two cases near boresight.

Similarly noting that

$$2\sin(x)\cos(y) = \sin(x+y) + \sin(x-y) \tag{3.14}$$

leads to the conclusion that the difference-channel antenna patterns in (3.6) and (3.10) both have a sum-of-sines form. As before, an appropriate choice of the parameters in (3.10) means that the difference-channel patterns for the two cases can be made to agree very well near boresight.

The same antenna elements are used to form both the sum- and difference-channel antenna beams in the phase-comparison case, so the parameters N_P, d_3 and e_n are common to both the sum and difference channels. This means that the values of these parameters must be a compromise between the values required to match the sum- and difference-channel antenna patterns. While this restriction reduces the accuracy with which the phase-comparison case approximates the general case somewhat, it does not change the fact that there will be a range of angles near boresight where the agreement is good.

The equivalence between the monopulse error in the general and phase-comparison cases can be established by noting that the monopulse errors in (3.8) and (3.11) both have the following form

$$M_X = \frac{\sum_{m=0}^{M} \gamma_m \sin(\epsilon_m x)}{\sum_{n=0}^{N} \zeta_n \cos(\kappa_n x)} \tag{3.15}$$

where M_X is any monopulse error, γ_m, ϵ_m, ζ_n and κ_n are real arbitrary constants, and M and N are arbitrary integer constants.

Appendix C provides proof that all even-order derivatives of (3.15) are equal to zero when x is equal to zero. This means that all the even-order derivatives of the monopulse errors for the two cases given in (3.8) and (3.11) are zero on boresight ($\theta = 0$). The antenna element spacings in the phase-comparison case (d_s and d_d) can now be used to make the first two odd-order derivatives of the monopulse errors equal on boresight, meaning that the first four derivatives of the monopulse errors will be equal on boresight. Under these conditions, the agreement between the general and phase-comparison monopulse errors will be excellent near boresight (i.e. when θ is small).

The two spacings in the phase-comparison case could also be chosen in other ways to allow the equivalence between the two cases to be established according to other definitions. For example, the spacings could be adjusted to produce the least-squares error between the general and phase-comparison monopulse errors over a given range of angles near boresight.

It is possible to extend the range of agreement by modifying the phase-comparison monopulse error in (3.11) to give

$$M_P = K \frac{\sin\left[\beta \frac{d_d}{2} \sin(\theta)\right]}{\cos\left[\beta \frac{d_s}{2} \sin(\theta - \theta_0)\right]} \tag{3.16}$$

where a scaling factor K and a sum-channel angular offset θ_0 have been added.

The inclusion of the scaling factor K allows the first six derivatives of (3.8) and (3.16) to be made equal through the appropriate choice of d_s, d_d and K. While there is no physical basis for adding the scaling factor K, including an additional constant is reasonable in a mathematical model. The addition of a scaling factor to the monopulse

error means that a scaling factor also has to be added to the difference-channel return in (3.10).

The angular offset θ_0 has been included in the sum channel to account for any squint of the sum-channel peak relative to the difference-channel zero. This approach was used under the assumption that boresight ($\theta = 0$) is chosen as the angle where the difference-channel antenna pattern is zero.

The result in (3.12) can also be generalised by adding a scaling factor to give

$$M_P = K \tan\left[\beta \frac{d_p}{2} \sin(\theta)\right] \tag{3.17}$$

which is less general than (3.16) because it has fewer degrees of freedom. However, (3.17) is significantly simpler than (3.16), making it easier to use.

3.3 Results and Discussion

The use of a generalised phase-comparison antenna to model any type of monopulse antenna is demonstrated in this section by approximating the measured patterns of two monopulse antennas.

The AN/FPQ-6 radar is an C-Band monopulse tracking radar whose antenna consists of a five-horn Cassegrain feed and a 29-foot reflector dish [30, 31, 70]. The fact that a five-horn feed is used is ideal for demonstrating the principles described above because the feed structures for the sum and difference channels are different.

The QCS15.5-17N(D1587) is a monopulse antenna manufactured by Q-par Angus Ltd and operates from 15.5 to 17 GHz. The antenna has a four-horn Cassegrain feed and a 1.2-m reflector [71]. The four-horn feed is widely used to construct amplitude-comparison monopulse antennas making this a useful test case.

Measured and approximated the sum- and difference-channel patterns, and monopulse errors are shown in Figures 3.1 and 3.2 based on plots of the sum- and difference-channel antenna patterns of an AN/FPQ-6 radar [70] and a Q-par Angus Ltd QCS15.5-17N(D1587) antenna [71]. The indicated angle cannot be calculated because this would require a knowledge of how the radar processes its signals, and this information is not available.

The origins of the curves in Figures 3.1 and 3.2 are described below. In all cases, the monopulse error on boresight was determined from the measured values at $\pm 0.1°$ for the AN/FPQ-6 radar and at $\pm 0.15°$ for the Q-par Angus Ltd antenna. If additional parameters were available, the minimax error value in (3.18) was minimised over the range $0.1° \leq |\theta| \leq 0.5°$ for the AN/FPQ-6 radar and over the range $0.15° \leq |\theta| \leq 1°$ for the Q-par Angus Ltd antenna.

$$E = \max_{\theta} \left[\frac{M_{meas}(\theta)}{M_{calc}(\theta)} - 1\right] \tag{3.18}$$

where E is the error, and $M_{meas}(\theta)$ and $M_{calc}(\theta)$ are the measured and calculated monopulse errors respectively. Angles very close to boresight are not considered because the small difference-channel gain near boresight means that the values near boresight are inaccurate due to measurement and transcription errors.

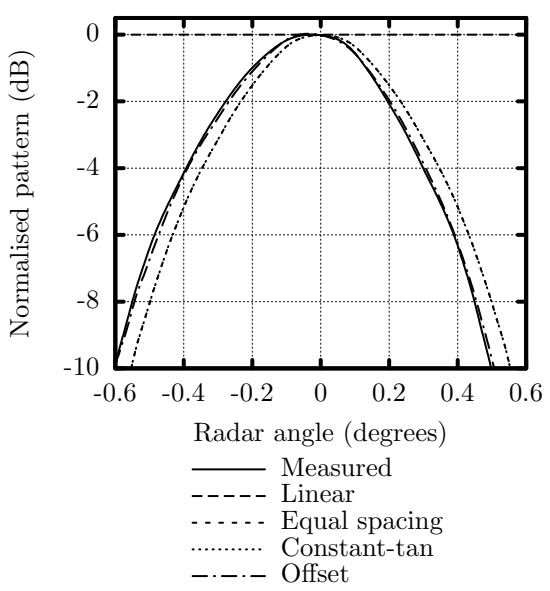

(a) Sum channel. Note that the measured and offset plots, and the equal spacing and constant-tan plots are very similar and thus difficult to distinguish.

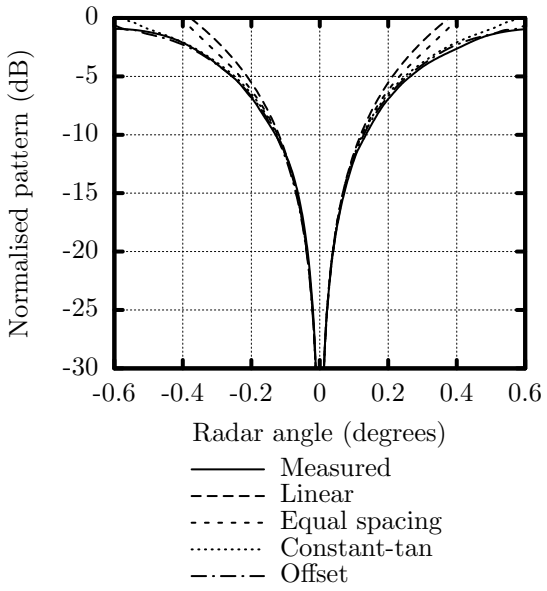

(b) Difference channel. Note that the measured, constant-tan and offset plots are very similar and thus difficult to distinguish.

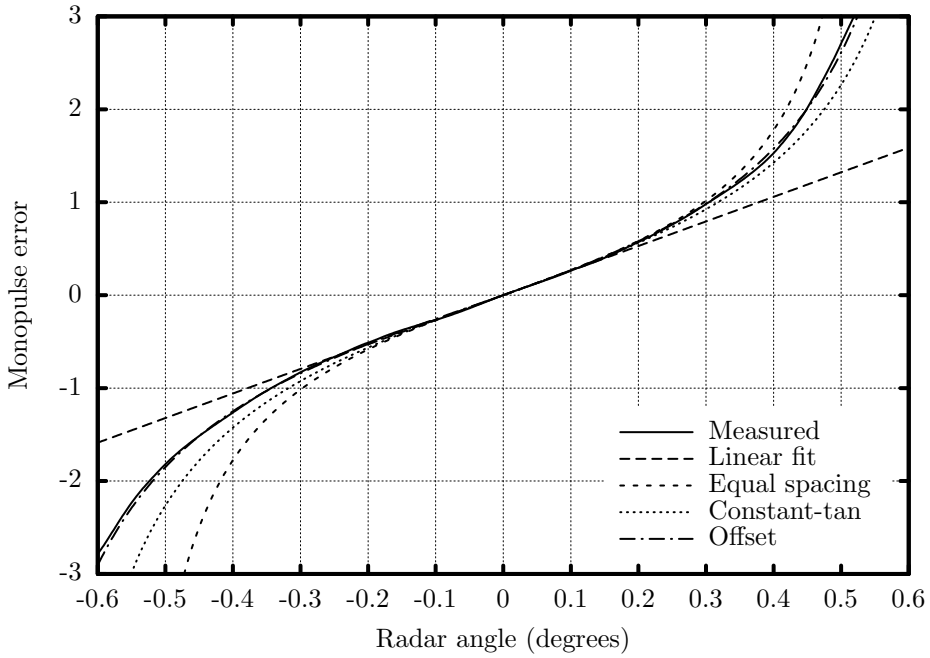

(c) Monopulse error. Note that the measured and offset plots are very similar and thus difficult to distinguish.

Figure 3.1: Measured and approximated sum- and difference-channel patterns and monopulse error for an AN/FPQ-6 radar [70]. (Reprinted, with permission, from [1]. ©2009 IEEE.)

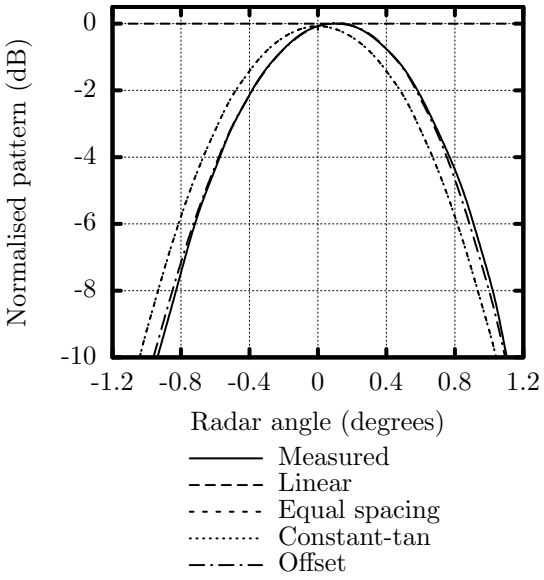

(a) Sum channel. Note that the measured and offset plots, and the equal spacing and constant-tan plots are very similar and thus difficult to distinguish.

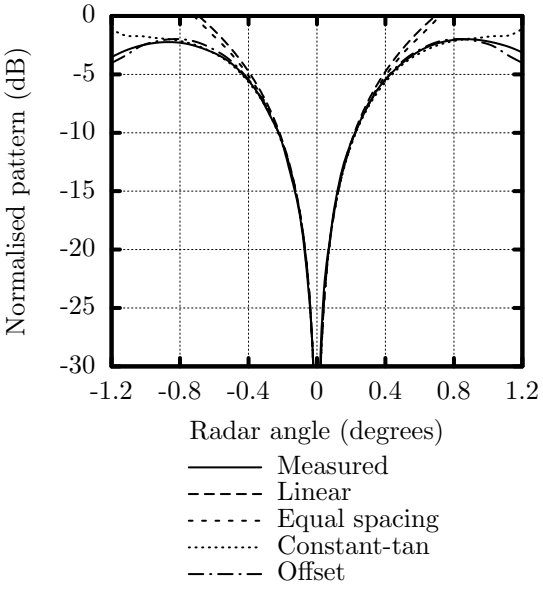

(b) Difference channel. Note that the measured, constant-tan and offset plots are very similar and thus difficult to distinguish.

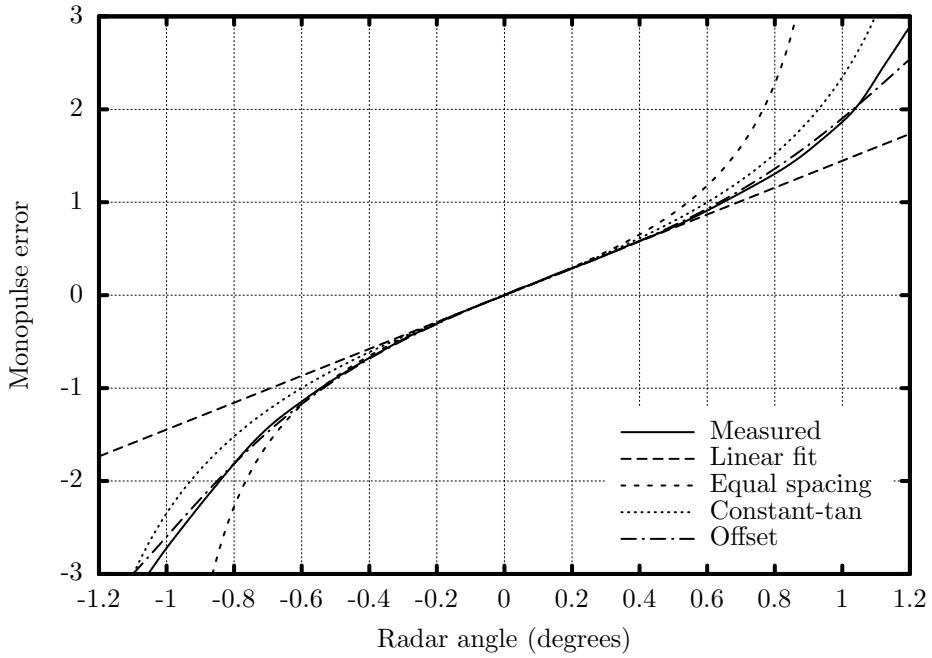

(c) Monopulse error. Note that the measured and offset plots are very similar and thus difficult to distinguish.

Figure 3.2: Measured and approximated sum- and difference-channel patterns and monopulse error for a monopulse antenna manufactured by Q-par Angus Ltd [71]. (Reprinted, with permission, from [1]. ©2009 IEEE.)

Measured: The measured sum- and difference-channel antenna patterns read from the graphs in [70, 71]. The monopulse error was calculated from the quotient of the magnitudes of the difference- and sum-channel antenna patterns.

Linear fit: A straight-line fit to the monopulse error that matches the monopulse error gradient on boresight.

Equal spacing: The phase-comparison monopulse approximation in (3.12) with d_p chosen to match the monopulse error gradient on boresight.

Constant-tan: The phase-comparison monopulse approximation with a scaling factor given in (3.17). The value of d_p was determined using a line search to minimise the error in (3.18). The monopulse error gradient on boresight was set equal to the measured value for each value of d_p by solving the gradient of (3.17) on boresight for K giving

$$K = \frac{2}{\beta d_p} \cdot \left. \frac{dM_P}{d\theta} \right|_{\theta=0}. \tag{3.19}$$

Offset: The general case shown in (3.16), but with equal antenna element spacings ($d_p = d_s = d_d$). The values of d_p and θ_0 were determined using the Nelder-Mead optimisation algorithm [72] to minimise the error in (3.18). The value of K was used to match the measured monopulse error boresight gradient for each combination of d_p and θ_0 by solving the gradient of (3.16) on boresight for K giving

$$K = \frac{2}{\beta d_p} \cos\left[\beta \frac{d_p}{2} \sin(\theta_0)\right] \left. \frac{dM_P}{d\theta} \right|_{\theta=0}. \tag{3.20}$$

The patterns of the symmetrical antenna elements comprising the phase-comparison systems were determined from the sum-channel antenna patterns because the difference-channel patterns are very small near boresight leading to large errors.

The agreement between the measured and approximated sum- and difference-channel patterns, and monopulse errors in Figures 3.1 and 3.2 is seen be good near boresight in all cases. The linear approximation rapidly diverges from the strongly nonlinear measured patterns as the 3 dB edges of the sum-channel antenna beam (approximately $-0.35°$ to $0.25°$ for the AN/FPQ-6 radar and $-0.5°$ to $0.7°$ for the Q-par Angus Ltd antenna) are approached. The equal-spacing phase-comparison approximation displays the same shape as the measurements, but still exhibits significant errors near the 3 dB edges of the sum-channel antenna beam. The addition of another degree of freedom by including a scaling factor improves agreement between the approximate and measured values to the point that the agreement is good even outside the sum-channel 3 dB beamwidth. While not shown in Figures 3.1 and 3.2, using different spacings for the sum- and difference-channel antenna elements gives results that are identical to this case. Almost perfect agreement over the entire range of angles considered is obtained when the angular offset of the sum-channel antenna pattern is accounted for. While not shown, using different spacings for the sum- and difference-channel antenna elements with a sum-channel angular offset gives results that are essentially identical to this case.

These results show that the use of different spacings for the sum- and difference-channel antenna elements does not add significantly to the accuracy of the results. The

use of a phase-comparison monopulse antenna with the same spacings for the sum- and difference-channel antenna elements with a scaling factor in the difference-channel return is thus sufficient to model any monopulse antenna.

The measured data used here are particularly challenging for most of the models considered because the sum-channel peak is offset from boresight as seen in Figures 3.1(a) and 3.2(a). Only the offset case considers this fact, and the other cases' inability to accommodate the resulting asymmetry limits the attainable accuracy. This can be seen in Figures 3.1(c) and 3.2(c) by noting that improving the accuracy of these approximations on one side of boresight will decrease the accuracy on the other side of boresight.

3.4 Concluding Remarks

A generalised phase-comparison monopulse antenna has been shown to be a good model for any monopulse antenna near boresight. The only restriction is that the monopulse antenna patterns must be symmetrical. This means that any analysis of monopulse radars only needs to consider the generalised phase-comparison case to be applicable to any monopulse radar.

The measured patterns of an AN/FPQ-6 monopulse radar and a monopulse antenna manufactured by Q-par Angus Ltd were used to demonstrate the accuracy that can be achieved using this approach. The agreement between the measured and approximated results improves as the complexity of the models is increased by adding additional degrees of freedom.

A phase-comparison monopulse system is used to analyse a cross-eye jamming scenario in Chapter 4. The equivalence proved above shows that the results of that analysis are applicable to any monopulse radar near boresight.

CHAPTER 4

MATHEMATICAL ANALYSIS

4.1 Introductory Remarks

This chapter outlines a comprehensive, rigorous mathematical analysis of an isolated, single-loop, retrodirective cross-eye jammer against a phase-comparison monopulse system. As shown in Chapter 3, a phase-comparison monopulse antenna is equivalent to any monopulse antenna near boresight. This analysis overcomes the limitations of the existing analyses of cross-eye jamming by minimising the number of assumptions required and by fully accounting for the retrodirective implementation of cross-eye jammers. The work described in this chapter forms the basis of a published journal paper [2].[1]

The analysis of single-loop, retrodirective cross-eye jamming is presented in Section 4.2, and the implications of this analysis are considered in Section 4.3 by evaluating a representative missile engagement. Section 4.4 provides concluding remarks.

4.2 Mathematical Analysis

A comprehensive, rigorous analysis of retrodirective cross-eye jamming of a phase-comparison monopulse radar is described in Section 4.2.1 and is shown to be equivalent to a number of results that are known to be accurate (including the phase-front analysis) in Section 4.2.2.

4.2.1 Extended Analysis of Cross-Eye Jamming

The geometry of an isolated single cross-eye jammer loop against a phase-comparison monopulse antenna is given in Figure 4.1. The phase centres of the radar and jammer antenna elements are denoted by circles and crosses respectively, and the position of the apparent target is shown by a square. The parameters used in Figure 4.1 are defined below:

d_p: The spacing of the phase centres of the phase-comparison monopulse antenna elements. Only the phase centres of the radar antenna elements are shown in Figure 4.1, and the radar antenna elements will generally be large enough to meet at the centre of the radar antenna. The same spacing is used for both the sum and difference channels because using different spacings leads to extremely complex results, and as shown in Section 3.3, the accuracy improvement when modelling other types of monopulse antenna is minimal.

[1] Portions of this chapter are reprinted, with permission, from [2].

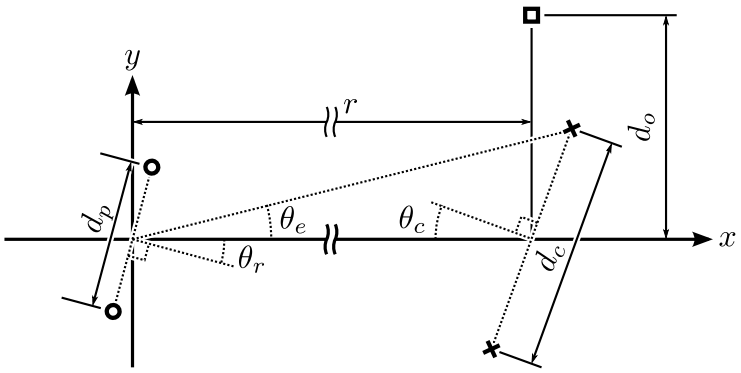

Figure 4.1: The geometry of a cross-eye jamming scenario with a phase-comparison monopulse radar and an isolated single-loop cross-eye jammer. The phase centres of the radar and jammer antenna elements are denoted by circles and crosses respectively, and the position of the apparent target is shown by a square.

d_c: The spacing of the phase centres of cross-eye jammer antenna elements. The jammer antenna elements can be large, but even large jammer antenna elements will have a substantial space between them.

d_o: The linear distance from the centre of the jammer to the position of the apparent target created by the cross-eye jammer. This error definition is motivated by the fact that the conventional analyses of cross-eye jamming suggest that a cross-eye jammer produces a fixed linear error as discussed in Section 2.4.1

r: The range from the centre of the radar antenna to the centre of the jammer.

θ_r: The angle to the centre of the cross-eye jammer measured from the radar's boresight.

θ_c: The rotation of the jammer system measured from the jammer's broadside direction to the centre of the radar. This rotation will generally be present in engagements because it is extremely unlikely that the radar being jammed will appear in the jammer's broadside direction.[2]

θ_e: Half the angular separation of the jammer antenna elements as seen by the radar. Exact and approximate values of θ_e and trigonometric functions of θ_e are considered in Appendix B.

From (3.9), the gain of the sum channel of the radar in the direction of the bottom jammer antenna element will be

$$S_b = \cos\left[\beta\frac{d_p}{2}\sin\left(\theta_r - \theta_e\right)\right] P_r\left(\theta_r - \theta_e\right) \tag{4.1}$$

[2]The radar being jammed can be placed exactly in the jammer's broadside direction if the jammer can be rotated. However, cross-eye jamming requires a large spacing between the jammer antenna elements (typically 10-20 m [19, 21]), and it is unlikely that such a large system will be mounted on a rotating pedestal. This means that the entire platform carrying the cross-eye jammer will have to be rotated to position the radar being jammed in the jammer's broadside direction. While rotating the platform can, and probably will be done, this will take time, so a sizable proportion of any engagement will take place with the radar being jammed off the jammer's broadside direction.

and the gain of the sum channel of the radar in the direction of the top jammer antenna element will be

$$S_t = \cos\left[\beta\frac{d_p}{2}\sin(\theta_r + \theta_e)\right] P_r(\theta_r + \theta_e) \tag{4.2}$$

where $P_r(\theta)$ is the pattern of the radar antenna elements. The constant factor 4 in (3.9) has been included in $P_r(\theta)$ in (4.1) and (4.2) to simplify the results. The gain of the difference channel of the radar in the direction of the bottom jammer antenna element can be found from (3.10) to be

$$D_b = j\sin\left[\beta\frac{d_p}{2}\sin(\theta_r - \theta_e)\right] P_r(\theta_r - \theta_e) \tag{4.3}$$

and the gain of the difference channel of the radar in the direction of the top jammer antenna element will be

$$D_t = j\sin\left[\beta\frac{d_p}{2}\sin(\theta_r + \theta_e)\right] P_r(\theta_r + \theta_e) \tag{4.4}$$

where the factor 4 in (3.10) has again been included in $P_r(\theta)$.

These equations can be simplified by noting that [73]

$$\sin(x \pm y) = \sin(x)\cos(y) \pm \cos(x)\sin(y) \tag{4.5}$$

to obtain

$$\beta\frac{d_p}{2}\sin(\theta_r \pm \theta_e) = \beta\frac{d_p}{2}\sin(\theta_r)\cos(\theta_e) \pm \beta\frac{d_p}{2}\cos(\theta_r)\sin(\theta_e) \tag{4.6}$$

$$= k \pm k_c \tag{4.7}$$

where the variables

$$k = \beta\frac{d_p}{2}\sin(\theta_r)\cos(\theta_e) \tag{4.8}$$

and

$$k_c = \beta\frac{d_p}{2}\cos(\theta_r)\sin(\theta_e) \tag{4.9}$$

have been introduced to simplify the notation. The approximations to the sine and cosine of θ_e described in Appendix B can be used to simplify the forms of (4.8) to (4.9) to

$$k \approx \beta\frac{d_p}{2}\sin(\theta_r) \tag{4.10}$$

$$k_c \approx \beta\frac{d_p}{2}\cos(\theta_r)\theta_e \tag{4.11}$$

under the reasonable assumption that θ_e is small, or equivalently, that $r \gg d_c$. Equation 6.34 on page 89 shows that k_c can be accurately approximated by

$$k_c \approx \beta\frac{d_r}{2}\theta_e \tag{4.12}$$

in the sum-channel main beam as long as the sum-channel antenna beam is narrow ($d_p \gg \lambda$).

The sum- and difference-channel gains in (4.1) to (4.4) can now be simplified to

$$S_b = \cos(k - k_c) P_r(\theta_r - \theta_e) \tag{4.13}$$

$$S_t = \cos(k + k_c) P_r(\theta_r + \theta_e) \tag{4.14}$$

$$D_b = j \sin(k - k_c) P_r(\theta_r - \theta_e) \tag{4.15}$$

and

$$D_t = j \sin(k + k_c) P_r(\theta_r + \theta_e). \tag{4.16}$$

As explained in Section 2.5.2, the fact that a retrodirective cross-eye jammer is considered means that the signals passing through the jammer in the two possible directions travel along exactly the same physical paths. The attenuation and phase shift due to range and any common elements are thus identical for the two paths through the jammer due to reciprocity [44, 45, 74]. The difference-channel return is normalised by the sum-channel return during monopulse processing, so the effects of any common factors are removed. The effects of range and common circuit elements are thus not explicitly shown below without loss of generality.

The derivation below assumes that the signal that passes through the cross-eye jammer from the top antenna element to the bottom antenna element has an amplitude gain of a and a phase shift of ϕ relative to the signal that passes from the bottom antenna element to the top antenna element.

The sum-channel signal received by the radar with thus be

$$\begin{aligned} S_J &= S_b P_c(\theta_c - \theta_e) S_t P_c(\theta_c + \theta_e) + a e^{j\phi} S_t P_c(\theta_c + \theta_e) S_b P_c(\theta_c - \theta_e) && (4.17)\\ &= \left(1 + a e^{j\phi}\right) S_b P_c(\theta_c - \theta_e) S_t P_c(\theta_c + \theta_e) && (4.18)\\ &= P_r(\theta_r - \theta_e) P_c(\theta_c - \theta_e) P_r(\theta_r + \theta_e) P_c(\theta_c + \theta_e) \times \\ &\quad \left(1 + a e^{j\phi}\right) \cos(k - k_c) \cos(k + k_c) && (4.19) \end{aligned}$$

where $P_c(\theta)$ is the pattern of the cross-eye jammer antenna elements.

Equation (4.19) can be simplified by using the following trigonometric identities [73]

$$\cos(x \pm y) = \cos(x)\cos(y) \mp \sin(x)\sin(y) \tag{4.20}$$

and

$$\begin{aligned} \cos(2x) &= 2\cos^2(x) - 1 && (4.21)\\ &= 1 - 2\sin^2(x) && (4.22) \end{aligned}$$

to simplify

$$\begin{aligned}\cos(k-k_c)\cos(k+k_c) &= [\cos(k)\cos(k_c)+\sin(k)\sin(k_c)]\times \\ &\quad [\cos(k)\cos(k_c)-\sin(k)\sin(k_c)] && (4.23)\\ &= \cos^2(k)\cos^2(k_c)-\sin^2(k)\sin^2(k_c) && (4.24)\\ &= \frac{1}{2}[1+\cos(2k)]\frac{1}{2}[1+\cos(2k_c)]- \\ &\quad \frac{1}{2}[1-\cos(2k)]\frac{1}{2}[1-\cos(2k_c)] && (4.25)\\ &= \frac{1}{4}[1+\cos(2k)+\cos(2k_c)+\cos(2k)\cos(2k_c)]- \\ &\quad \frac{1}{4}[1-\cos(2k)-\cos(2k_c)+\cos(2k)\cos(2k_c)] && (4.26)\\ &= \frac{1}{2}[\cos(2k)+\cos(2k_c)] && (4.27)\end{aligned}$$

which can now be substituted into (4.19) to give

$$\begin{aligned}S_J = P_r(\theta_r-\theta_e)P_c(\theta_c-\theta_e)P_r(\theta_r+\theta_e)P_c(\theta_c+\theta_e)\times \\ \frac{1}{2}\left(1+ae^{j\phi}\right)[\cos(2k)+\cos(2k_c)]. \qquad (4.28)\end{aligned}$$

The difference-channel signal received by the radar will be

$$\begin{aligned}D_J &= S_bP_c(\theta_c-\theta_e)D_tP_c(\theta_c+\theta_e)+ae^{j\phi}S_tP_c(\theta_c+\theta_e)D_bP_c(\theta_c-\theta_e) && (4.29)\\ &= P_r(\theta_r-\theta_e)P_c(\theta_c-\theta_e)P_r(\theta_r+\theta_e)P_c(\theta_c+\theta_e)\times \\ &\quad j\left[\cos(k-k_c)\sin(k+k_c)+ae^{j\phi}\cos(k+k_c)\sin(k-k_c)\right]. && (4.30)\end{aligned}$$

This can be simplified by using (4.5), (4.20), [73]

$$\sin^2(x)+\cos^2(x)=1 \qquad (4.31)$$

and

$$\sin(2x)=2\sin(x)\cos(x) \qquad (4.32)$$

to simplify

$$\begin{aligned}\cos(k\mp k_c)\sin(k\pm k_c) &= [\cos(k)\cos(k_c)\pm\sin(k)\sin(k_c)]\times \\ &\quad [\sin(k)\cos(k_c)\pm\cos(k)\sin(k_c)] && (4.33)\\ &= \sin(k)\cos(k)\cos^2(k_c)\pm\cos^2(k)\sin(k_c)\cos(k_c)\pm \\ &\quad \sin^2(k)\sin(k_c)\cos(k_c)+\sin(k)\cos(k)\sin^2(k_c) && (4.34)\\ &= \sin(k)\cos(k)\left[\sin^2(k_c)+\cos^2(k_c)\right]\pm \\ &\quad \sin(k_c)\cos(k_c)\left[\sin^2(k)+\cos^2(k)\right] && (4.35)\\ &= \sin(k)\cos(k)\pm\sin(k_c)\cos(k_c) && (4.36)\\ &= \frac{1}{2}[\sin(2k)\pm\sin(2k)] && (4.37)\end{aligned}$$

which can be substituted into (4.30) give

$$D_J = P_r(\theta_r - \theta_e) P_c(\theta_c - \theta_e) P_r(\theta_r + \theta_e) P_c(\theta_c + \theta_e) \times j\frac{1}{2}\left\{[\sin(2k) + \sin(2k_c)] + ae^{j\phi}[\sin(2k) - \sin(2k_c)]\right\} \quad (4.38)$$

$$= P_r(\theta_r - \theta_e) P_c(\theta_c - \theta_e) P_r(\theta_r + \theta_e) P_c(\theta_c + \theta_e) \times j\frac{1}{2}\left[\left(1 + ae^{j\phi}\right)\sin(2k) + \left(1 - ae^{j\phi}\right)\sin(2k_c)\right]. \quad (4.39)$$

An exact monopulse processor forms its error signal by normalising the difference-channel return in (4.39) by the sum-channel return in (4.28), and taking the imaginary part of the result [15, 30] giving

$$M_J = \Im\left\{\frac{D_J}{S_J}\right\} \quad (4.40)$$

$$= \Im\left\{\frac{j\left[\left(1 + ae^{j\phi}\right)\sin(2k) + \left(1 - ae^{j\phi}\right)\sin(2k_c)\right]}{\left(1 + ae^{j\phi}\right)[\cos(2k) + \cos(2k_c)]}\right\} \quad (4.41)$$

$$= \frac{1}{\cos(2k) + \cos(2k_c)}\left[\sin(2k) + \sin(2k_c)\,\Re\left\{\frac{1 - ae^{j\phi}}{1 + ae^{j\phi}}\right\}\right] \quad (4.42)$$

where M_J is the monopulse error. The antenna patterns in the first lines of (4.28) and (4.39) are common to both the sum- and difference-channel returns and have thus been cancelled. The real part of the complex factor in (4.42) can be simplified as follows

$$\Re\left\{\frac{1 - ae^{j\phi}}{1 + ae^{j\phi}}\right\} = \Re\left\{\frac{1 - ae^{j\phi}}{1 + ae^{j\phi}} \times \frac{1 + ae^{-j\phi}}{1 + ae^{-j\phi}}\right\} \quad (4.43)$$

$$= \Re\left\{\frac{1 - ae^{j\phi} + ae^{j\phi} - a^2}{1 + ae^{j\phi} + ae^{-j\phi} + a^2}\right\} \quad (4.44)$$

$$= \frac{\Re\{1 - a^2 - j2a\sin(\phi)\}}{1 + a^2 + 2a\cos(\phi)} \quad (4.45)$$

$$= \frac{1 - a^2}{1 + a^2 + 2a\cos(\phi)} \quad (4.46)$$

where the relationships [73]

$$\cos(x) = \frac{e^{jx} + e^{-jx}}{2} \quad (4.47)$$

and

$$\sin(x) = \frac{e^{jx} - e^{-jx}}{2j} \quad (4.48)$$

were used. The result in (4.46) can now be substituted into (4.42) to give

$$M_J = \frac{1}{\cos(2k) + \cos(2k_c)}\left[\sin(2k) + \sin(2k_c)\frac{1 - a^2}{1 + a^2 + 2a\cos(\phi)}\right]. \quad (4.49)$$

Using the definition of the cross-eye gain [9]

$$G_C = \frac{1 - a^2}{1 + a^2 + 2a\cos(\phi)} \quad (4.50)$$

reduces (4.49) to

$$M_J = \frac{\sin(2k) + \sin(2k_c)\, G_C}{\cos(2k) + \cos(2k_c)}. \tag{4.51}$$

As noted in Section 3.2.3, it is possible to add a constant scaling factor to (4.51) as was done in (3.17) on page 32. This adds another degree of freedom, improving the accuracy of this result when it is used as a model of other types of monopulse radar.

The process of normalising the difference-channel return by the sum-channel return in (4.40) means that the amplitude and phase of the difference-channel return are normalised to the amplitude and phase of the sum-channel return. Taking the imaginary part of this result means that only that portion of the difference-channel return that is in phase quadrature with the sum-channel return is used to compute the monopulse error. This portion of the difference-channel return can be obtained from the monopulse error by multiplying the monopulse error in (4.49) by the sum-channel return in (4.28) giving

$$\begin{aligned} D_{JM} &= jM_J S_J && (4.52)\\ &= j\frac{\sin(2k) + \sin(2k_c)\, G_C}{\cos(2k) + \cos(2k_c)} \times \\ &\quad P_r(\theta_r - \theta_e)\, P_c(\theta_c - \theta_e)\, P_r(\theta_r + \theta_e)\, P_c(\theta_c + \theta_e) \times \\ &\quad \frac{1}{2}\left(1 + ae^{j\phi}\right)\left[\cos(2k) + \cos(2k_c)\right] && (4.53)\\ &= P_r(\theta_r - \theta_e)\, P_c(\theta_c - \theta_e)\, P_r(\theta_r + \theta_e)\, P_c(\theta_c + \theta_e) \times \\ &\quad j\frac{1}{2}\left(1 + ae^{j\phi}\right)\left[\sin(2k) + \sin(2k_c)\, G_C\right] && (4.54) \end{aligned}$$

where the complex factor j has also been included to account for the fact that the imaginary part of the quotient is used.

4.2.2 Equivalence to Other Results

The results derived in Section 4.2.1 are validated below by comparing them to other results that are known to be accurate. Single targets are considered first, followed by an analysis of a retrodirective beacon, and finally a comparison to the phase-front analysis of glint and cross-eye jamming is given.

Point Targets

The analysis in Section 4.2.1 should reduce to the results presented in Section 3.2.2 for a single target under suitable conditions. The simplest way to adapt the results in Section 4.2.1 to the single-target case is to make the spacing between the jammer antenna elements zero (implying $d_c \to 0$, so $\theta_e \to 0$ and $k_c \to 0$).

The sum-channel return in (4.28) becomes

$$\begin{aligned} S_1 &= \left[P_r(\theta_r)\, P_c(\theta_c)\right]^2 \frac{1}{2}\left(1 + ae^{j\phi}\right)\left[\cos(2k) + 1\right] && (4.55)\\ &= \frac{1}{2}\left[P_r(\theta_r)\cos(k)\right]^2 \left[P_c(\theta_c)\right]^2 \left(1 + ae^{j\phi}\right) && (4.56) \end{aligned}$$

where (4.21) was used. The first term in square brackets in (4.56) is equal to the phase-comparison sum-channel antenna pattern given in (3.9) on page 30 squared because the sum-channel antenna beam is used for both transmission and reception in this case. The remainder of (4.56) is related to the RCS of the target.

The difference-channel return in (4.39) becomes

$$D_1 = \left[P_r\left(\theta_r\right) P_c\left(\theta_c\right)\right]^2 j\frac{1}{2}\left(1 + ae^{j\phi}\right)\sin\left(2k\right) \tag{4.57}$$

$$= \frac{1}{2}\left[P_r\left(\theta_r\right)\cos\left(k\right)\right]\left[jP_r\left(\theta_r\right)\sin\left(k\right)\right]\left[P_c\left(\theta_c\right)\right]^2\left(1 + ae^{j\phi}\right) \tag{4.58}$$

where (4.32) was used. The first term in square brackets in (4.58) is equal to the phase-comparison sum-channel antenna pattern given in (3.9) on page 30 because the sum-channel antenna beam is used for transmission. The second term in square brackets in (4.58) is equal to the phase-comparison difference-channel antenna pattern given in (3.10) on page 30 because the difference-channel antenna beam is used for reception. The remainder of (4.58) is again related to the RCS of the target, and is seen to be identical to the portion of 4.56 that determines the RCS of the target.

The monopulse error is now determined from the imaginary part of the quotient of (4.58) and (4.56) which is given by

$$M_1 = \Im\left\{\frac{D_1}{S_1}\right\} \tag{4.59}$$

$$= \Im\left\{\frac{\left[2P_r\left(\theta_r\right)\cos\left(k\right)\right]\left[2jP_r\left(\theta_r\right)\sin\left(k\right)\right]\left[P_c\left(\theta_c\right)\right]^2\left(1 + ae^{j\phi}\right)}{\left[2P_r\left(\theta_r\right)\cos\left(k\right)\right]^2\left[P_c\left(\theta_c\right)\right]^2\left(1 + ae^{j\phi}\right)}\right\} \tag{4.60}$$

$$= \tan\left(k\right) \tag{4.61}$$

which is seen to be equal to (3.12) on page 30 which was derived for a point target. The results in Section 4.2.1 thus agree with the results for a phase-comparison monopulse antenna when a single target is considered.

Another possibility for generating a single target is to let a tend to either zero or infinity to eliminate one of the paths through the jammer. The main problem with this approach is that the sum- and difference-channel returns become infinite when a approaches infinity. Additionally, the relative phase shift of the two directions through the jammer has no meaning here because allowing a to tend to either zero or infinity means that signals only propagate through the jammer in one direction. Both these problems are removed by normalising the sum- and difference-channel returns to $\left(1 + ae^{j\phi}\right)$.

The normalised sum- and difference-channel returns from (4.28) and (4.39) are given

by

$$\frac{S_2}{1+ae^{j\phi}} = P_r(\theta_r-\theta_e)\,P_c(\theta_c-\theta_e)\,P_r(\theta_r+\theta_e)\,P_c(\theta_c+\theta_e)\times \frac{1}{2}\left[\cos(2k)+\cos(2k_c)\right] \tag{4.62}$$

$$= P_r(\theta_r-\theta_e)\,P_c(\theta_c-\theta_e)\,P_r(\theta_r+\theta_e)\,P_c(\theta_c+\theta_e)\times \frac{1}{2}\left\{\cos\left[\beta d_p\sin(\theta_r)\cos(\theta_e)\right]+\cos\left[\beta d_p\cos(\theta_r)\sin(\theta_e)\right]\right\} \tag{4.63}$$

$$= P_r(\theta_r-\theta_e)\,P_c(\theta_c-\theta_e)\,P_r(\theta_r+\theta_e)\,P_c(\theta_c+\theta_e)\times \frac{1}{2}\left\{\cos\left[\beta\frac{d_p}{2}\sin(\theta_r+\theta_e)+\beta\frac{d_p}{2}\sin(\theta_r-\theta_e)\right]+ \cos\left[\beta\frac{d_p}{2}\sin(\theta_r+\theta_e)-\beta\frac{d_p}{2}\sin(\theta_r-\theta_e)\right]\right\} \tag{4.64}$$

$$= P_r(\theta_r-\theta_e)\,P_c(\theta_c-\theta_e)\,P_r(\theta_r+\theta_e)\,P_c(\theta_c+\theta_e)\times \cos\left[\beta\frac{d_p}{2}\sin(\theta_r+\theta_e)\right]\cos\left[\beta\frac{d_p}{2}\sin(\theta_r-\theta_e)\right] \tag{4.65}$$

and

$$\frac{D_2}{1+ae^{j\phi}} = P_r(\theta_r-\theta_e)\,P_c(\theta_c-\theta_e)\,P_r(\theta_r+\theta_e)\,P_c(\theta_c+\theta_e)\times j\frac{1}{2}\left[\sin(2k)\pm\sin(2k_c)\right] \tag{4.66}$$

$$= P_r(\theta_r-\theta_e)\,P_c(\theta_c-\theta_e)\,P_r(\theta_r+\theta_e)\,P_c(\theta_c+\theta_e)\times j\frac{1}{2}\left\{\sin\left[\beta d_p\sin(\theta_r)\cos(\theta_e)\right]\pm\sin\left[\beta d_p\cos(\theta_r)\sin(\theta_e)\right]\right\} \tag{4.67}$$

$$= P_r(\theta_r-\theta_e)\,P_c(\theta_c-\theta_e)\,P_r(\theta_r+\theta_e)\,P_c(\theta_c+\theta_e)\times j\frac{1}{2}\left\{\sin\left[\beta\frac{d_p}{2}\sin(\theta_r+\theta_e)+\beta\frac{d_p}{2}\sin(\theta_r-\theta_e)\right]\pm \sin\left[\beta\frac{d_p}{2}\sin(\theta_r+\theta_e)-\beta\frac{d_p}{2}\sin(\theta_r-\theta_e)\right]\right\} \tag{4.68}$$

$$= P_r(\theta_r-\theta_e)\,P_c(\theta_c-\theta_e)\,P_r(\theta_r+\theta_e)\,P_c(\theta_c+\theta_e)\times j\begin{cases}\sin\left[\beta\frac{d_p}{2}\sin(\theta_r+\theta_e)\right]\cos\left[\beta\frac{d_p}{2}\sin(\theta_r-\theta_e)\right] & \text{for } a\to 0\\ \cos\left[\beta\frac{d_p}{2}\sin(\theta_r+\theta_e)\right]\sin\left[\beta\frac{d_p}{2}\sin(\theta_r-\theta_e)\right] & \text{for } a\to\infty\end{cases} \tag{4.69}$$

where the trigonometric identities (4.5), (4.20) and [73]

$$2\sin(x)\cos(y)=\sin(x+y)+\sin(x-y) \tag{4.70}$$

were used. The positive and negative signs in the difference-channel returns are the cases where a tends to zero and infinity respectively.

The results in (4.65) and (4.69) are not the same as (3.9) on page 30 and (3.10) on page 30 because the results above are valid for a retrodirective implementation of the

system while the results in Section 3.2.2 only consider a point target. This means that the above results include signals to both the target antenna element that receives the signal from the radar and the target antenna element that transmits the signal back to the radar. The results in Section 3.2.2 only give the results in the direction of the single target.

The monopulse error is now determined from the imaginary part of the quotient of (4.69) and (4.65) which is given by

$$M_2 = \Im\left\{\frac{D_2}{S_2}\right\} \tag{4.71}$$

$$= \tan\left[\beta\frac{d_p}{2}\sin\left(\theta_r \pm \theta_e\right)\right] \tag{4.72}$$

which agrees perfectly with (3.12) on page 30 for a target in the relevant direction.

While it might appear surprising that the monopulse errors above and in Section 3.2.2 agree despite the fact that their sum- and difference-channel returns differ, this result is actually expected. In the above case, the sum-channel gain in the direction of the jammer antenna element used for reception from the radar is common to both the sum- and difference-channel returns, so it cancels. The same process happens in Section 3.2.2, except that the sum-channel gain for the transmitted signal is in the same direction as the received signal and is thus not explicitly shown. Only the sum- and difference-channel gains in the direction of the target antenna element that transmits the signal back to the radar remain in both cases, leading to the same result.

Retrodirective Beacon

The analysis presented in Section 4.2.1 is performed with the objective of analysing cross-eye jamming, but the result is general enough to be applied to other scenarios. A retrodirective beacon (Van Atta array) consisting of two antenna elements with signals that can propagate in both directions is one of the cases that is also covered by the analysis in Section 4.2.1. A retrodirective beacon appears as a point target between the its two antenna elements in its far-field region.

For a retrodirective beacon, $a = 1$ and $\phi = 0$, so the sum- and difference-channel returns from (4.28) and (4.39) are given by

$$\begin{aligned} S_B &= P_r\left(\theta_r - \theta_e\right) P_c\left(\theta_c - \theta_e\right) P_r\left(\theta_r + \theta_e\right) P_c\left(\theta_c + \theta_e\right) \times \\ &\quad \left[\cos\left(2k\right) + \cos\left(2k_c\right)\right] \qquad (4.73) \\ &= P_r\left(\theta_r - \theta_e\right) P_c\left(\theta_c - \theta_e\right) P_r\left(\theta_r + \theta_e\right) P_c\left(\theta_c + \theta_e\right) \times \\ &\quad \left[2\cos^2\left(k\right) - 1 + \cos\left(2k_c\right)\right] \qquad (4.74) \end{aligned}$$

and

$$\begin{aligned} D_B &= P_r\left(\theta_r - \theta_e\right) P_c\left(\theta_c - \theta_e\right) P_r\left(\theta_r + \theta_e\right) P_c\left(\theta_c + \theta_e\right) \times \\ &\quad j\sin\left(2k\right) \qquad (4.75) \\ &= P_r\left(\theta_r - \theta_e\right) P_c\left(\theta_c - \theta_e\right) P_r\left(\theta_r + \theta_e\right) P_c\left(\theta_c + \theta_e\right) \times \\ &\quad 2j\sin\left(k\right)\cos\left(k\right) \qquad (4.76) \end{aligned}$$

where (4.21) and (4.32) were used. These results assume that the radar antenna is not in the far-field region of the beacon system, but a retrodirective beacon will generally be used in its far-field region. The far-field assumption means that the range is increased to the point that θ_e becomes essentially equal to zero making k_c zero, and giving a sum-channel return of

$$S_B = 2\left[P_r\left(\theta_r\right)\cos\left(k\right)\right]^2\left[P_c\left(\theta_c\right)\right]^2 \tag{4.77}$$

and a difference-channel return of

$$D_B = 2\left[P_r\left(\theta_r\right)\cos\left(k\right)\right]\left[jP_r\left(\theta_r\right)\sin\left(k\right)\right]\left[P_c\left(\theta_c\right)\right]^2 \tag{4.78}$$

clearly showing the antenna beams used for transmission and reception. The factor 2 in (4.77) and (4.78) is due to the fact that there are two directions through the beacon whose returns combine.

Based on (4.73) and (4.75), the monopulse error is given by

$$M_B = \Im\left\{\frac{D_B}{S_B}\right\} \tag{4.79}$$

$$= \frac{\sin\left(2k\right)}{\cos\left(2k\right)+\cos\left(2k_c\right)} \tag{4.80}$$

which simplifies to

$$M_B = \frac{2\sin\left(k\right)\cos\left(k\right)}{2\cos^2\left(k\right)} \tag{4.81}$$

$$= \tan\left(k\right) \tag{4.82}$$

when (4.77) and (4.78) are used. Given that θ_e is essentially zero, the $\cos\left(\theta_e\right)$ term in k becomes 1, and (4.82) reduces to

$$M_B = \tan\left[\beta\frac{d_p}{2}\sin\left(\theta_r\right)\right] \tag{4.83}$$

which is identical to the result for a point target given by (3.12) on page 30. As expected, the result in (4.83) shows that a retrodirective beacon behaves like a point target in its far-field region.

Phase-Front Analysis

The analyses of glint have been shown to be accurate through extensive measurements over many years [31].[3] The results derived in Section 4.2.1 should thus give the same results as the analyses of glint described in Section 2.4.1 under the conditions for which those analyses are valid.

[3]This thesis is based on overcoming the limitations of glint analyses when applied to the special case of retrodirective cross-eye jamming, so the inaccuracies of conventional glint analyses applied to this special case are highlighted throughout. However, this should not be interpreted as implying that glint analyses are inaccurate when applied to glint. Retrodirective cross-eye jamming is a special case that is not representative of glint in general, and approximations inherent in glint analyses that are inaccurate when applied to retrodirective cross-eye jamming are accurate when applied to glint.

As shown in Section 2.4.1, the monopulse indicated angle predicted by the conventional glint analyses is given by (2.8) and (2.9) on page 13, which are repeated below for convenience.

$$\Re\{\theta_i\} = \theta_r + \theta_e \frac{1-a^2}{1+a^2+2a\cos(\phi)} \tag{4.84}$$

$$= \theta_r + \theta_e G_C \tag{4.85}$$

The monopulse error in (4.51) can be converted to a monopulse indicated angle using (3.11) on page 30 to give

$$\tan\left[\beta\frac{d_p}{2}\sin(\theta_i)\right] = \frac{\sin(2k)+\sin(2k_c)\,G_C}{\cos(2k)+\cos(2k_c)} \tag{4.86}$$

where θ_r in (3.11) has been replaced by θ_i.

The main difference between (4.85) and (4.86) is the trigonometric functions in (4.86). If it can be assumed that the arguments of all the trigonometric functions in (4.86) are small, the following simplifications to (4.86) result

$$\beta\frac{d_p}{2}\sin(\theta_i) \approx \frac{2k+2k_cG_C}{1+1} \tag{4.87}$$

$$\beta\frac{d_p}{2}\sin(\theta_i) \approx k + k_cG_C \tag{4.88}$$

$$\beta\frac{d_p}{2}\sin(\theta_i) \approx \beta\frac{d_p}{2}\sin(\theta_r)\cos(\theta_e) + \beta\frac{d_p}{2}\cos(\theta_r)\sin(\theta_e)\,G_C \tag{4.89}$$

$$\sin(\theta_i) \approx \sin(\theta_r)\cos(\theta_e) + \cos(\theta_r)\sin(\theta_e)\,G_C \tag{4.90}$$

$$\sin(\theta_i) \approx \sin(\theta_r) + \theta_eG_C \tag{4.91}$$

$$\theta_i \approx \theta_r + \theta_eG_C \tag{4.92}$$

where approximations in Appendix B have been used, and θ_i and θ_r have been assumed to be small.

Equation (4.85) is thus approximately equal to (4.86) when the arguments of all the trigonometric functions in (4.86) are small. This implies the following assumptions:

- The right-hand-side of (4.86) is small because otherwise the argument of the tangent on the left-hand side of (4.86) will be large, echoing Ostrovityanov's result [48] presented in Section 2.4.2. This means that the product of the cross-eye gain and jammer antenna element spacing must be small, providing the motivation for Vakin and Shustov's bound [12,16] considered in Section 2.4.2. However, a cross-eye jammer seeks to create the largest possible error, and this requires high cross-eye gain and large jammer antenna element spacing.
- The range is much greater than the jammer antenna element spacing ($r \gg d_c$). This assumption is shown to be very accurate in relative terms in Appendix B.[4]
- The target is not far from the radar's boresight (θ_r is small). This assumption limits the agreement to angles near the radar's boresight. Again, this requirement is counter to the objective of cross-eye jamming, which is to cause the largest possible error to move the jammer as far from the radar's boresight as possible.

[4]Appendix B also shows that this assumption is not necessarily accurate in absolute terms, so it does not imply that the radar being jammed is in the cross-eye jammer's far-field region – a condition which would violate the one of the requirements for successful cross-eye jamming [19, 21].

- The indicated angle is small (θ_i is small). This assumption means that agreement will be poor in the cross-eye jamming case where large indicated angles are sought.

The agreement between the extended and phase-front analyses will thus be good near boresight for closely-spaced jammer antenna elements and/or small cross-eye gains. This is in agreement with Vakin and Shustov's requirements that $a \geq 0.9$ or $a \leq 1.1$, and $2\theta_e \leq 10\%$ of the radar's 3-dB beamwidth [12]. However, only the second assumption above is valid in a cross-eye jamming scenario, again confirming the limitations of glint analyses when applied to cross-eye jamming.

Another way of ensuring that the arguments of all the trigonometric functions in (4.86) are small enough to make it approximately equal to (4.85) is to make the radar antenna infinitesimally small by letting d_p tend to zero. This provides further confirmation that the linear-fit analysis implicitly assumes an infinitesimally small antenna as stated in Section 2.4.2.

4.3 Results and Discussion

In this section, the extended analysis of cross-eye jamming derived in Section 4.2 is examined and compared to the linear-fit analysis for a typical cross-eye jamming scenario. A number of cases that highlight differences between the results are considered, and the implications of the results derived in Section 4.2 are highlighted. A far wider range of parameters is considered in Chapter 5, where both the extended and linear-fit analyses are compared to laboratory measurements.

The following parameters typical of a missile threat against an aircraft or ship will be used in this section:

- 10° radar antenna beamwidth ($d_r = 2.54$ wavelengths, and each radar antenna element is a uniformly-excited aperture 2.54 wavelengths long),
- the jammer antenna elements are uniformly-excited apertures 2.54 wavelengths long,
- 1 km jammer range ($r = 1$ km),
- 10 m jammer antenna element separation ($d_c = 10$ m),
- 30° jammer rotation ($\theta_c = 30°$), and
- 0.5 dB jammer amplitude mismatch ($a = 0.9441$).

The total angular separation of the cross-eye jammer antenna elements as seen by the radar for the parameters above is 0.4962° ($\theta_e = 0.2481°$), which is 5.0% of the radar antenna's 3-dB beamwidth. The value of the jammer phase match (ϕ) and the resulting cross-eye gain (G_C) will be specified on the figures below.

Results for a number of phase-match (and consequently cross-eye gain) cases are shown in Figures 4.2 to 4.4 when the radar antenna is rotated. The case with the best phase match (highest cross-eye gain) in Figure 4.4 is also considered at a range of 10 km in Figure 4.5 to show the effect of varying the jammer antenna element spacing. Results for the case where the jammer system is rotated are in given Figure 4.6 again for the case in Figure 4.4 to show the effect of rotating the jammer system.

Results are given for both the extended analysis outlined in Section 4.2.1 and Sherman's linear-fit analysis [30, 40] described in Section 2.4.1. The linear-fit analysis is used here because the other analyses do not explicitly consider the sum- and difference-

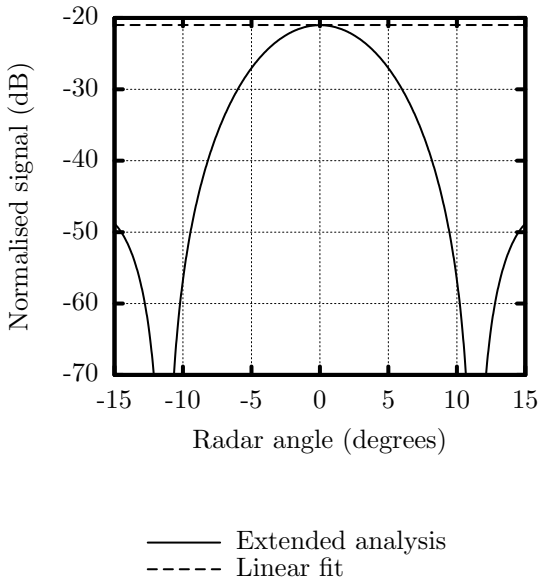

(a) Sum-channel return.

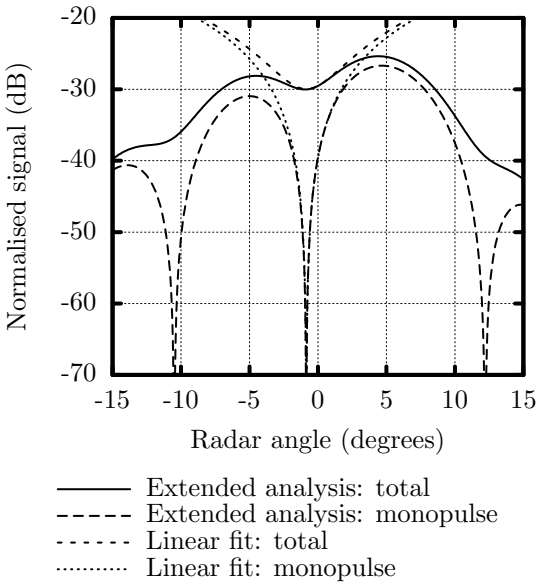

(b) The total difference-channel return and the portion of the difference-channel return used to form the monopulse indicated angle.

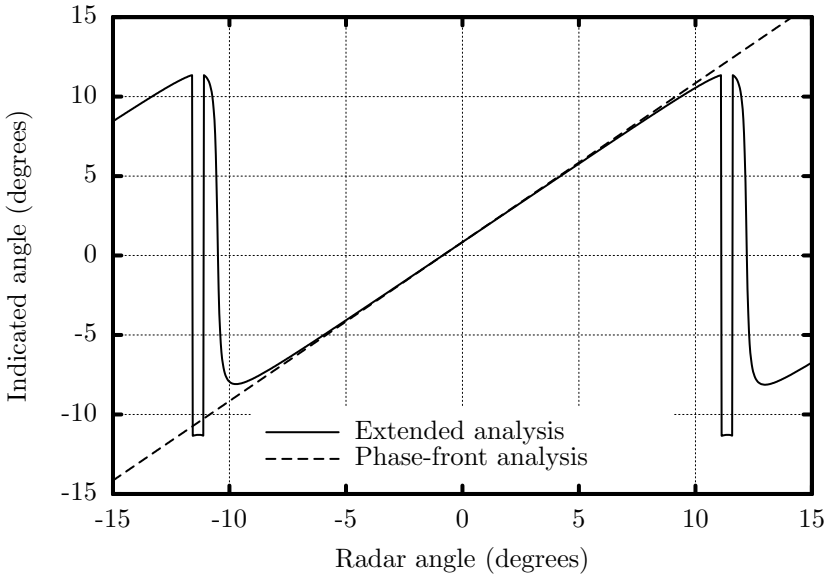

(c) Indicated angle.

Figure 4.2: Monopulse signals when the radar antenna was rotated for a relative amplitude and phase shift of 0.5 dB and 170° respectively giving a cross-eye gain of 3.42, and a jammer antenna element spacing of 5.0% of the radar antenna beamwidth.

channel returns, apart from stating that the sum-channel return will be maximised when the antenna aligns itself with the phase fronts or the Poynting-vector direction. Furthermore, the equivalence of the various glint analyses is shown in Section 2.4.1 [12,13,46,47], so the results are applicable to all glint analyses.

The (a) and (b) portions of each figure show the sum- and difference-channel returns

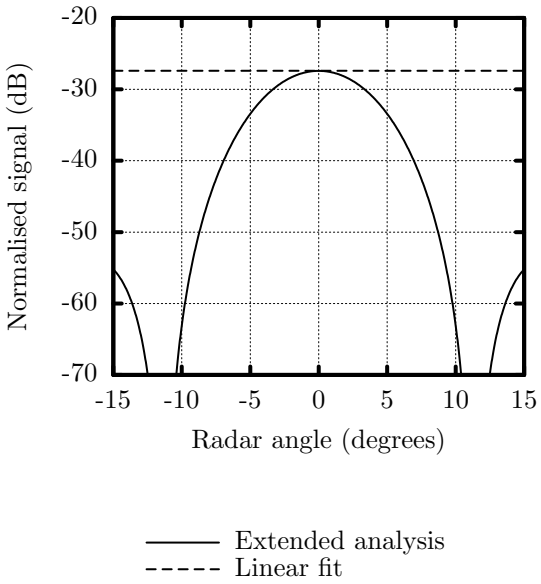

(a) Sum-channel return.

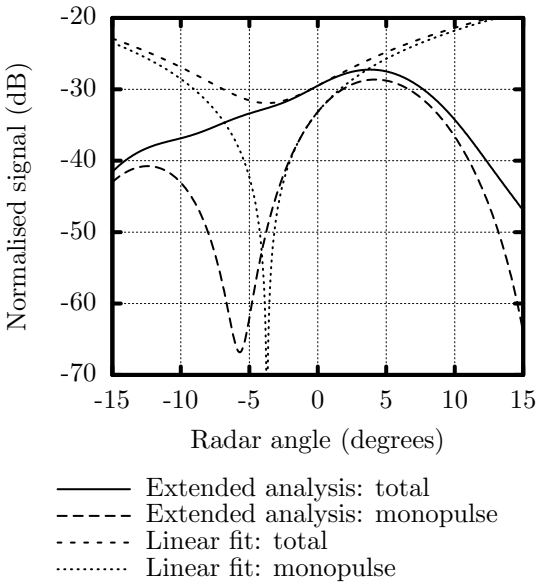

(b) The total difference-channel return and the portion of the difference-channel return used to form the monopulse indicated angle.

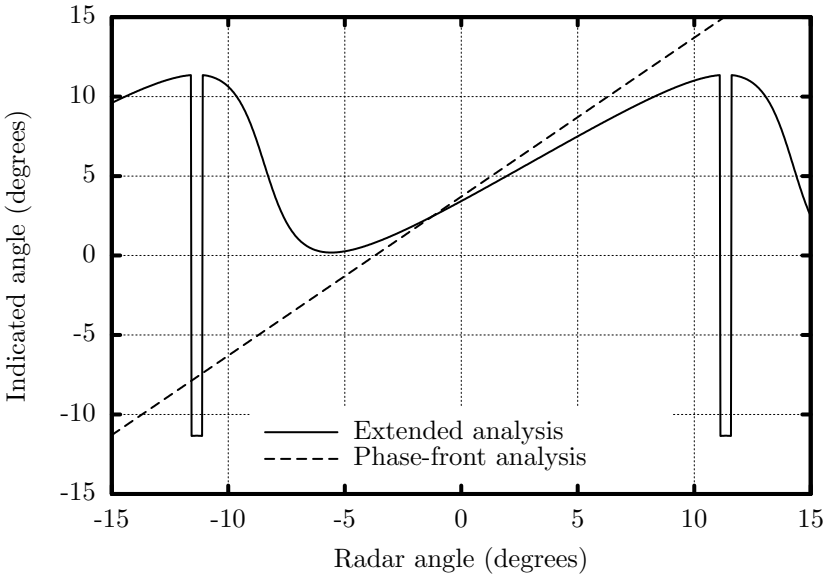

(c) Indicated angle.

Figure 4.3: Monopulse signals when the radar antenna was rotated for a relative amplitude and phase shift of 0.5 dB and 176.2° respectively giving a cross-eye gain of 14.94, and a jammer antenna element spacing of 5.0% of the radar antenna beamwidth.

for each case, normalised to the returns that would have been received from a retrodirective beacon ($a = 1$ and $\phi = 0°$) that is being perfectly tracked ($\theta_r = 0°$). The (b) portions of each figure show both the total difference-channel return from (4.39) and the portion of the difference-channel return used to form the monopulse error from (4.54). Lastly, the monopulse indicated angle is plotted in the (c) portions of each figure.

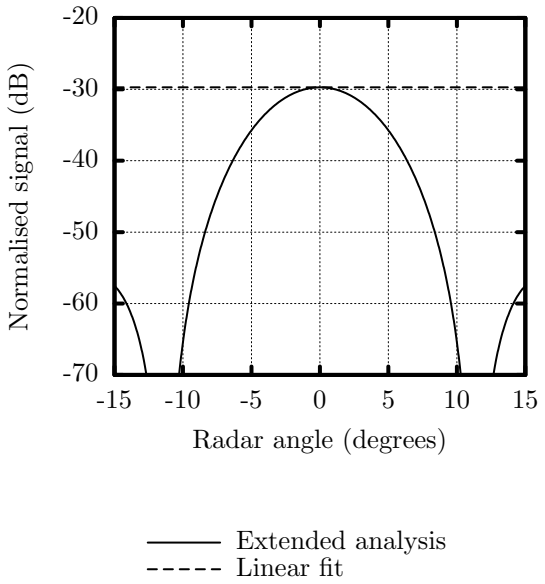

(a) Sum-channel return.

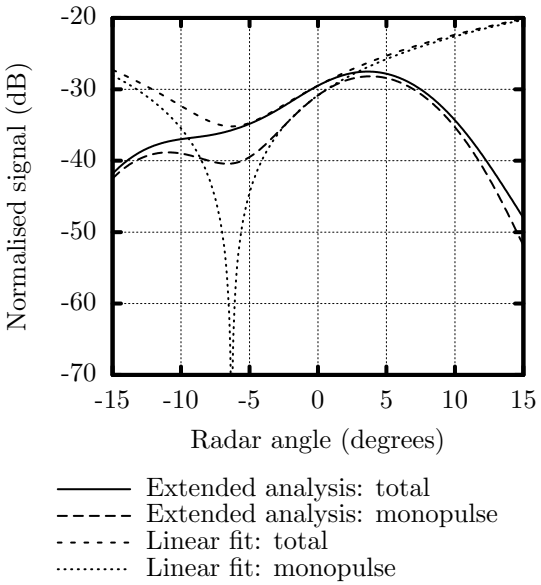

(b) The total difference-channel return and the portion of the difference-channel return used to form the monopulse indicated angle.

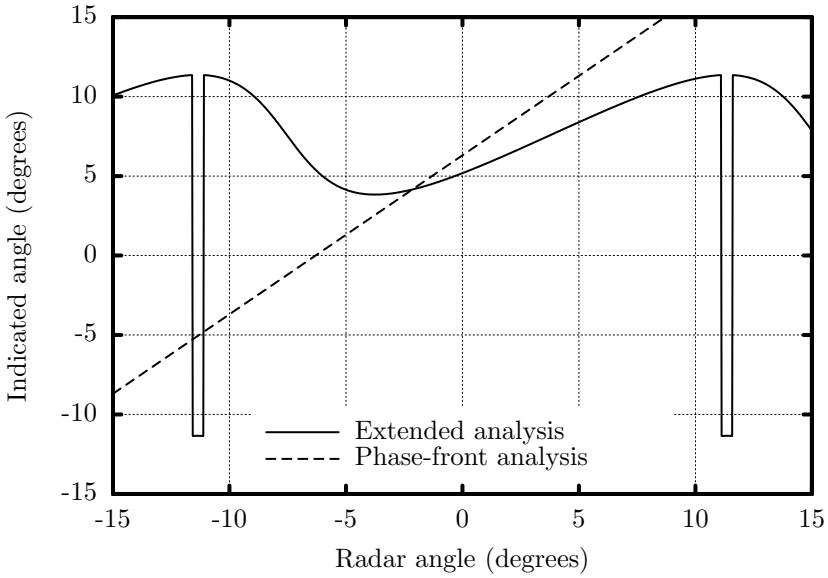

(c) Indicated angle.

Figure 4.4: Monopulse signals when the radar antenna was rotated for a relative amplitude and phase shift of 0.5 dB and 178° respectively giving a cross-eye gain of 25.41, and a jammer antenna element spacing of 5.0% of the radar antenna beamwidth.

Figure 4.2 shows a case where the cross-eye gain is small, so the differences between the linear-fit and extended analyses are expected to show good agreement. The differences between the sum- and difference-channel returns using the two analyses are mainly due to the fact that the linear-fit analysis only considers the antenna patterns near boresight. Despite this, the agreement near boresight is still very good. The agree-

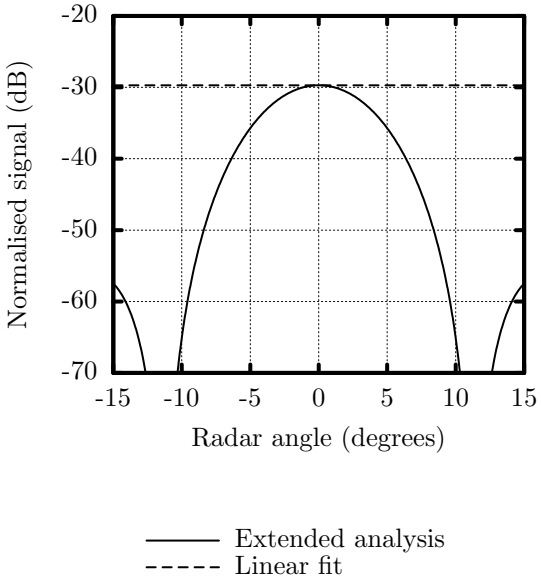

(a) Sum-channel return.

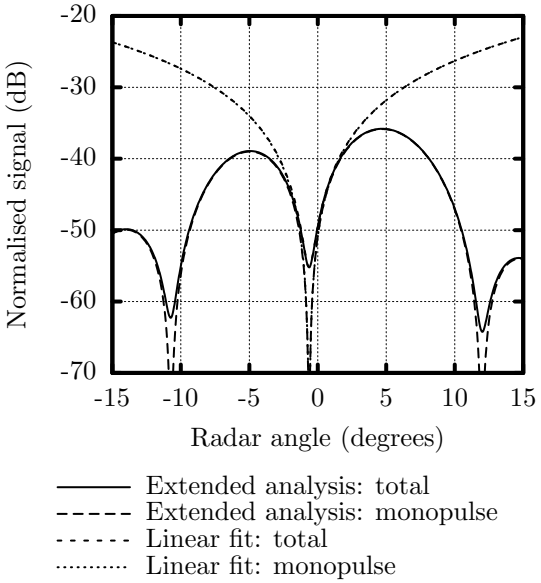

(b) The total difference-channel return and the portion of the difference-channel return used to form the monopulse indicated angle.

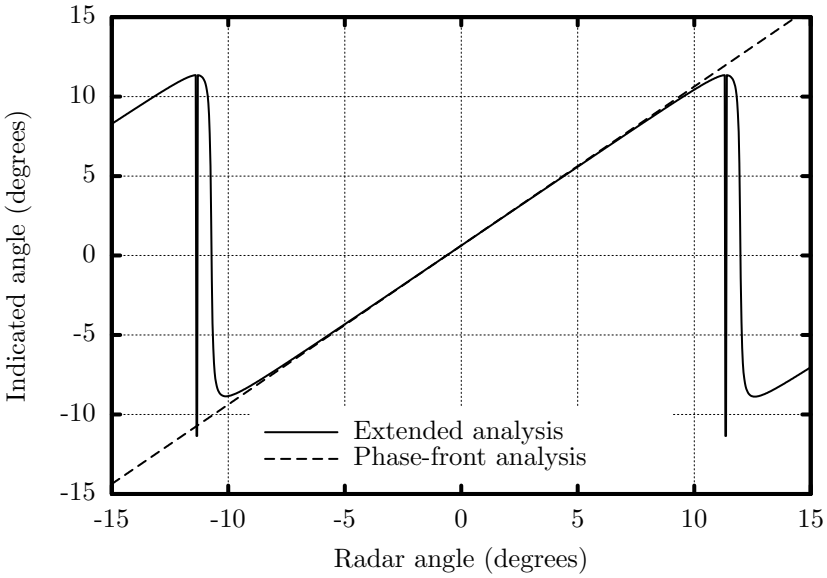

(c) Indicated angle.

Figure 4.5: Monopulse signals when the radar antenna was rotated for a relative amplitude and phase shift of 0.5 dB and 178° respectively giving a cross-eye gain of 25.41, at a range of 10 km giving a jammer antenna element spacing of 0.50% of the radar antenna beamwidth.

ment between the indicated angles for the two analyses are excellent even well outside the radar's 3 dB beamwidth ($-5°$ to $5°$).

The vertical lines in the indicated-angle plots for the extended analysis are due to sign changes in the sum-channel return near its first null. This behaviour is obviously

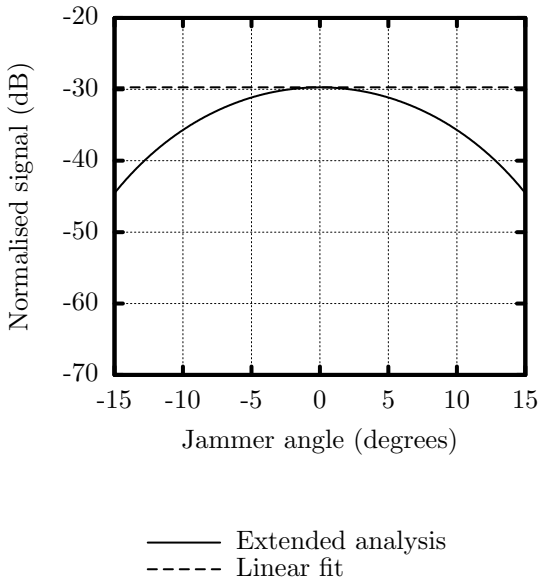

(a) Sum-channel return.

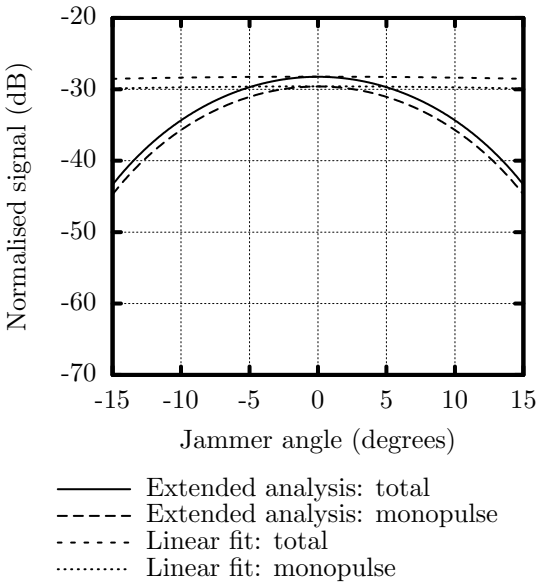

(b) The total difference-channel return and the portion of the difference-channel return used to form the monopulse indicated angle.

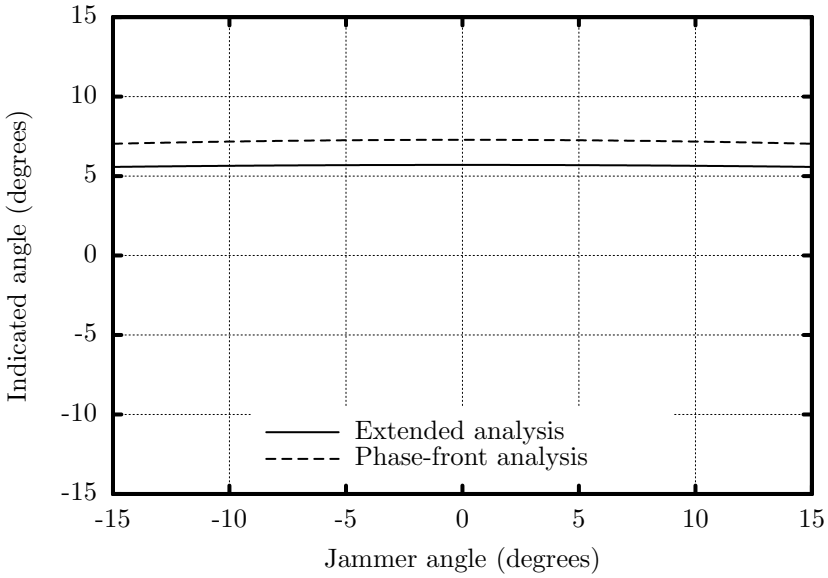

(c) Indicated angle.

Figure 4.6: Monopulse signals when the jammer antenna was rotated for a relative amplitude and phase shift of 0.5 dB and 178° respectively giving a cross-eye gain of 25.41, and a jammer antenna element spacing of 5.0% of the radar antenna beamwidth.

not seen in the linear-fit results because the linear-fit analysis only considers the antenna patterns near boresight.

The extended-analysis indicated-angle plot is zero at more than one radar rotation angle. However, only the zero nearest boresight is stable because the signs of the indicated angle will drive the radar away from the position of the other indicated-angle

zero. Combinations of stable and unstable monopulse error zeros have been observed by other researchers [8, 34].

As in Section 4.2.2, the results in Figure 4.2 thus serve to validate the extended analysis because they show that the extended analysis agrees well with the linear-fit analysis under the conditions for which the linear-fit analysis is known to be accurate.

A higher cross-eye gain is used in Figure 4.3, and differences between the linear-fit and extended analyses start to emerge. As before, the sum- and difference-channel returns display good agreement near boresight, but differences in the difference-channel return used to form the monopulse error are apparent. The agreement in the indicated angle is significantly poorer than for Figure 4.2, but is still reasonable. As explained in Section 4.2.2, the agreement is expected to be good near boresight, but to diverge as the target moves away from the radar's boresight, and this behaviour is clearly seen in Figure 4.3(c). The most significant difference is that the linear-fit analysis predicts an angular error that is well within the 3 dB beamwidth of the radar antenna, while the extended analysis shows that the indicated angle is not zero at any angle.

Figure 4.4 gives the results for a high cross-eye gain. As expected from the discussion in Section 4.2.2, the agreement between the two analyses is poor. Only the sum- and difference-channel returns show reasonable agreement, and even then, only near boresight.

The same case considered in Figure 4.4 is shown in Figure 4.5 at a range of 10 km to reduce the angular separation of the jammer antenna elements to 0.04962° ($\theta_e = 0.02481°$). The agreement between the linear-fit and extended analyses is again seen to be excellent because the large cross-eye gain is compensated by the very small jammer antenna element angular separation as expected from Section 4.2.2. The spacing of the vertical lines has also decreased to match the reduced spacing of the jammer antenna elements.

The case considered in Figure 4.4 is again considered in Figure 4.6, but for the case where the jammer is kept on the radar's boresight and the jammer system is rotated. The agreement is generally good because the jammer is always on the radar's boresight and the agreement has already been shown to be good in this case. The extended-analysis plots clearly show variations due to the jammer antenna element patterns which are not considered in the equivalent linear-fit plots. However, these variations do not appear in the indicated angle plots in Figure 4.6(c) because, as shown in Section 4.2.1, the jammer antenna element patterns cancel out when the monopulse error is formed.

The very slight variations with angle for the linear-fit analysis in Figure 4.6(b) and both analyses in Figure 4.6(c) are due to changes in the projected spacing of the jammer antenna elements as seen by the radar.

The first important conclusion from these results is that the sum-channel return decreases as the cross-eye gain increases. This is caused by the fact that the relative phase shift of the two directions through the jammer is very close to 180°, so the jammer returns cancel at the radar. This fact is well-known in the literature and is generally considered one of the drawbacks of cross-eye jamming [6–11, 13, 15, 17, 19–22, 25, 34, 35]. A cross-eye jammer must thus have a very high gain, particularly when the jammer return has to compete with a platform's skin return.

The gain of the jammer antenna elements has no effect on the angular error induced in the radar being jammed. This suggests that constructing a cross-eye jammer using

low-gain, wide-beamwidth antenna elements would be beneficial by allowing the jammer to cover wide angular regions. However, the signal received by the radar being jammed is typically small, so the use of antenna elements with higher gains is beneficial because it decreases the gain and power required from the jammer system [19, 21].

A very significant new result from the extended analysis is that the direction of the peak of the sum-channel return is not affected by a retrodirective cross-eye jammer. This means that any radar system that uses the same antenna beam for transmission and reception (e.g. some types of conical-scan radar) will not be affected by a retrodirective cross-eye jammer. This disagrees with the widely-held view that cross-eye jamming affects all types of radar (e.g. [6, 9–11, 14, 18, 20, 22, 25, 34, 64]). However, this result is not surprising because both directions through a retrodirective cross-eye jammer pass through both jammer antenna elements and the sum-channel antenna beam is used for both transmission and reception. This means that the sum-channel gain to each jammer antenna element appears in the signal received from both directions through the cross-eye jammer, so the total sum-channel gain for each direction through the jammer is identical. This is not the case for glint because the sum-channel gain will differ in the directions to the two scatterers.

The total difference-channel return is seen to vary very little between the cases considered here with the notable exception of the long-range case. However, the portion of the difference-channel return used to form the monopulse error varies dramatically, approaching the total difference-channel return as the cross-eye gain increases. The portion of the difference-channel return used to form the monopulse error never becomes zero in the sum-channel main beam when the cross-eye gain and jammer antenna element spacings are large (Figures 4.3(b) and 4.4(b)). This means that, in the ideal case, the settling angle will not exist under these conditions, and a monopulse radar will not be able to track the target generated by the cross-eye jammer.

The behaviour of the indicated angle mirrors that of the difference-channel return, but with a slightly better agreement between the two analyses. As in the difference-channel case, the indicated angle never becomes zero in the cases where the cross-eye gain and jammer antenna element separation are large (Figures 4.3(c) and 4.4(c)), confirming that, under ideal conditions, a monopulse radar will not be able to track the target formed by a cross-eye jammer in this case. This is an exceedingly important new result which suggests that a well-matched retrodirective cross-eye jammer will actually be able to break a radar's lock. This result is in stark contrast to the widely-held view that the largest error a cross-eye jammer can produce is smaller than the 3-dB beamwidth of the radar being jammed [8, 12, 16, 24, 25, 34]. The conditions under which the indicated angle never becomes zero are investigated in Chapter 6.

The behaviour of the difference-channel return and the indicated angle can be explained by noting the form of the difference-channel returns in (4.39) and (4.54), and the monopulse error in (4.51). All these equations contain a term that is minimised (the term containing k) and another term that is maximised (the term containing k_c) when the radar is perfectly tracking the cross-eye jammer. The cross-eye gain determines which of these two terms dominates the overall difference-channel return and monopulse error, with higher cross-eye gains causing larger errors.

The indicated angle on boresight for the extended analysis is smaller than for the linear-fit analysis. This result is expected because the phase-front analysis linearises

an arctangent function [48] as described in Section 2.4.1, and the true value of the arctangent function is always less than or equal to the linearised value used.

The results presented in Figure 4.2 violate Vakin and Shustov's bound [12, 16] considered in Section 2.4.2 because the relative amplitude of the two directions through the jammer is outside the allowable range, suggesting that the phase-front analysis will be inaccurate in this case. Despite this, the agreement between the results based on the phase-front analysis and the extended analysis is excellent, suggesting that Vakin and Shustov's bound does not adequately consider all the factors that determine the accuracy of the phase-front analysis.

4.4 Concluding Remarks

A comprehensive, rigorous analysis of the effect of an isolated, single-loop, retrodirective cross-eye jammer on a monopulse radar was performed. The equivalence of the new results and a number of results known to be accurate was demonstrated. Plots comparing the traditional and extended analyses were provided.

Results which are known in the literature and are supported by the new analysis are listed below.

- The sum-channel return decreases as the amplitude and phase match approach the ideal conditions for a cross-eye jammer.
- Higher cross-eye gains lead to larger angular errors.
- Increasing the angular separation of the jammer antenna elements increases the angular error induced in the radar being jammed.
- The gain of the cross-eye jammer antenna elements does not affect the induced angular error, but does affect the strength of the signal received by the radar being jammed.
- The monopulse indicated angle predicted by the traditional analysis on boresight is optimistic.

A number of new results that arise from a consideration of the extended analysis are listed below.

- The sum-channel return does not display any angular error against a retrodirective cross-eye jammer. This result will apply to any radar that uses the same antenna beam for transmission and reception (e.g. some types of conical-scan radar).
- The portion of the difference-channel return used to form the monopulse error as a proportion of the total difference-channel return increases with increasing cross-eye gain.
- The angular error predicted by the conventional analyses is conservative.
- There are cases where the monopulse error never becomes zero inside the radar's sum-channel antenna beam.

The theoretical results derived in this chapter are validated by the laboratory experiments described in Chapter 5.

CHAPTER 5

EXPERIMENTS

5.1 Introductory Remarks

The extended analysis of retrodirective cross-eye jamming given in Chapter 4 leads to a number of new conclusions about cross-eye jamming. Given the significance of these conclusions, it is important to have experimental data to validate the theoretical analysis. This chapter describes experiments conducted for this purpose. The work described in this chapter forms the basis of a submitted journal paper [3].[1]

The laboratory setup is described in Section 5.2 and the processing of the measured data is considered in Section 5.3. Section 5.4 presents results and compares them to both the conventional phase-front analysis and the extended analysis developed in Chapter 4. Finally, concluding remarks are given in Section 5.5.

5.2 Experimental Setup

The measurement setup is described in this section. The overall layout of the experiments is considered in Section 5.2.1, and the radar and jammer systems are considered in detail in Sections 5.2.2 and 5.2.3 respectively.

5.2.1 Overall Layout

The experiments were conducted in an anechoic chamber to minimise the effects of systems and scatterers that are not part of either the radar or jammer systems. The largest facility available for this purpose was the University of Pretoria's compact measurement range.

The compact range was completely reconfigured to allow it to be used as an anechoic chamber rather than as a compact range. This was done by placing one set of antennas at the back of the compact range, and the other set of antennas on the positioner in the middle of the compact range to allow them to be rotated. Unfortunately, the reflector normally used for measurements in the compact range is an integral part of the compact range and cannot be moved from the front of the range, so the reflector is present in the measurements as an unwanted scatterer.

One of the conclusions of the extended analysis in Chapter 4 is that the patterns of the antenna elements used to form the radar and jammer have no effect on the resulting monopulse indicated angle. This conclusion can be confirmed by rotating both the radar and jammer systems relative to one another. The relative rotation of the radar and jamming systems was achieved by first rotating the radar system using the positioner

[1] Portions of this chapter are reprinted, with permission, from [3].

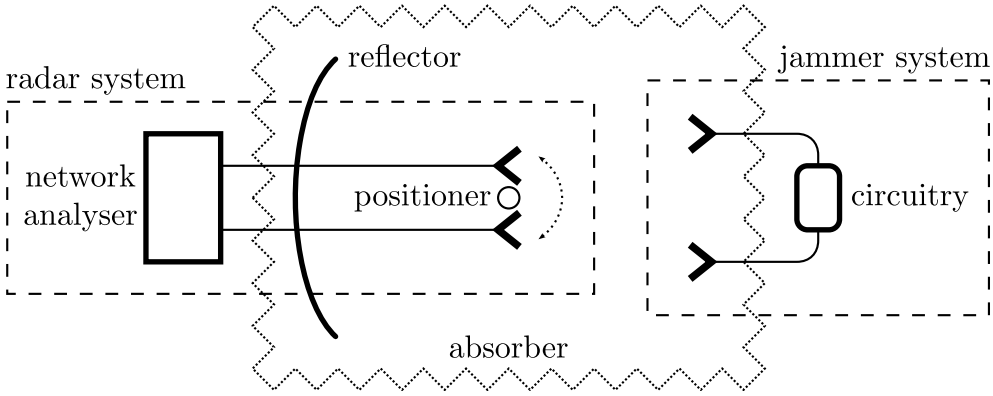

(a) Radar is rotated.

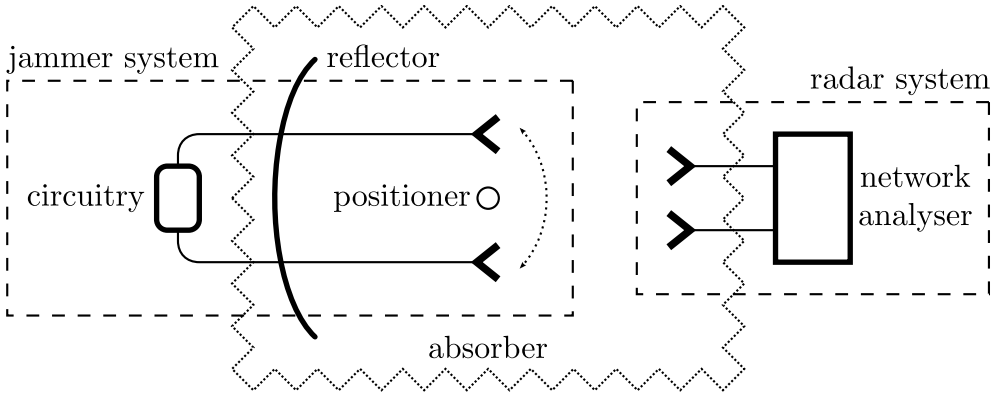

(b) Jammer is rotated.

Figure 5.1: The two configurations used for the experimental validation. The compact range's reflector is included to indicate the positions of the systems in the compact range, but was not used during the measurements (though it was present as an undesired scatterer).

Table 5.1: Measured system dimensions.

Parameter	Value	
	Radar rotated	Jammer rotated
Radar antenna spacing	70 mm	70 mm
Jammer antenna spacing	552/398 mm	483 mm
Range from radar to jammer	6.3 m	6.3 m

in the anechoic chamber while keeping the jammer system at a fixed orientation, and subsequently rotating the jammer system using the positioner while keeping the radar system at a fixed orientation. The two configurations used for the measurements are shown in Figure 5.1.

The measured dimensions of the system are shown in Table 5.1. Two cases using different jammer circuitry and jammer antenna spacings were considered when the radar was rotated to demonstrate the robustness of the analysis. A laser was used to align the radar and jammer antennas to point at one another's centres when the rotation angle was zero. Minor errors in the measured values and alignment are not critical because

precise values are calculated during the data processing described in Section 5.3.

5.2.2 Radar System

The phase-comparison monopulse radar system was constructed from two wideband ridged horn antennas connected to a Hewlett-Packard 8720D network analyser. The antennas were connected to the network analyser ports and samplers (for transmission and reception respectively) using four 15 m coaxial cables. Each radar antenna element was connected to a circulator to isolate the transmitted and received signals, and a Low-Noise Amplifier (LNA) was used to compensate for the cable loss. The radar antenna configuration is shown in Figure 5.2(a).

This configuration was used because it provides extremely high isolation between the signals transmitted and received by the network analyser while maintaining low measurement noise. High isolation is achieved by inserting the cable loss and circulator isolation between the network analyser's sources and samplers, though the LNA does reduce this isolation somewhat. Low measurement noise is achieved by including LNAs at the radar antenna elements and by directly accessing the network analyser's samplers for the received signals, thereby removing the loss associated with the network analyser's couplers during reception.

The network analyser used has a connector for direct access to the source, allowing the network analyser's couplers and their loss to be bypassed on transmission. However, using this direct connection would have required either external circuitry or additional measurements to switch transmission between the two radar antenna elements. The additional complexity this would have entailed was not justified because the Signal-to-Noise Ratio (SNR) of the measurements was already high.

The sum- and difference-channel returns can be computed from the calibrated S parameters measured with the network analyser by noting that the total signal received by each of the radar antenna elements is

$$R_1 = S_{11} + S_{12} \tag{5.1}$$
$$R_2 = S_{21} + S_{22} \tag{5.2}$$

where R_1 and R_2 are the returns received by the two radar antenna elements. The sum- and difference-channel returns can be calculated using

$$S_m = R_1 + R_2 \tag{5.3}$$
$$= S_{11} + S_{12} + S_{21} + S_{22} \tag{5.4}$$
$$D_m = R_1 - R_2 \tag{5.5}$$
$$= S_{11} + S_{12} - S_{21} - S_{22} \tag{5.6}$$

where S_m and D_m are the measured sum- and difference-channel returns respectively.

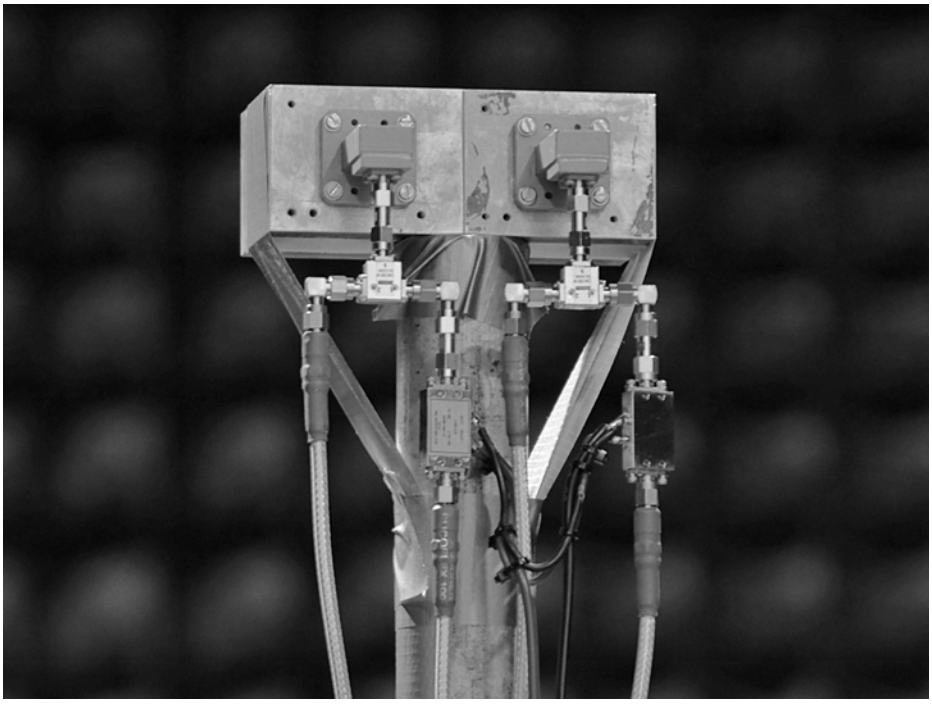

(a) Photo of the radar system showing the antennas, circulators, LNAs and cables.

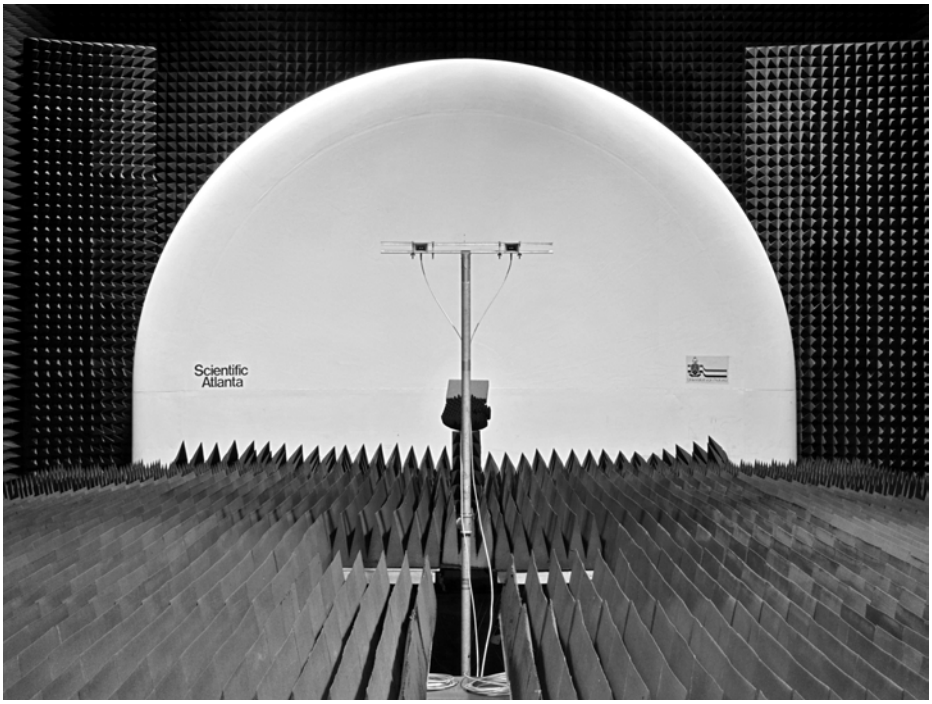

(b) Photo of the antennas representing the jammer system. The compact range's reflector (not used during these measurements) is visible in the background.

Figure 5.2: Photographs of the measurement setup. (Reprinted, with permission, from [3]. ©2009 IEEE.)

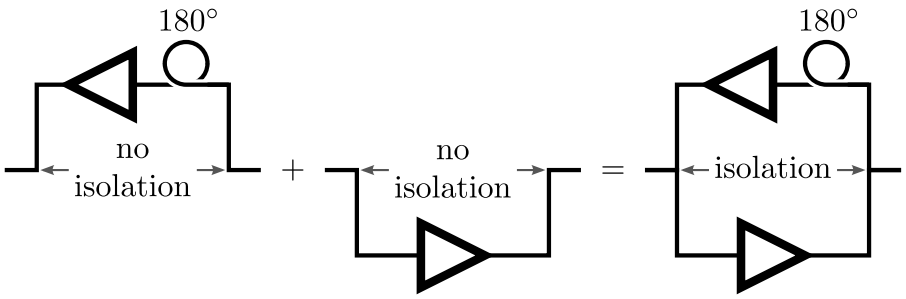

Figure 5.3: The use of superposition allows a high-gain cross-eye jammer to be simulated without requiring high isolation. (Reprinted, with permission, from [3]. ©2009 IEEE.)

5.2.3 Jammer System

The jammer system is shown in Figure 5.2(b) and consisted of two wideband ridged horn antennas connected by one 15 m coaxial cable and one 2 m coaxial cable when the radar system rotated (Figure 5.1(a)) and by two 15 m coaxial cables when the jammer system was rotated (Figure 5.1(b)). The main benefit of using such long cables was that the jammer return was delayed so that it appeared to be outside the physical extent of the anechoic chamber. This allowed the jammer return to be isolated from other stray returns inside the anechoic chamber using time-domain techniques. Having returns outside the physical dimensions of the anechoic chamber means that the measurements only have to compete with weaker multiple reflections. This was particularly important because it was not possible to remove the compact range's reflector, so it was present in the measurements as a large unwanted scatterer.

The main problem with implementing a cross-eye jammer is obtaining a jammer gain that is high enough to produce a detectable signal in the radar being jammed while maintaining sufficient isolation between the two directions through the jammer to avoid oscillation. This problem was avoided here by performing one measurement using high-gain amplifiers in one direction through the jammer, performing a second measurement with the jammer amplifiers in the other direction, and then combining the two measurements to obtain the final result as shown in Figure 5.3. This approach produces good results in a temperature-controlled environment when high-quality measurement equipment is used because system variations between the measurements are small. The data processing described in Section 5.3 considers any variations between measurements to be due to the jammer system, so such variations do not adversely affect the results.

It is extremely difficult to simultaneously obtain relative amplitudes and phase shifts close to 0 dB and 180° respectively over wide bandwidths, and variations from these desired values were present in the measured results. This is actually beneficial here because a wide range of jammer parameters were obtained. Two cases with different jammer circuitry and jammer antenna spacings were measured when the radar was rotated to obtain an even wider range of jammer parameters.

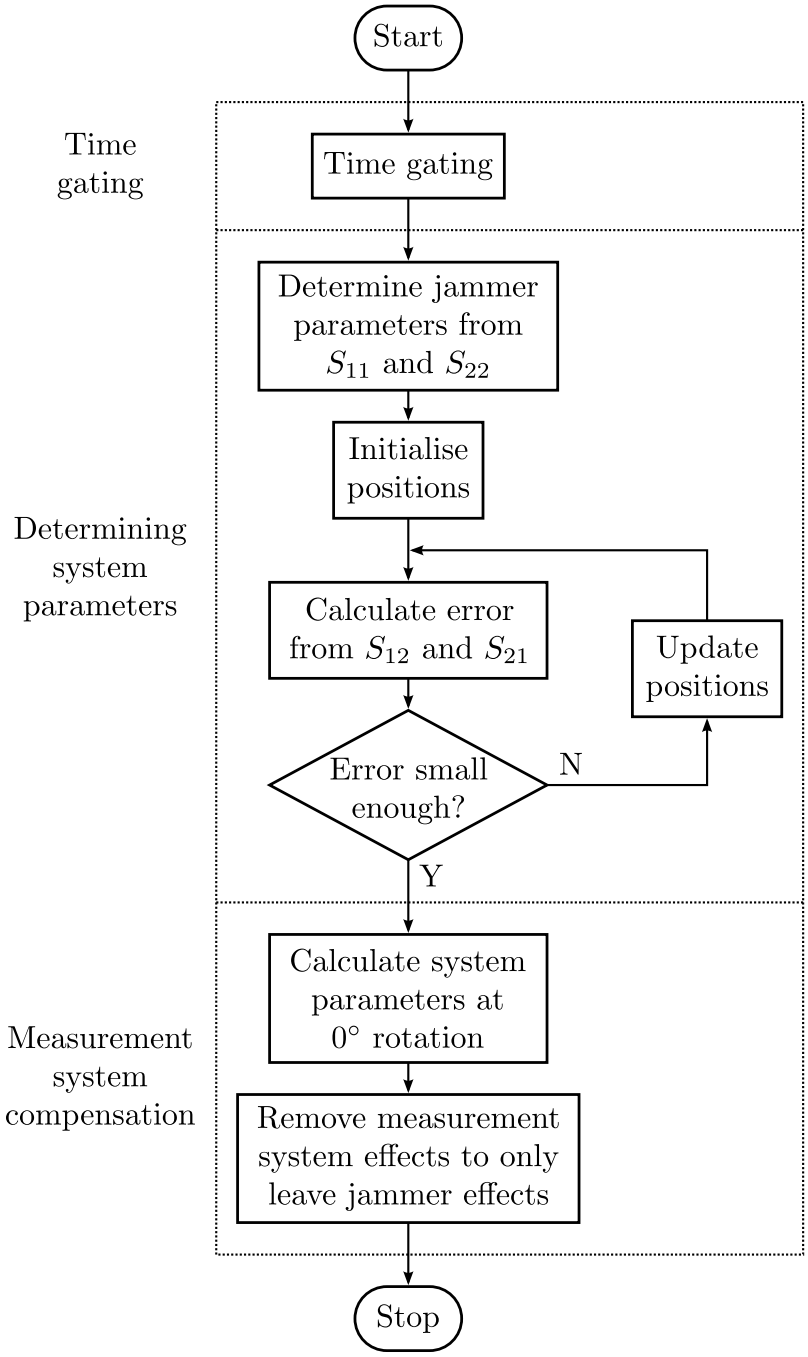

Figure 5.4: A flow chart summarising the data processing procedure.

5.3 Data Processing

The data must be processed to remove the effects of the measurement equipment. The process used here consists of the following three steps:

1. time gating,
2. determining system parameters, and
3. measurement system compensation.

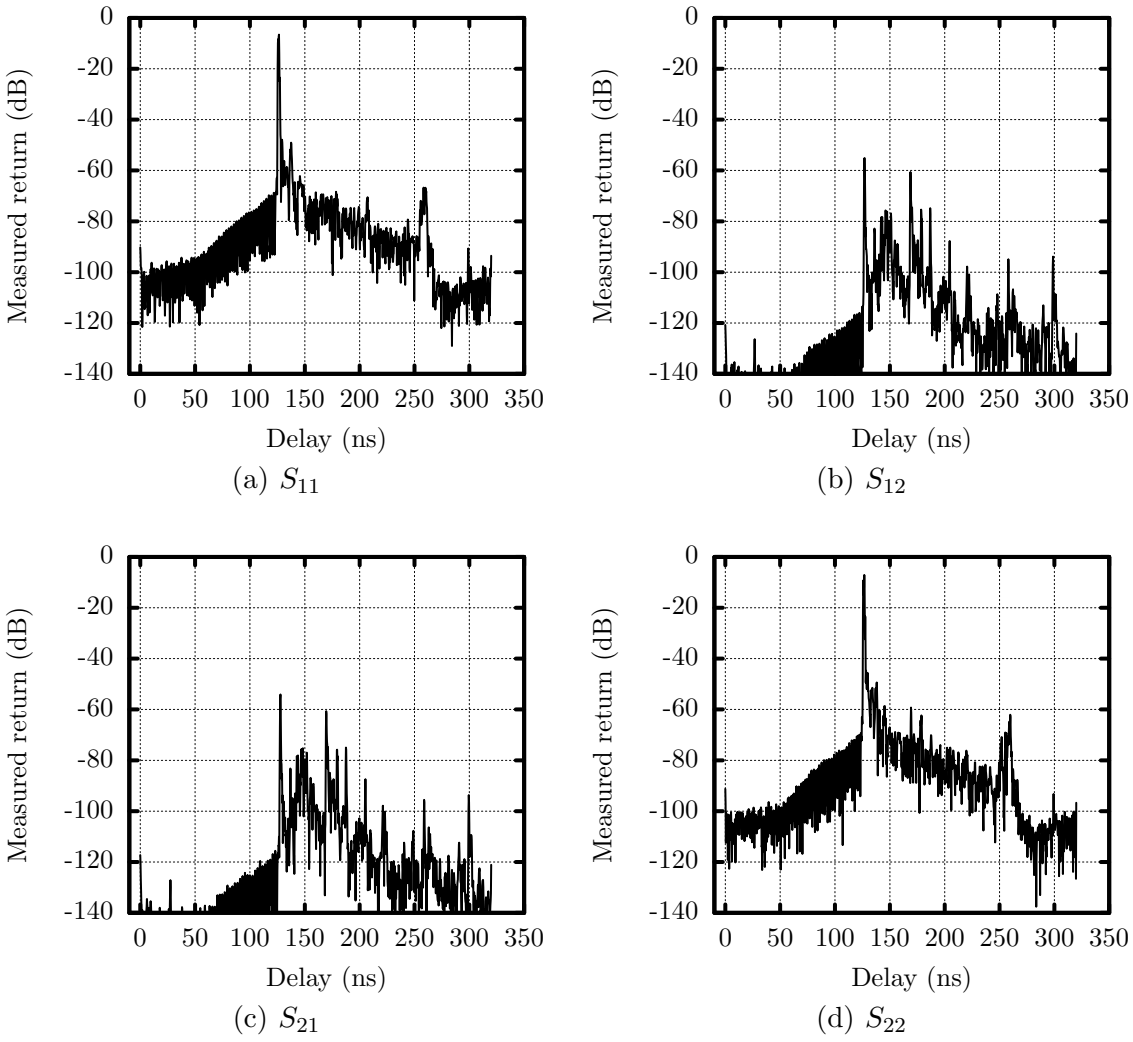

Figure 5.5: Time-domain plots of the measured S parameters for the configuration where the radar was rotated as shown in Figure 5.1(a), but with the jammer antennas terminated by matched loads.

These steps are considered in Sections 5.3.1, 5.3.2 and 5.3.3 respectively. The data processing procedure is summarised in the flow chart shown in Figure 5.4.

5.3.1 Time Gating

The purpose of the time gating performed on the measured data is to extract the jammer return from the measured data by suppressing all other returns. Although the anechoic chamber is lined with absorbing material, a number of stray reflections are still present in the measured data.

Windowing was applied to the time-domain plots in this section to suppress the sidelobes of the very high peaks. A Blackman window was used as a compromise between a narrow passband and low sidelobes [75].

Figure 5.5 shows time-domain plots of the S parameters measured by the network

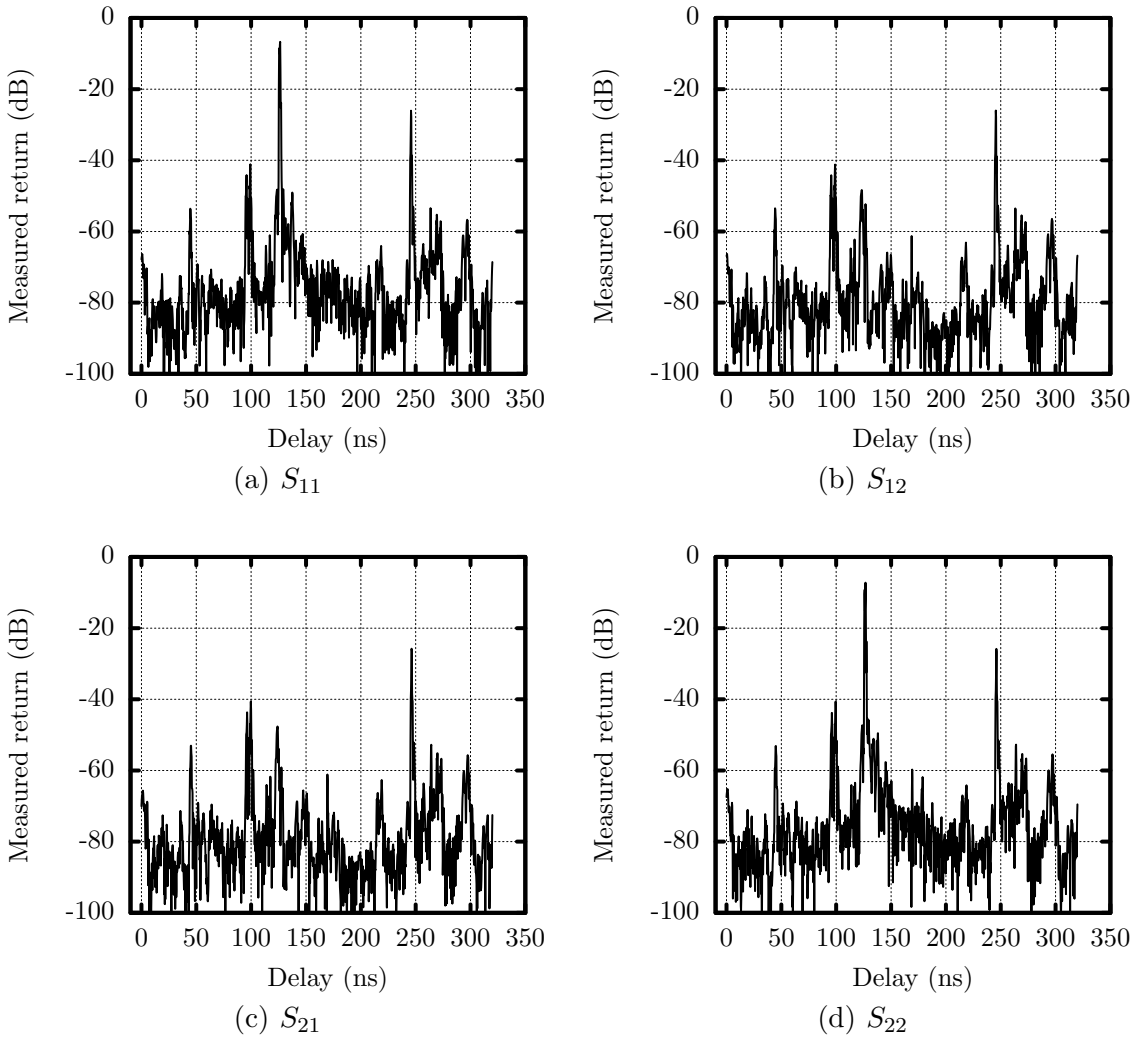

Figure 5.6: Time-domain plots of the measured S parameters for one direction through the jammer for case 1 when the radar was rotated as shown in Figure 5.1(a).

analyser with the jammer antennas terminated in matched loads to minimise their reflections. Time-domain plots of the measured data at a rotation of 0° when the radar and jammer systems were rotated are shown in Figures 5.6 and 5.7 respectively (note the scale change from Figure 5.5).

The sources of some of the reflections are identified in Table 5.2. The background measurements in Figure 5.5 clearly show the sidelobes due to phase noise in the network analyser's synthesisers, particularly around the radar antenna reflections at 126 ns. The presence of the compact range's reflector as an undesired scatterer and source of multiple reflections is clearly shown in all cases. Some of the multiple reflections appear to come from inside the cable between the network analyser and the radar antenna elements because the time-domain processing causes ranges to alias to lower values when they exceed the unambiguous range (320 ns in this case). The multiple reflections are greater when the radar is rotated because the high-gain jammer system at the back of the anechoic chamber is pointing towards the compact range's large reflector at the front of

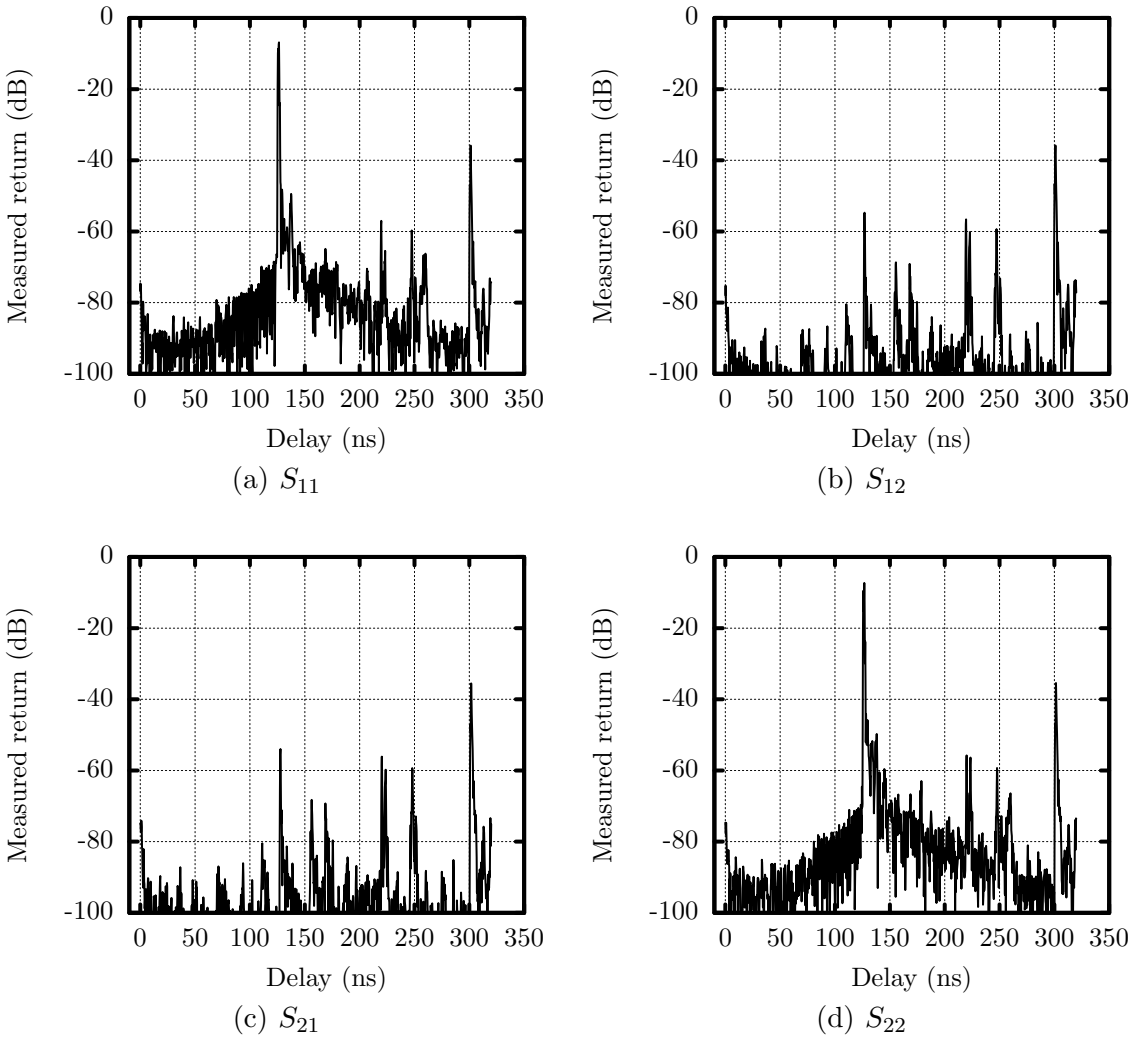

Figure 5.7: Time-domain plots of the measured S parameters for one direction through the jammer when the jammer system was rotated as shown in Figure 5.1(b).

Table 5.2: Sources of reflections.

Source	Delay (ns)	
	Figures 5.5 and 5.6	Figure 5.7
Radar antennas	126	126
Jammer pedestal	169	169
Back wall/range reflector	178	222
Jammer system	246	302
First multiple reflection	417/97	none
Second multiple reflection	685/45	none

the compact range as shown in Figure 5.1(a).

Comparing Figure 5.5 to Figures 5.6 and 5.7 shows that the jammer signals are much stronger than the background reflections at the same time delays. However, the jammer signal is not strong enough to dominate the total signal when the signals at all

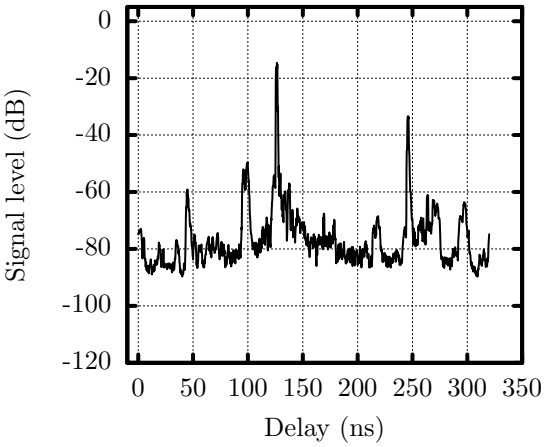

(a) Envelope.

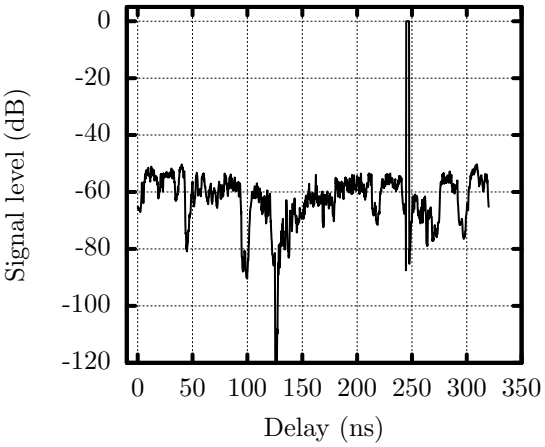

(b) Desired attenuation.

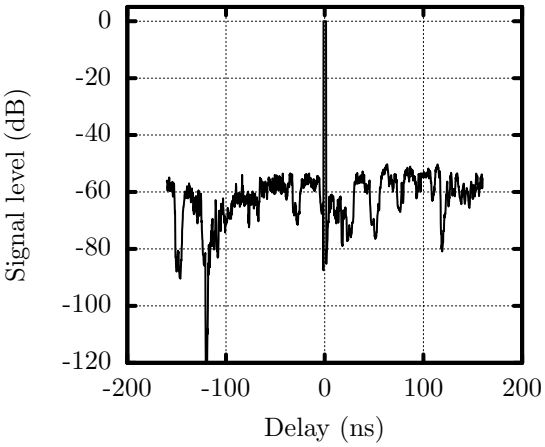

(c) Desired attenuation around zero.

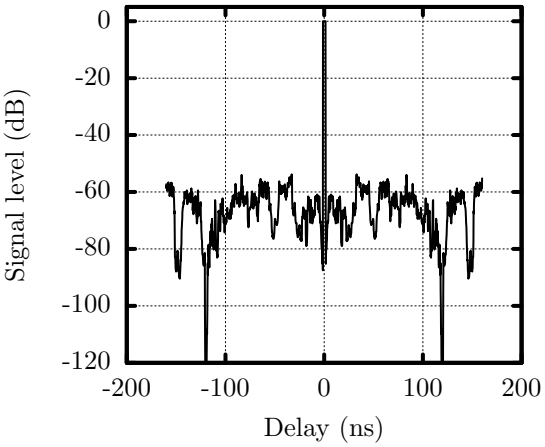

(d) Symmetrical desired attenuation.

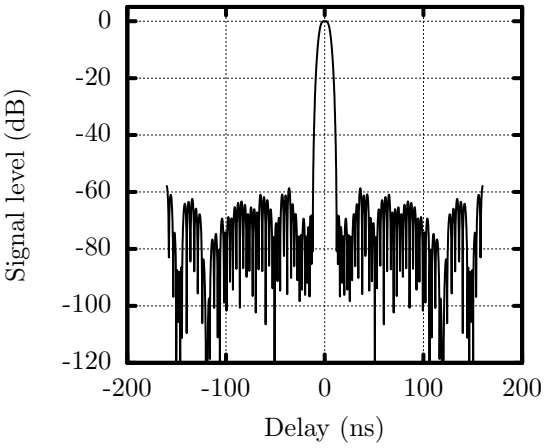

(e) Filter amplitude response.

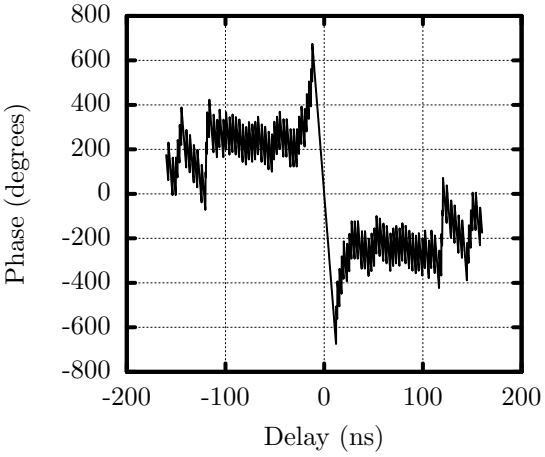

(f) Filter phase response.

Figure 5.8: Steps in the process of designing the FIR filters used for time gating. Note the change in the time axis from (c) onwards.

ranges are considered, particularly for the S_{11} and S_{22} measurements where the radar antenna element reflections at 126 ns are large. The need for time gaining to reduce the strong undesired signals at delays removed from the jammer signals' delays is thus clearly demonstrated.

Time-gating filters were used to extract the desired jammer contribution from the measured data and to eliminate the unwanted reflections. The time-gating filters used were 101-coefficient Finite Impulse Response (FIR) filters whose attenuations were optimised to be highest where the unwanted reflections are strongest. The filter design procedure is summarised in Figure 5.8 for case 1 when the radar was rotated.

The first step was to find the maximum return at each range by considering all the S parameters at all rotation angles for both directions through the jammer giving the envelope shown in Figure 5.8(a). The desired attenuation at each range was determined by calculating the attenuation necessary to reduce the envelope to a constant level as shown in Figure 5.8(b). Figure 5.8(b) also shows that the desired attenuation at the signal's delay (the passband) is zero. A linear phase shift was added to the desired attenuation to shift the passband to the origin as shown in Figure 5.8(c) and the desired attenuation was made symmetrical as shown in Figure 5.8(d). The FIR filter was designed using the approach described below giving the amplitude and phase responses shown in Figures 5.8(e) and 5.8(f) respectively. The steps in the phase response in Figure 5.8(f) are due to roots on the unit circle which cause phase inversions. Lastly, the passband was moved back to the appropriate delay by adding the inverse of the linear phase shift used to move the passband to the origin, giving results like those shown in Figure 5.9.

A FIR filter with its passband at the origin will have a linear phase response (constant group delay) as long as the its impulse response is real and symmetric or antisymmetric [76]. This places the following requirements on a linear-phase FIR filter's roots [76]:

- all roots that are on the unit circle must occur in complex conjugate pairs, and
- all roots that are not on the unit circle must occur in groups of two complex conjugate pairs, where the magnitude of each complex conjugate pair is the inverse of the magnitude of the other complex conjugate pair.

The second condition reduces to a single pair of roots each of whose magnitude is the inverse of the other's when the roots are on the real axis.

The 101-coefficient FIR filters used have 100 roots of which 98 were placed on the unit circle in complex conjugate pairs, and 2 of which were placed on the positive real axis to broaden the passband. The positions of the roots were adjusted using the Nelder-Mead algorithm [72] to minimise the passband variation while ensuring that the highest sidelobe values were equal to the desired attenuation.

The very high order of the filters meant that each of the filters had to be realised by cascading two 51-coefficient FIR filters to avoid rounding errors. The roots on the unit circle were alternately assigned to the 51-coefficient FIR filters in complex conjugate pairs to ensure that adjacent roots were not in the same filter. Each of the 51-coefficient FIR filters was assigned one of the two roots that were not on the unit circle.

The result of applying the time-gating filters to the responses in Figures 5.9(a) and 5.9(b) is shown in Figures 5.9(c) and 5.9(d) respectively. The effect of the filter design is seen by the fact that the filter responses in Figures 5.9(c) and 5.9(d) have high attenuations where the signals in Figures 5.9(a) and 5.9(b) have large returns. For

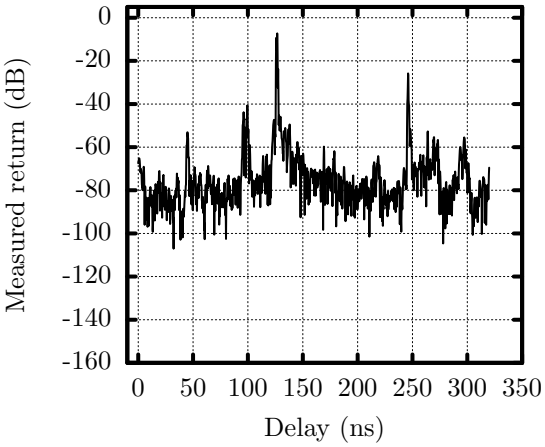

(a) Raw response when the radar was rotated.

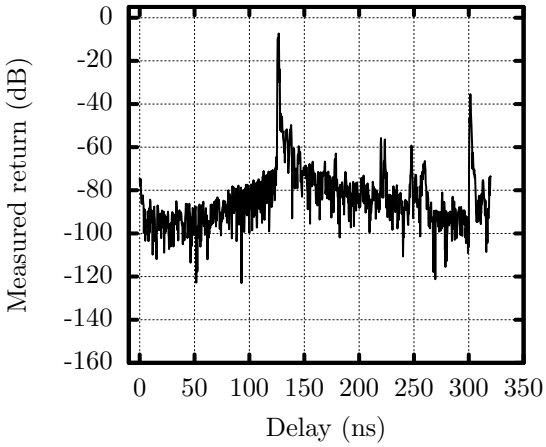

(b) Raw response when the jammer was rotated.

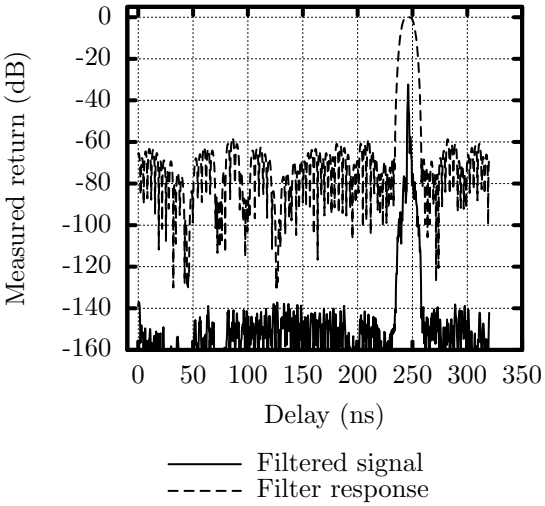

(c) Time-gated response when the radar was rotated.

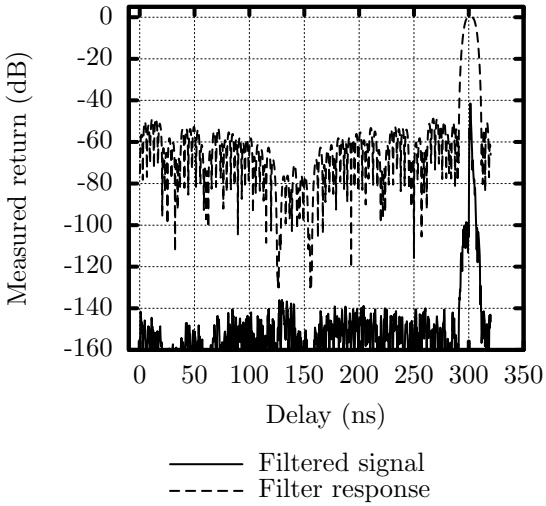

(d) Time-gated response when the jammer was rotated.

Figure 5.9: Time-domain plots of the measured S_{22} data for one direction through the jammer before and after time gating.

example, the return from the compact range's reflector at 222 ns in Figure 5.9(b) is strongly attenuated by the time-gating filter as shown in Figure 5.9(d). The almost constant signal level away from the jammer system return in Figures 5.9(c) and 5.9(d) again reflects the FIR filter design procedure used.

5.3.2 Determining System Parameters

The parameters and positions of the radar and jammer systems must be determined as a prelude to determining the measurement equipment effects.

The fact that, as shown in Figure 5.3, two measurements were performed for each setup shown in Figure 5.1 means that a total of eight S parameters were measured at

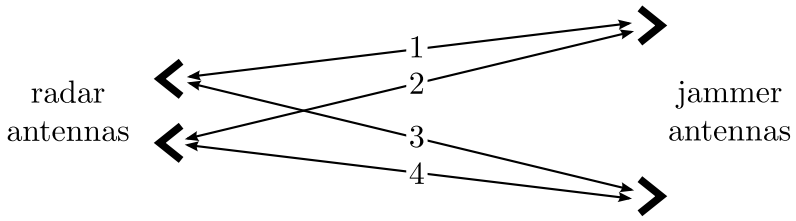

Figure 5.10: The paths between the radar and jammer antenna elements for the two sets of S parameter measurements. (Reprinted, with permission, from [3]. ©2009 IEEE.)

each frequency and aspect angle. The desired parameters are estimated using these eight measured S parameters.

Considering the model in Figure 5.10, the physical path lengths for S_{11} of measurement one (paths 1 and 3) and of measurement two (paths 3 and 1) are exactly the same, though the direction through the jammer is reversed. The same is true for the path lengths for S_{22} of measurement one (paths 2 and 4) and of measurement two (paths 4 and 2). This means that the relative amplitude and phase shift through the jammer can be determined directly from the two sets of S_{11} and S_{22} measurements.

This approach assumes that all differences between the S_{11} and S_{22} measurements for the two directions through the jammer are due to the jammer system. As mentioned in Section 5.2.3, any variations caused by reversing the jammer amplifiers will thus be considered to be part of the jammer. This means that such variations are not a problem here because the objective of these experiments is to investigate retrodirective cross-eye jamming over a wide range of system parameters.

The relative amplitudes and phases obtained using the procedure described above for the three cases considered here are plotted in Figure 5.11. The fact that case 1 when the radar was rotated and the case when the jammer was rotated used the same jammer circuitry is evident from Figures 5.11(a) and 5.11(c). While between Figures 5.11(a) and 5.11(c) are evident, the robustness of the process to determine the jammer parameters is clearly demonstrated by the fact that the mean amplitude and phase differences are less than 0.4 dB and less than 4° respectively, while the maximum differences are less than 1.4 dB and less than 7° respectively. These differences are acceptable because phase-stable cables were not used, two connections had to be loosened and fastened whenever the jammer amplifiers were reversed, and different cables were used in the two cases highlighted.

The antenna positions were estimated from the two sets of S_{12} and S_{21} measurements. The S_{12} and S_{21} measurements have different physical path lengths as a consequence of the change of direction through the jammer. The S_{12} measurements travel along paths 2 and 3, and paths 4 and 1 in Figure 5.10 for measurements one and two respectively. For the S_{21} measurements, the signals travel along paths 1 and 4, and paths 3 and 2 in Figure 5.10 for measurements one and two respectively. The phase differences between the S_{12} measurements for the two directions through the jammer and the phase differences between the S_{21} measurements for the two directions through the jammer can thus be used as error functions that must be minimised to estimate the path lengths between the antennas in Figure 5.10.

The path phase shifts depend on the positions of the radar and jammer antenna

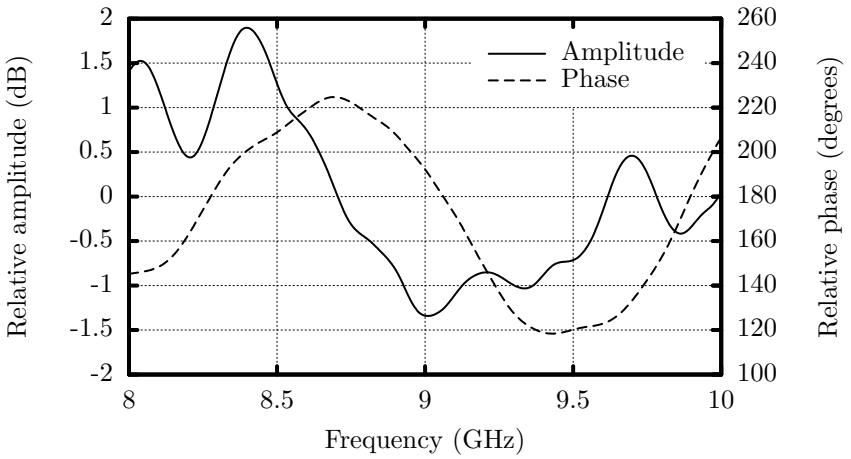

(a) Radar rotated, case 1.

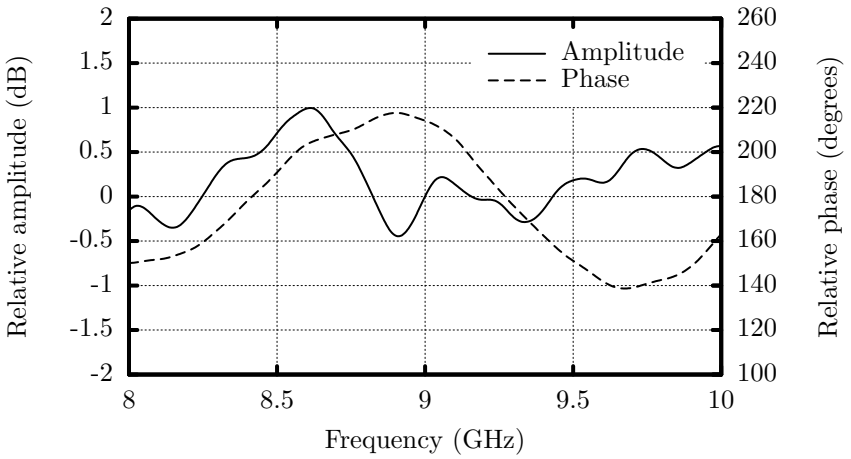

(b) Radar rotated, case 2.

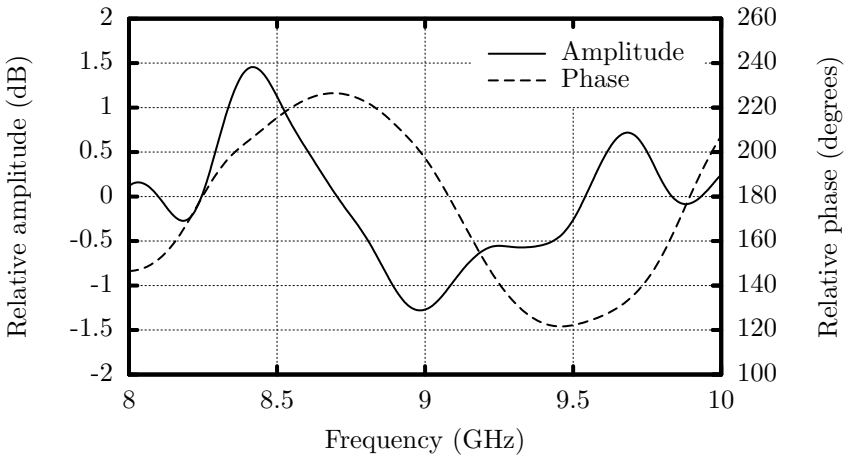

(c) Jammer rotated.

Figure 5.11: The relative amplitude and phase of the cross-eye jammer systems used during the measurements.

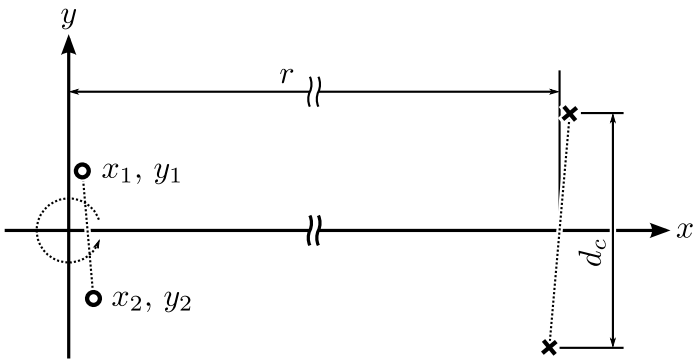

Figure 5.12: The model of the antenna positions used for data processing.

Table 5.3: Computed system dimensions.

Parameter	Value		
	Radar rotated		Jammer rotated
	Case 1	Case 2	
x_1	35.78 mm	35.67 mm	72.19 mm
y_1	35.17 mm	35.16 mm	246.5 mm
x_2	35.70 mm	35.50 mm	72.09 mm
y_2	−35.23 mm	−35.12 mm	−242.2 mm
d_c	550.8 mm	397.5 mm	70.96 mm
r	6.300 m	6.304 m	6.303 m
Antenna spacing	70.39 mm	70.29 mm	488.7 mm
Antenna rotation	−0.06°	−0.14°	−0.01°

elements as a function of both frequency and rotation angle. The model used for the system is shown in Figure 5.12. The system being rotated (radar or jammer) is placed at the origin while the other system is placed at some distance from the origin. Four degrees of freedom are required for the antennas being rotated to allow for angular offset, down-range offset, cross-range offset and antenna spacing. The fixed antennas are positioned symmetrically around the x axis because any angular offset is included in the rotated antenna positions. The fact that the fixed antennas do not rotate means that only the projected spacing of the fixed antennas can be determined.

The parameters in Figure 5.12 were fitted to the measured data using the Nelder-Mead local optimisation algorithm [72] because this algorithm does not require gradient information and good starting values were available in the form of the measured antenna positions. The jammer phase shift calculated from S_{11} and S_{22} as described above, and the phase shift due to the positions of the antennas shown in Figure 5.12 were removed from the phases of the S_{12} and S_{21} measurements. As explained above, this procedure should only leave the effect of the measurement equipment, so the remaining phases of the S_{12} and S_{21} measurements should thus be identical for each of the two directions through the cross-eye jammer. The positions of the antennas were then adjusted by the optimisation algorithm to minimise the differences between the remaining S_{12} and S_{21} phases for each of the two directions through the cross-eye jammer. The positions determined using the technique described above are given in Table 5.3.

Comparisons between the measured values in Table 5.1 and the computed values in Table 5.3 show excellent agreement. Furthermore, the agreement between the values of the common parameters for cases 1 and 2 when the radar was rotated demonstrates the robustness of the position calibration procedure. The down-range positions (x_1 and x_2) arise because the antennas' phase centres were not aligned with the axis of rotation. However, even here the agreement is good because the antennas are 70 mm long, and their midpoints and backs were aligned with the axis of rotation when the radar and jammer systems were rotated respectively.

5.3.3 Measurement System Compensation

Once the relative amplitude and phase shift of the two directions through the jammer and the accurate positions of the antennas are known, the effects of the measurement equipment (amplitude and phase variations due to the network analyser, antennas, cables, amplifiers and circulators) can be determined. These equipment effects are then removed from the measured data, leaving only the desired jammer and spatial orientation effects of the radar and jammer systems.

The measurement equipment effects are estimated for each of the transmit and receive paths as a function of frequency. This is done by removing the jammer system effects and the phase shifts due to the radar and jammer antenna element positions calculated previously from the measured data at a rotation of 0°, leaving only the measurement equipment effects. These measurement equipment effects are then removed from the measurements at all angles so that only the desired radar and jammer effects as a function of frequency and angle remain.

5.4 Results and Discussion

Measured and computed results over a wide range of jammer parameters are plotted in Figures 5.13 and 5.14 when the radar was rotated, and in Figure 5.15 when the jammer was rotated. Specific cases are then considered in more detail in Figures 5.16 to 5.19.

The magnitude of the monopulse error is plotted on a logarithmic scale in Figures 5.13 to 5.15 because this format accentuates the differences between the measured and calculated results. The angular error predicted by the conventional phase-front theory is plotted in Figures 5.13 and 5.14 as a white line. Figures 5.13 and 5.14 plot the results as a function of both frequency and angle, while Figure 5.15 only plots the results as a function of frequency because, as shown in Figures 4.2 to 4.6 on pages 50 to 54, radar rotation has a significant effect on the monopulse error while jammer rotation only produces a small effect on the monopulse error. The measurement system compensation was performed at a rotation of 0°, so the results in Figure 5.15 are plotted at a jammer rotation of 5°.

The angles of the first monopulse error peaks in Figures 5.13 and 5.14 move closer to boresight as the frequency increases. This is because the radar antenna element spacing as a function of wavelength increases with frequency, thereby narrowing radar antenna patterns.

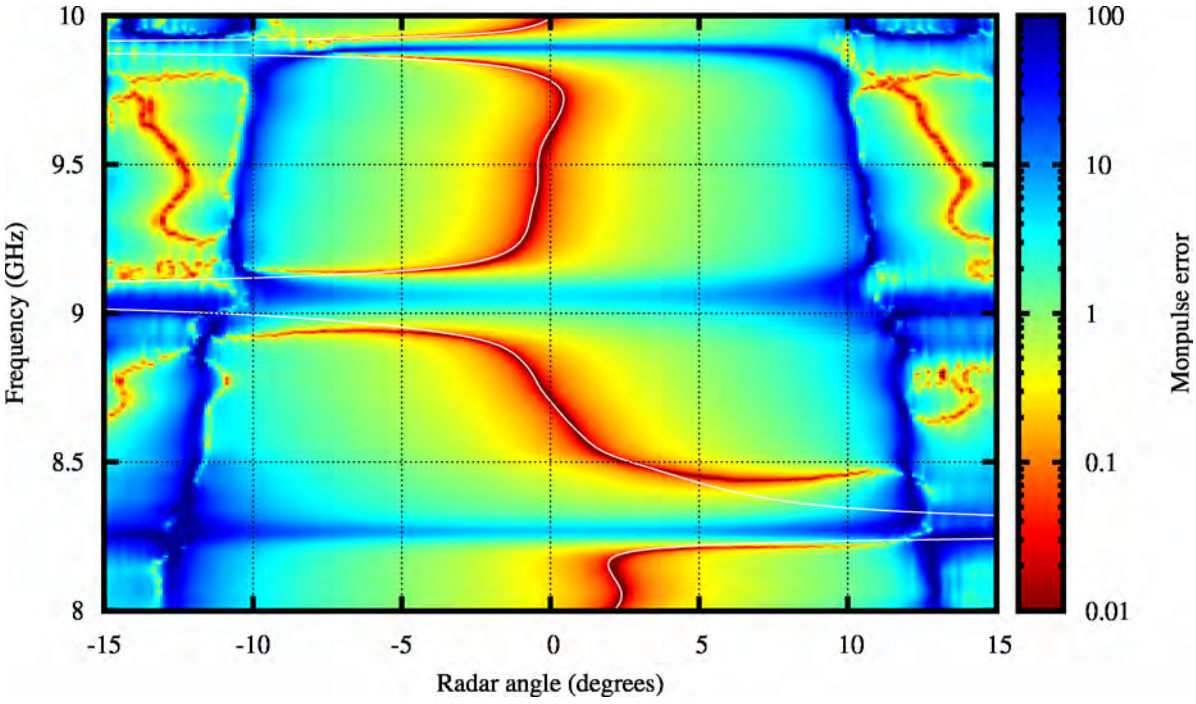

(a) Measured.

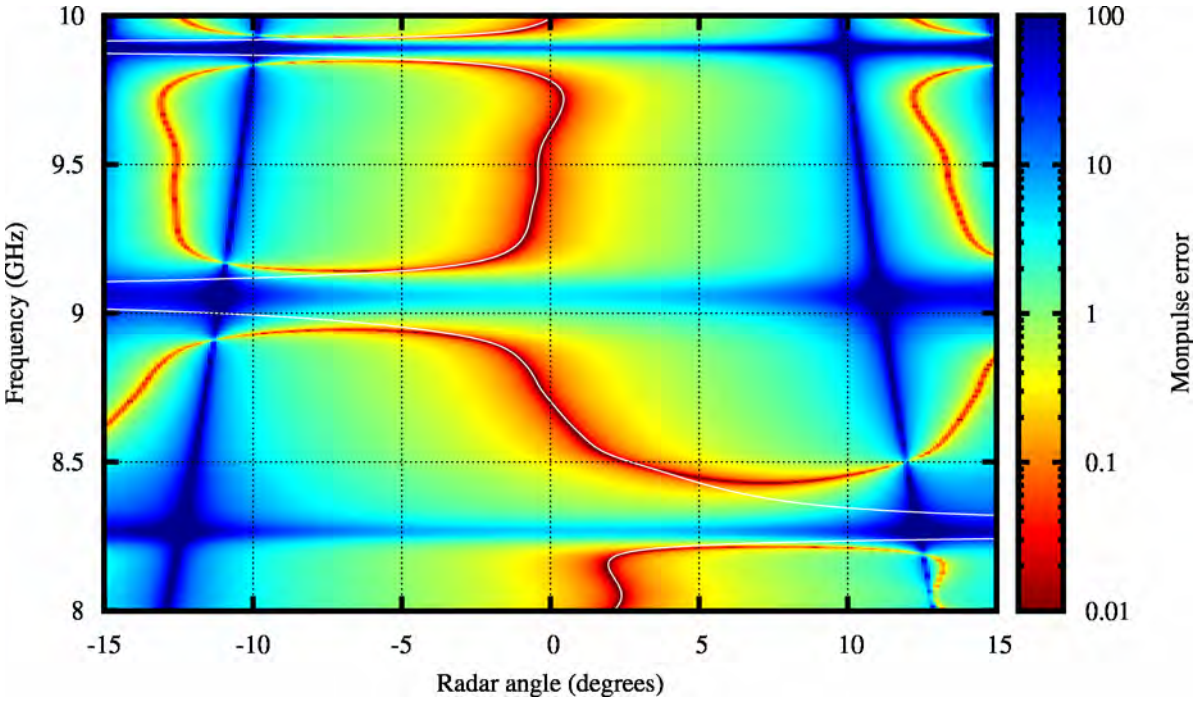

(b) Calculated.

Figure 5.13: Magnitude of the monopulse error for case 1 when the radar was rotated. The jammer parameters are given in Figure 5.11(a), and the jammer antenna element spacing is 5.006° as seen by the radar. The white line shows the error predicted by the phase-front analysis.

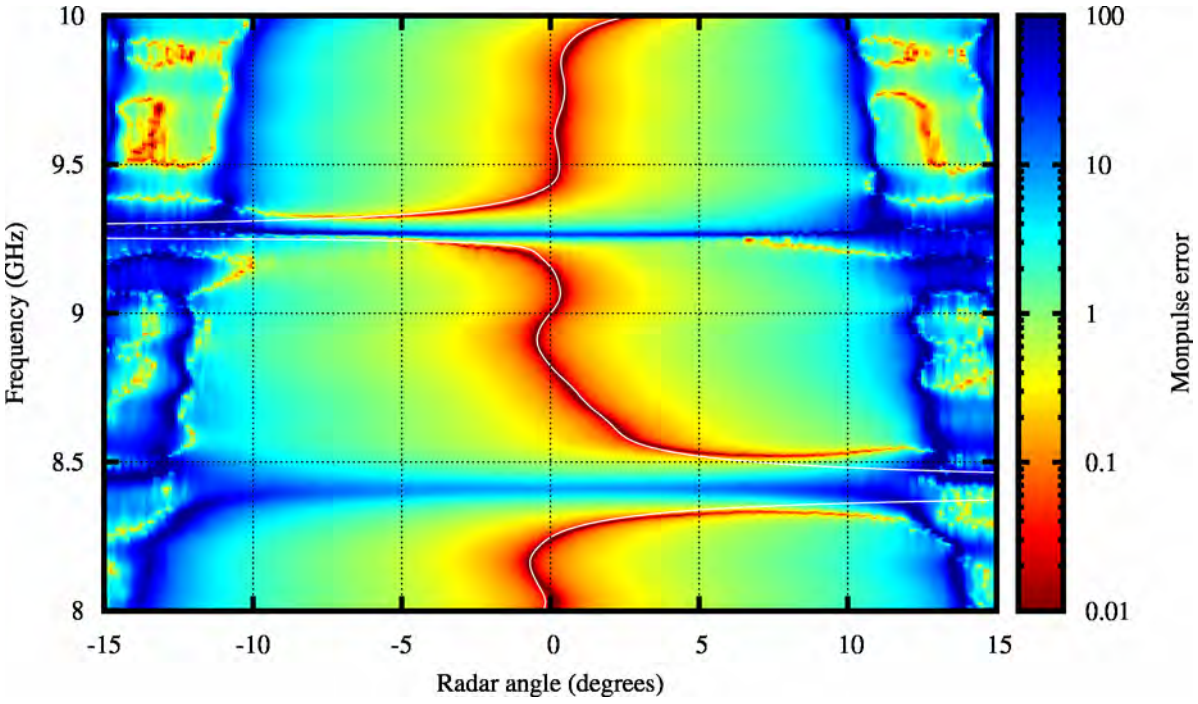

(a) Measured.

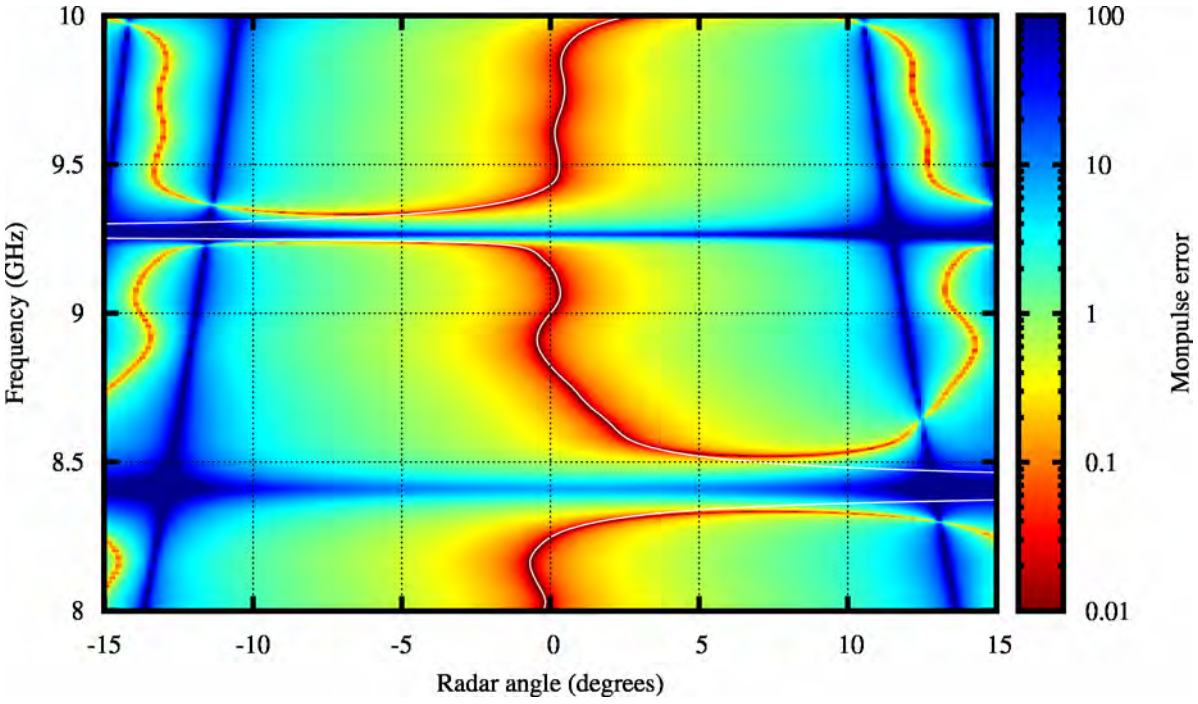

(b) Calculated.

Figure 5.14: Magnitude of the monopulse error for case 2 when the radar was rotated. The jammer parameters are given in Figure 5.11(b), and the jammer antenna element spacing is 3.612° as seen by the radar. The white line shows the error predicted by the phase-front analysis.

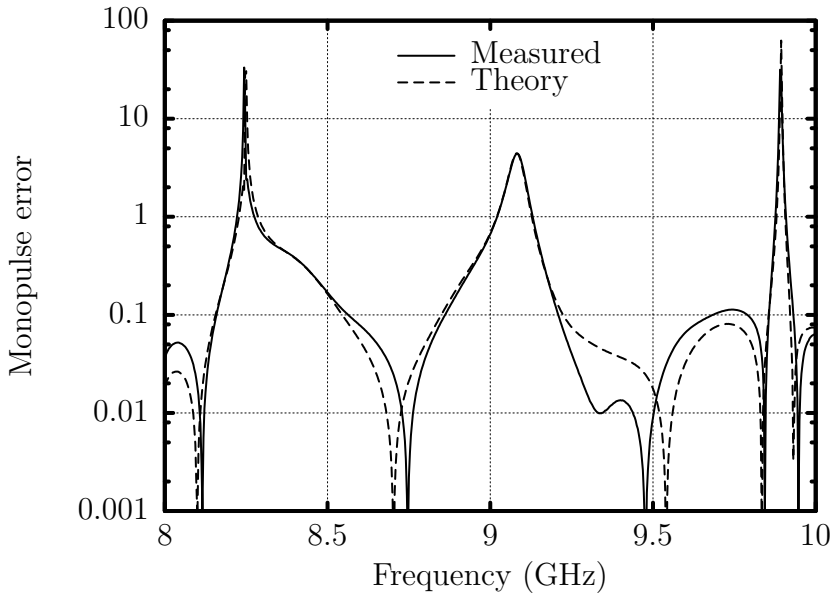

Figure 5.15: Magnitude of the monopulse error when the jammer was rotated at 5° rotation. The jammer parameters are given in Figure 5.11(c), and the jammer antenna element spacing is 4.440° as seen by the radar.

Apart from differences due to jammer circuitry, the most significant difference between Figures 5.13 and 5.14 is that the first monopulse error peak is nearer boresight in case 1 shown in Figure 5.13, echoing the results in Figures 4.4 and 4.5 on pages 52 and 53. This effect is caused by the wider spacing of the jammer antenna elements used in case 1. The first monopulse error peak occurs when the sum-channel antenna beam's first null is pointing directly at one of the jammer antenna elements. This causes the sum-channel returns from both directions through the retrodirective cross-eye jammer to be minimised because both directions use the jammer antenna element which has a null pointed towards it. A minimum in the sum-channel return leads to a maximum in the monopulse error because the sum-channel return appears in the denominator of the monopulse error.

The agreement between the measured results in Figures 5.13(a) and 5.14(a), and the calculated results in Figures 5.13(b) and 5.14(b) is remarkably good over the entire range of parameters considered. The largest differences are seen to occur outside the angle of the first monopulse error peak, and this is readily explained by the fact that the antennas used to form the phase-comparison monopulse radar are not matched and calibration is performed on boresight. The largest differences between the measured and theoretical results in Figure 5.15 occur when the monopulse error is extremely small and are again due to the fact that the radar antenna patterns are not matched.

Comparing Figure 5.11 and Figures 5.13 to 5.15 shows that the largest errors induced in the radar occur at those angles where the relative phase of the two directions through the cross-eye jammer is closest to 180°. This is anticipated because a relative phase shift of 180° results in the smallest sum-channel return and the largest cross-eye gain.

The largest differences between the phase-front theory, and the measurements and the extended analysis in Figures 5.13 and 5.14 are also seen to occur when the relative

phase of the two directions through the retrodirective cross-eye jammer is close to 180° (see Figure 5.11). This supports the assertion that the phase-front analysis is most inaccurate under precisely the conditions for which cross-eye jammers are designed.

Detailed comparisons between the measured and theoretical results when the radar antenna is rotated are given for three cases of amplitude and phase matching in Figures 5.16 to 5.18 which consider similar cases to Figures 4.2 to 4.4 on pages 50 to 52. Figures 4.2 and 5.16 show cases where the agreement between the phase-front and extended analyses is good, Figures 4.3 and 5.17 present cases where the settling angle only just ceases to exist, and Figures 4.4 and 5.18 consider cases where the settling angle does not exist. A single case where the jammer antenna elements are rotated is considered in Figure 5.19.

The main difference between the results in Figures 4.2 to 4.4 and 4.6, and Figures 5.16 to 5.19 is that a significantly lower cross-eye gain is required to achieve comparable errors in the measured results. This is due to the fact that the angular separation for the measurements ($\theta_e = 2.503°$ for Figures 5.16 to 5.18, and $\theta_e = 2.220°$ for Figure 5.19) is significantly larger than for the scenario considered in Section 4.3 ($\theta_e = 0.2865°$).

The (a) and (b) portions of Figures 5.16 to 5.19 compare the measured sum- and difference-channel returns with theoretical results based on the extended analysis. These results are normalised to the return that would be received if the radar was perfectly tracking a retrodirective beacon ($\theta_r = 0$, $a = 1$ and $\phi = 0°$). The linear-fit analysis is not shown here to avoid having too many curves on each plot. As in Figures 4.2 to 4.6 on pages 50 to 54, both the total difference-channel return and the portion of the difference-channel return used for monopulse processing are shown in the (b) portions of Figures 5.16 to 5.19. The measured monopulse indicated angles and the theoretical results for both the phase-front and extended analyses are shown in the (c) portions of Figures 5.16 to 5.19.

All the theoretical results were calculated assuming that both the radar and jammer antenna elements were omnidirectional. The effect of this assumption is clearly seen in the sum- and difference-channel returns in Figures 5.16 to 5.19 where the measured signals drop below the theoretical signals as the radar system is rotated. As predicted by the extended analysis, the monopulse indicated angles in Figures 5.16 to 5.18 do not show this effect because the indicated angle is not affected by the radar antenna element patterns. However the noise increases at large rotations because the antenna gain roll off decreases the amplitude of the received signals leading to lower SNR values. Differences between the measured data and the extended analysis are mainly due to inevitable measurement noise and to the fact that the antenna element patterns are not matched. Remarkably, the agreement continues to be good even well outside the sum-channel 3 dB beamwidth (roughly -5° to 5°) despite the assumption of omnidirectional antennas.

As predicted by the extended analysis, the cross-eye jammer does not induce any angular error in the sum-channel signal. This important result means that a cross-eye jammer will not cause an error in a radar that uses the same antenna beam for transmission and reception (e.g. some types of conical-scan radar). This behaviour is not predicted by the phase-front analysis because the phase-front analysis assumes that any radar antenna will align itself with the distorted phase front leading to the same angular error in all cases.

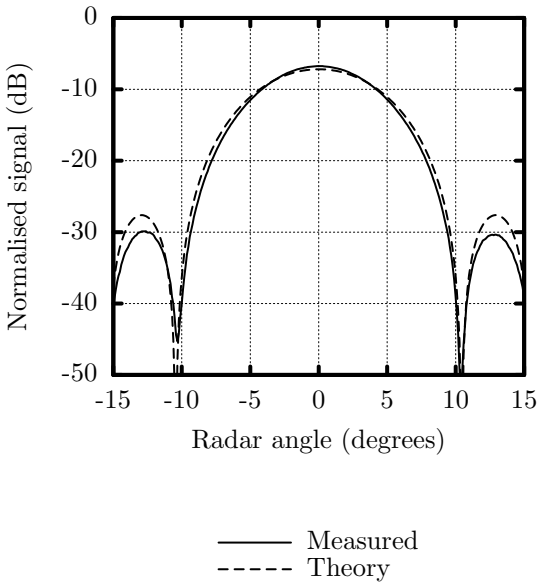

(a) Sum-channel return.

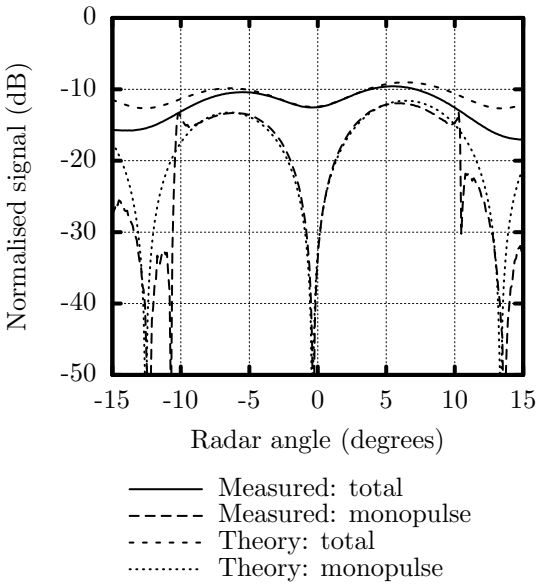

(b) The total difference-channel return and the portion of the difference-channel return used to form the monopulse indicated angle.

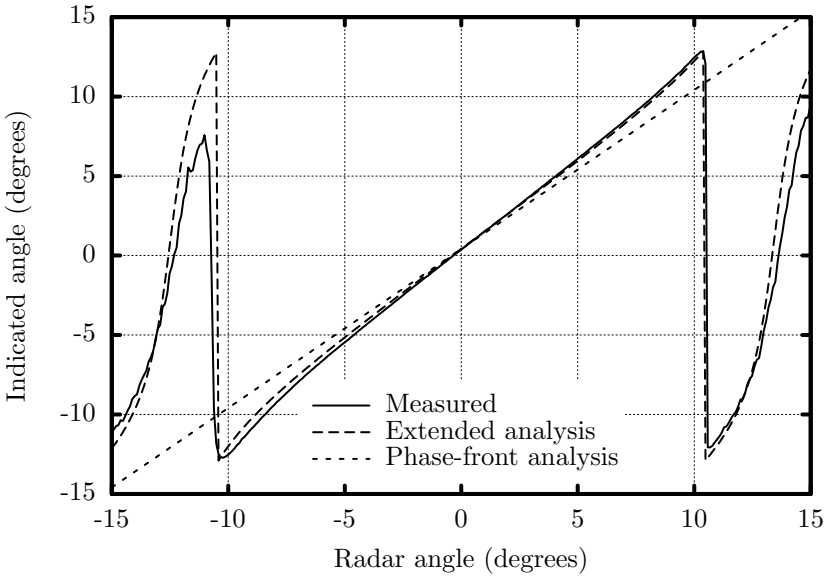

(c) Indicated angle.

Figure 5.16: Monopulse signals at 9.5 GHz for case 1 when the radar antennas were rotated. The relative amplitude and phase shift are −0.72 dB and 120.1° respectively giving a cross-eye gain of 0.16, and the jammer antenna element spacing is 45% of the radar antenna beamwidth. (Reprinted, with permission, from [3]. ©2009 IEEE.)

The agreement between the measured data and the phase-front analysis is good in Figure 5.16(c) where the jammer phase shift is far from 180° making the cross-eye gain small. However, significant differences between the measured data and the phase-front analysis are seen in Figures 5.17(c) and 5.18(c) where the jammer phase shift is closer

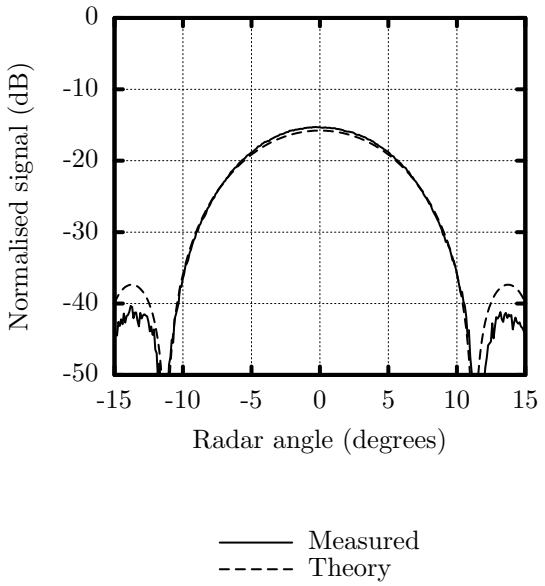

(a) Sum-channel return.

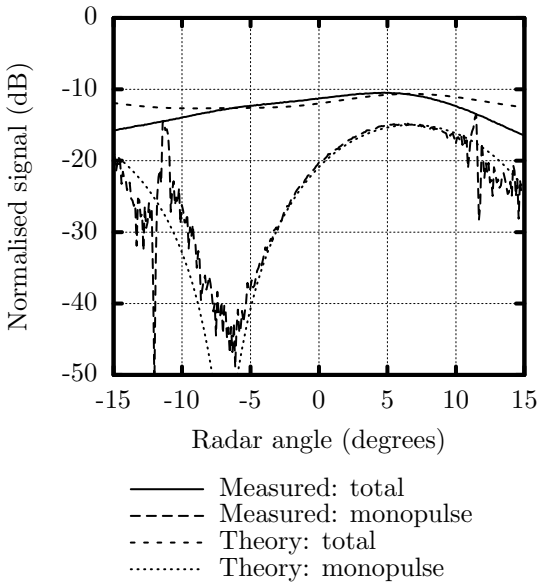

(b) The total difference-channel return and the portion of the difference-channel return used to form the monopulse indicated angle.

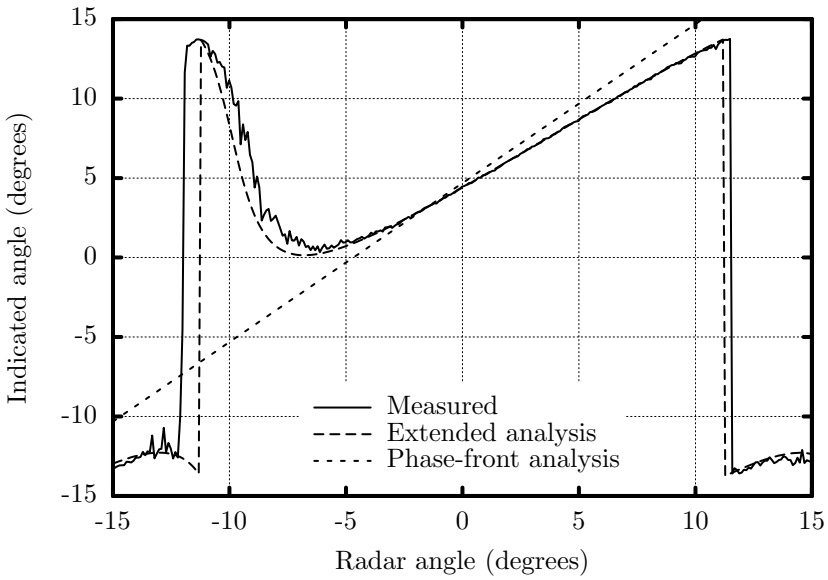

(c) Indicated angle.

Figure 5.17: Monopulse signals at 8.953 GHz for when case 1 the radar antennas were rotated. The relative amplitude and phase shift are −1.17 dB and 200.4° respectively giving a cross-eye gain of 1.9, and the jammer antenna element spacing is 39% of the radar antenna beamwidth. (Reprinted, with permission, from [3]. ©2009 IEEE.)

to 180°, increasing the cross-eye gain.

The agreement on boresight (0°) is very good in Figure 5.17(c) as expected based on the analysis in Section 4.2.2. However, the phase-front analysis predicts an error that is inside the sum-channel 3 dB beamwidth, while the measurements and extended

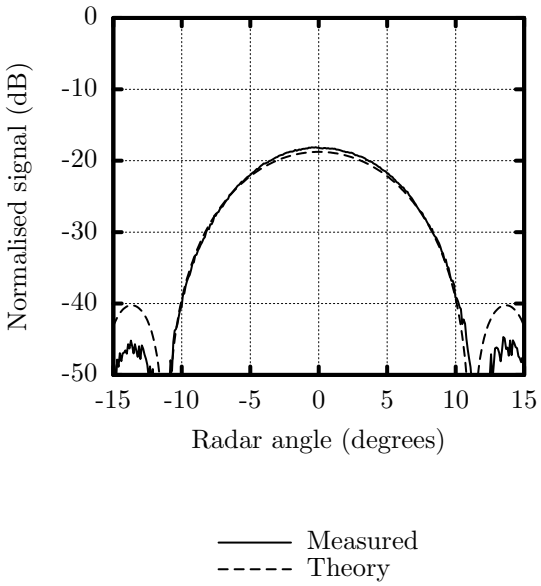

(a) Sum-channel return.

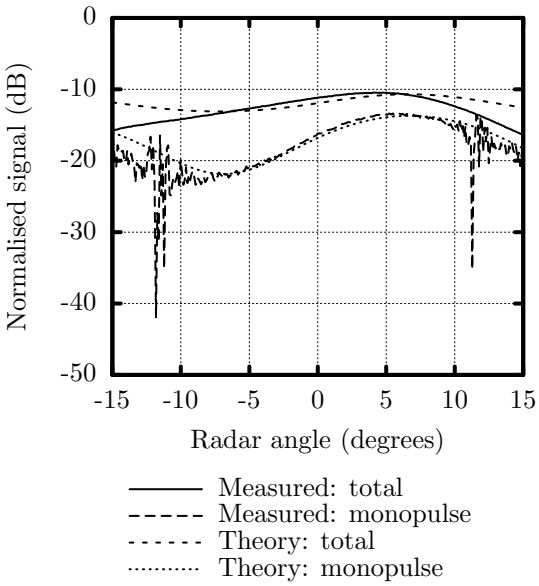

(b) The total difference-channel return and the portion of the difference-channel return used to form the monopulse indicated angle.

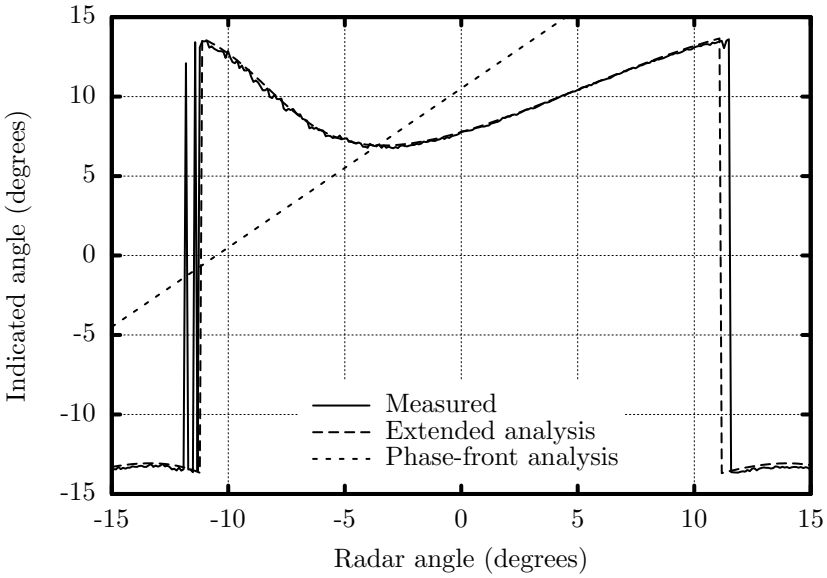

(c) Indicated angle.

Figure 5.18: Monopulse signals at 9.0 GHz for case 1 when the radar antennas were rotated. The relative amplitude and phase shift are −1.34 dB and 192.9° respectively giving a cross-eye gain of 4.2, and the jammer antenna element spacing is 40% of the radar antenna beamwidth. (Reprinted, with permission, from [3]. ©2009 IEEE.)

analysis show that the monopulse indicated angle never becomes zero anywhere in the sum-channel main beam. The error inherent in the phase-front analysis is even more significant in Figure 5.18(c) where jammer phase shift is close to 180° giving a high cross-eye gain.

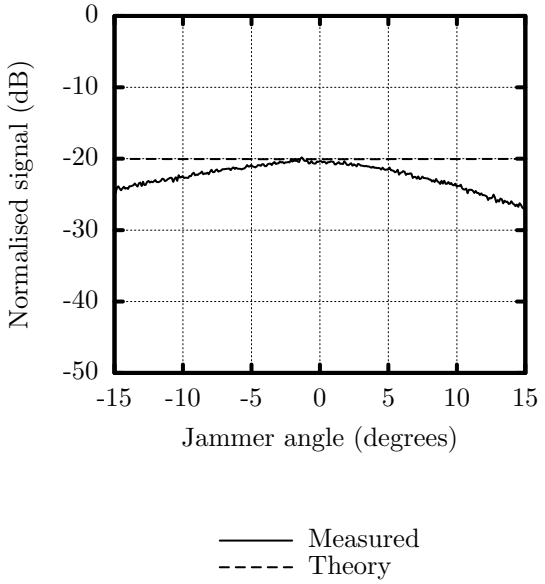

(a) Sum-channel return.

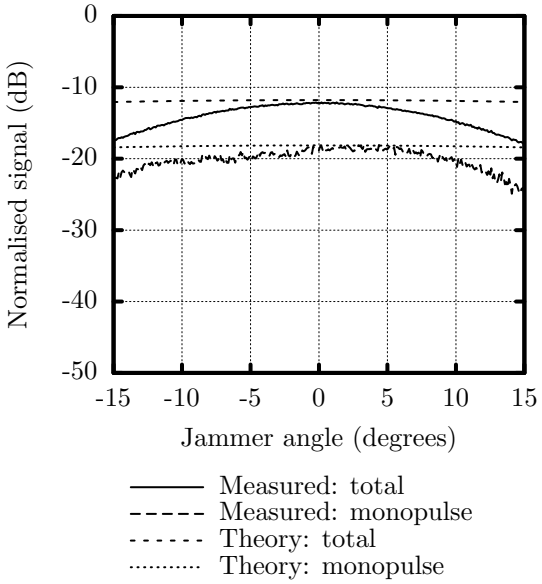

(b) The total difference-channel return and the portion of the difference-channel return used to form the monopulse indicated angle.

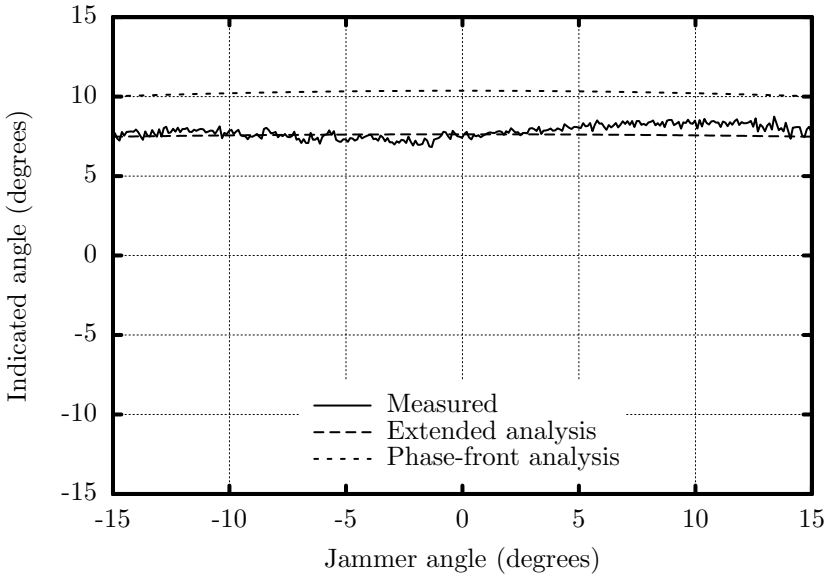

(c) Indicated angle.

Figure 5.19: Monopulse signals at 9.1219 GHz when the jammer antennas were rotated. The relative amplitude and phase shift are 0.84 dB and 190.2° respectively giving cross-eye gain of −4.7, and the jammer antenna element spacing is 46% of the radar antenna beamwidth.

The results when the jammer was rotated are presented in Figure 5.19. The main objective of these measurements was to validate the extended analysis' assertion that the jammer antenna element patterns have no effect on the monopulse indicated angle. The phase-front analysis implicitly echoes this conclusion because the gain of the jammer

antenna elements will not affect the phase-fronts created by the jammer as long as the antennas are identical.

The variations due to the antenna element patterns are again clearly visible in the sum- and difference-channel returns in Figures 5.19(a) and 5.19(b). However, the variation due to the jammer antenna element patterns is absent from the monopulse indicated angle in Figure 5.19(c) as expected. The small variations with angle seen in the difference-channel returns and indicated angle plots in Figure 5.19 are due to the fact that the projected spacing of the jammer antenna elements from the radar's perspective changes as the jammer system rotates.

The relative amplitude and jammer antenna element spacing as a proportion of the radar antenna's 3-dB beamwidth in Figure 5.16 are 0.9205 and 45% respectively, both of which violate Vakin and Shustov's bound [12, 16] highlighted in Section 2.4.2. Despite this, the agreement between the measurements and the phase-front analysis is good, confirming Section 2.4.2's assertion that Vakin and Shustov's bound does not adequately address all the factors that affect the validity of the phase-front analysis.

5.5 Concluding Remarks

Experimental results validating the extended analysis of retrodirective cross-eye jamming developed in Chapter 4 are presented in this chapter. The experiments properly approximate a retrodirective cross-eye jamming scenario by using the radar system for both transmission and reception, and by simulating a retrodirective cross-eye jammer. The experimental layout and data processing procedure used to achieve these objectives are outlined.

The measured data are compared to the traditional phase-front analysis as well as to the extended analysis of retrodirective cross-eye jamming. The results confirm the validity of the extended analysis for a wide range of amplitude and phase mismatch conditions between the two directions through the cross-eye jammer. The predicted monopulse indicated angle based on the phase-front analysis differs significantly from the measured results for relative phase shifts close to 180° which give high cross-eye gains.

Now that the extended analysis developed in Chapter 4 has been validated, Chapter 6 will analyse the amplitude and phase matching required between the two directions through a cross-eye jammer to achieve a specified angular error.

CHAPTER 6

TOLERANCE ANALYSIS

6.1 Introductory Remarks

The main objective of the research described in this thesis was to gain a more complete understanding of cross-eye jamming as a prelude to constructing practical systems. Chapter 4 presented an extended analysis of cross-eye jamming which was validated by the experiments described in Chapter 5. This chapter completes the analysis by considering the relationship between the magnitude of the angular error induced in the radar being jammed, and the amplitude and phase matching of the two directions through a retrodirective cross-eye jammer. The work described in this chapter forms the basis of a submitted journal paper [4].[1]

Closed-form solutions for the matching required from a retrodirective cross-eye jammer to achieve a specified angular error are derived in Section 6.2 for both the phase-front and extended analyses. Results are presented and compared in Section 6.3, and concluding remarks are provided in Section 6.4.

6.2 Mathematical Analysis

The basis of the analysis will be determining the angle where the monopulse indicated angle is zero. This angle will be referred to as the "settling angle." The settling angle is trivial to determine for the phase-front analysis, but as demonstrated in Section 4.3, might not exist for the extended analysis.

The performance of a cross-eye jammer implementation can be characterised by an "angle factor" defined as

$$G_\theta = \left|\frac{\theta_s}{\theta_e}\right| \tag{6.1}$$

where θ_s is the setting angle. When the angle factor is greater than one, the apparent target created by a cross-eye jammer will be outside the physical extent of the cross-eye jammer at all except very short ranges where the angular separation of the jammer antenna elements becomes large enough for the radar to resolve them.

The angle factor and the magnitude of the cross-eye gain will be shown to be identical in the phase-front analysis case (part of the motivation for the definition of cross-eye gain), but not for the extended analysis. To avoid confusion, the term "angle factor" will be used when the relationship between settling angle and jammer antenna separation is intended, while the term "cross-eye gain" will be reserved for the relationship in (2.10) on page 13.

[1] Portions of this chapter are reprinted, with permission, from [4].

6.2.1 Phase-Front Analysis

The indicated angle for the phase-front analysis is given by (2.9) on page 13 and is repeated below for reference.

$$\theta_i = \theta_r + \theta_e G_C \tag{6.2}$$

where the cross-eye gain G_C is defined in (2.10) on page 13 as [9]

$$G_C = \frac{1 - a^2}{1 + a^2 + 2a\cos(\phi)}. \tag{6.3}$$

The relationship between the cross-eye gain and settling angle for phase-front analysis can be determined by substituting θ_s for θ_r in (6.2) and solving for $\theta_i = 0$ giving

$$G_C = -\frac{\theta_s}{\theta_e}. \tag{6.4}$$

The magnitude of the cross-eye gain is thus equal to the angle factor defined in (6.1) for the phase-front analysis.

The definition of the tangent of θ_s gives

$$\tan(\theta_s) = \frac{d_o}{r} \tag{6.5}$$

$$\theta_s \approx \frac{d_o}{r} \tag{6.6}$$

where d_o is the distance from the centre of the jammer to the apparent target shown in Figure 4.1 on page 38, and θ_s is assumed to be small ($r \gg G_C d_c$). Using (6.6) and the accurate approximation to θ_e given in (B.12) on page 110 allows (6.4) to be rewritten as

$$\theta_s = -G_C \theta_e \tag{6.7}$$

$$\frac{d_o}{r} \approx -G_C \frac{d_c}{2r}\cos(\theta_c) \tag{6.8}$$

$$|d_o| \approx \left| G_C \frac{d_c}{2}\cos(\theta_c) \right| \tag{6.9}$$

where the approximation is due to the assumption that θ_s is small. Equation (6.9) suggests that a cross-eye jammer induces a linear offset that does not change with range in the radar being jammed, confirming the widely-held view highlighted in Section 2.4.1 [9,18,34]. This property of cross-eye jamming is particularly valuable because, as mentioned in Section 2.4.1, a fixed angular offset would not cause a missile to miss its target [24,34].

Relationships between a and ϕ that give a specified angle factor can now be derived by solving the cross-eye gain in (6.3) for a as ϕ as shown below.

$$G_S = \frac{1 - a^2}{1 + a^2 + 2a\cos(\phi)} \tag{6.10}$$

$$a^2 G_S + a2G_S\cos(\phi) + G_S = 1 - a^2 \tag{6.11}$$

$$a^2(G_S + 1) + a[2G_S\cos(\phi)] + (G_S - 1) = 0 \tag{6.12}$$

where G_S is the magnitude of the specified cross-eye gain (which, as shown in (6.4), is identical to the angle factor for the phase-front analysis). Equation (6.11) can be solved using the well-known solution to

$$ax^2 + bx + c = 0 \tag{6.13}$$

given by [73]

$$x = \frac{-b \pm \sqrt{b^2 - 4ac}}{2a} \tag{6.14}$$

leading to

$$a = \frac{-2G_S \cos(\phi) \pm \sqrt{4G_S^2 \cos^2(\phi) - 4(G_S + 1)(G_S - 1)}}{2(G_S + 1)} \tag{6.15}$$

$$= \frac{-G_S \cos(\phi) \pm \sqrt{G_S^2 \cos^2(\phi) + 1 - G_S^2}}{G_S + 1} \tag{6.16}$$

$$= \frac{-G_S \cos(\phi) \pm \sqrt{1 - [G_S \sin(\phi)]^2}}{1 + G_S} \tag{6.17}$$

where (4.31) on page 41 was used. Solving for ϕ starts with (6.11) and proceeds as shown below.

$$2aG_s \cos(\phi) = 1 - a^2 - G_S(1 + a^2) \tag{6.18}$$

$$\phi = \pm \arccos\left[\frac{1}{2a}\left(\frac{|1 - a^2|}{G_S} - 1 - a^2\right)\right] \tag{6.19}$$

where the relationship [73]

$$\cos(x) = \cos(-x) \tag{6.20}$$

was used. Using the fact that [73]

$$\cos(\pi \pm x) = -\cos(x) \tag{6.21}$$

and substituting $\phi = \pi \pm \phi_0$ into (6.19) gives

$$\phi_0 = \pm \arccos\left[-\frac{1}{2a}\left(\frac{|1 - a^2|}{G_S} - 1 - a^2\right)\right] \tag{6.22}$$

which restates the phase result in terms of how close the relative phase must be to 180°. These results can be used to determine the amplitude matching required to obtain a specified cross-eye gain for a given phase match, and the phase matching required to obtain a specified cross-eye gain for a given amplitude match.

Equations (6.17), (6.19) and (6.22) give the matching required to achieve exactly the specified cross-eye gain G_S. The cross-eye gain will be larger than G_S when a is between the two solutions to (6.17) and when ϕ_0 is between the two solutions to (6.22). This can be verified by evaluating the cross-eye gain in (6.3) for $a = -G_S \cos(\phi)/(1 + G_S)$ and $\phi = 180°$ ($\phi_0 = 0$) to confirm that $|G_C| > G_S$ in these cases.

Importantly, (6.19) and (6.22) give the same result when $a = x$ and when $a = 1/x$. These two cases are equivalent because they both signify that the gain of one direction through a cross-eye jammer differs from the gain in the other direction by the factor x.

Equation (6.17) only gives values of a with magnitudes less than 1, but the inverse of these results is clearly also valid. Values of a with magnitudes greater than 1 can be obtained from (6.17) by using $-G_S$ instead of G_S.

A very important result that arises from (6.17) is that the range of values of a for a given ϕ that gives a cross-eye gain magnitude of greater than G_S does not include $a = 1$ unless $\phi = 180°$. This means that the cross-eye gain can decrease as the amplitude match between the two directions through a cross-eye jammer approaches one.

6.2.2 Extended Analysis

The monopulse indicated angle obtained using the extended analysis derived in Section 4.2.1 is given in (4.86) on page 48, and is repeated below for reference.

$$\tan\left[\beta\frac{d_r}{2}\sin\left(\theta_i\right)\right] = \frac{\sin\left(2k\right) + \sin\left(2k_c\right)G_C}{\cos\left(2k\right) + \cos\left(2k_c\right)} \tag{6.23}$$

where k and k_c are defined as

$$k = \beta\frac{d_r}{2}\sin\left(\theta_r\right)\cos\left(\theta_e\right) \tag{6.24}$$

and

$$k_c = \beta\frac{d_r}{2}\cos\left(\theta_r\right)\sin\left(\theta_e\right) \tag{6.25}$$

in (4.8) and (4.9) on page 39. Clearly the relationship between the settling angle and the jammer parameters is more complex for the extended analysis than for the phase-front analysis in the previous section. However, the problem of determining the settling angle is greatly simplified by noting that only the numerator of the right-hand side (6.23) has to be considered because the denominator of the right-hand side of (6.23) cannot be infinite.

Infinite Error

As noted in Section 4.3, there are conditions under which the monopulse indicated angle will never become zero implying that the settling angle does not always exist. This occurs when the numerator of the right-hand side of (6.23) is never equal to zero for all values of θ_r within the sum-channel's main beam. Determining whether this occurs requires a knowledge of how k_c varies within the sum-channel's main beam.

The signal received in the sum channel is given in (4.28) on page 41 and is repeated below for reference.

$$\begin{aligned} S_J = {} & P_r\left(\theta_r - \theta_e\right)P_c\left(\theta_c - \theta_e\right)P_r\left(\theta_r + \theta_e\right)P_c\left(\theta_c + \theta_e\right) \times \\ & \frac{1}{2}\left(1 + ae^{j\phi}\right)\left[\cos\left(2k\right) + \cos\left(2k_c\right)\right]. \end{aligned} \tag{6.26}$$

Comparing (6.23) and (6.26), it can be seen that the only portion of the sum-channel return that remains after monopulse processing is the trigonometric sum in the square brackets on the second line of (6.26). The first nulls of the radar's sum-channel beam will thus be when the denominator of the right-hand side of (6.23) is equal to zero.

The trigonometric portion of the sum-channel return given in (6.26) (the denominator of the right-hand side of (6.23)) can be rewritten as

$$\frac{1}{2}\left[\cos\left(2k\right)+\cos\left(2k_c\right)\right]=\cos\left(k-k_c\right)\cos\left(k+k_c\right) \tag{6.27}$$

$$=\cos\left[\beta\frac{d_r}{2}\sin\left(\theta_r\right)\cos\left(\theta_e\right)-\beta\frac{d_r}{2}\cos\left(\theta_r\right)\sin\left(\theta_e\right)\right]\times \cos\left[\beta\frac{d_r}{2}\sin\left(\theta_r\right)\cos\left(\theta_e\right)+\beta\frac{d_r}{2}\cos\left(\theta_r\right)\sin\left(\theta_e\right)\right] \tag{6.28}$$

$$=\cos\left[\beta\frac{d_r}{2}\sin\left(\theta_r-\theta_e\right)\right]\cos\left[\beta\frac{d_r}{2}\sin\left(\theta_r+\theta_e\right)\right] \tag{6.29}$$

where (4.5) on page 39 was used. Given that the radar must not be able to resolve the two cross-eye jammer antenna elements, θ_e must be much smaller than the value of θ_r where the sum-channel pattern becomes zero. This value can thus accurately be approximated by setting (6.29) equal to zero, assuming θ_e is negligible and solving for θ_r as shown below.

$$\cos\left[\beta\frac{d_r}{2}\sin\left(\theta_r\pm\theta_e\right)\right]=0 \tag{6.30}$$

$$\beta\frac{d_r}{2}\sin\left(\theta_r\right)\approx\pm\frac{\pi}{2} \tag{6.31}$$

$$\sin\left(\theta_r\right)\approx\pm\frac{\pi}{\beta d_r} \tag{6.32}$$

$$\theta_{rz}\approx\pm\arcsin\left(\frac{\lambda}{2d_r}\right) \tag{6.33}$$

where θ_{rz} is angle of the first null of the sum-channel pattern and λ is the wavelength, and the well-known relationship $\beta=2\pi/\lambda$ (e.g. [44, 45, 74]) was used to simplify the result. This result is slightly conservative because a nonzero value of θ_e will make the first sum-channel pattern zeros slightly nearer boresight than suggested by (6.33) as discussed in Section 5.4.

Noting that k_c reaches its maximum value when $\theta_r=0$ and substituting (6.33) into (6.25) gives

$$\beta\frac{d_r}{2}\theta_e\sqrt{1-\left(\frac{\lambda}{2d_r}\right)^2}<k_c\leq\beta\frac{d_r}{2}\theta_e \tag{6.34}$$

in the sum-channel main beam where a modified version of (4.31) on page 41 given by

$$\cos\left(x\right)=\sqrt{1-\sin^2\left(x\right)} \tag{6.35}$$

was used. The square-root factor in (6.34) will be very close to 1 because $2d_r$ is significantly larger than a wavelength (i.e. the beamwidth is narrow) in tracking radars, so it can be assumed that k_c does not vary appreciably within the sum-channel main beam.

As stated above, the settling angle will not exist when the numerator of the right hand side of (6.23) never becomes zero in the sum-channel main beam, so

$$\sin(2k) + \sin(2k_c)\, G_C \neq 0 \tag{6.36}$$
$$\sin(2k_c)\, G_C \neq -\sin(2k)\,. \tag{6.37}$$

Noting that (6.31) applies at the edges of the sum-channel main beam when θ_e is negligible leads to

$$\beta\frac{d_r}{2}\sin(\theta_r) \lessapprox \frac{\pi}{2} \tag{6.38}$$
$$k \lessapprox \frac{\pi}{2} \tag{6.39}$$
$$2k \lessapprox \pi \tag{6.40}$$

in the sum-channel main beam, which means that

$$|\sin(2k)| \leq 1 \tag{6.41}$$

in the sum-channel main beam because the argument of the sine includes the values $\pm\pi/2$. Using (6.41) in (6.37) gives

$$|\sin(2k_c)|\, G_I > 1 \tag{6.42}$$
$$G_I > \left|\frac{1}{\sin(2k_c)}\right| \tag{6.43}$$

where G_I is the minimum cross-eye gain magnitude required to ensure that the settling angle does not exist. Expanding k_c using the simplest form in (6.34) and eliminating θ_e using (B.12) on page 110 allows (6.43) to be rewritten as

$$G_I \gtrsim \frac{1}{\sin(\beta d_r \theta_e)} \tag{6.44}$$
$$\gtrsim \frac{\lambda}{\pi d_r} \times \frac{r}{d_c \cos(\theta_c)} \tag{6.45}$$

assuming that the angular separation of the jammer antennas (θ_e) is much smaller than the radar beamwidth (determined by the factor βd_r). The values of a, ϕ and ϕ_0 can now be obtained from (6.17), (6.19) and (6.22) by using the value of G_I from (6.45) for G_S.

Finite Error

The settling angle will exist when the above conditions are not satisfied, and is determined by the angle where the monopulse error is zero.

Solving (6.23) for the cross-eye gain when $\theta_i = 0$ gives

$$G_C = -\frac{\sin(2k)}{\sin(2k_c)}. \tag{6.46}$$

Expanding k when θ_e is small and using the largest value of k_c from (6.34) modifies (6.46) to give

$$G_C \approx -\frac{\sin\left[\beta d_r \sin\left(\theta_s\right)\right]}{\sin\left(\beta d_r \theta_e\right)} \tag{6.47}$$

which slightly underestimates the required cross-eye gain because the largest value of the denominator was used, though this is partially compensated by a small overestimation of the numerator.

Equation (6.47) reduces to the same form as the phase-front analysis result in (6.4) when both the settling angle (θ_s) and half the angular separation of the jammer antenna elements (θ_e) are much smaller than the radar beamwidth (determined by βd_r).

Noting that $G_S = |G_C|$ by definition and that $|\theta_s| = G_\theta \theta_e$ from (6.1), allows (6.47) to be rewritten as

$$G_S \approx \frac{\sin\left[\beta d_r \sin\left(G_\theta \theta_e\right)\right]}{\sin\left(\beta d_r \theta_e\right)} \tag{6.48}$$

allowing the values of a, ϕ and ϕ_0 for a specified angle factor to be obtained by determining G_S from (6.48) and using (6.17), (6.19) and (6.22) to calculate a, ϕ and ϕ_0.

The trigonometric functions in (6.48) mean that it is not possible to obtain a simple relationship between the linear error and either the cross-eye gain or the angle factor for the extended analysis. However, the trigonometric functions can be approximated by their arguments when the angular separation of the jammer antenna elements is much smaller than the radar beamwidth ($\theta_e \ll \beta d_r$) and the product of the angle factor and the jammer antenna element angular separation is small ($G_\theta \theta_e$ is small) reducing (6.48) to

$$G_S \approx \frac{\beta d_r G_\theta \theta_e}{\beta d_r \theta_e} \tag{6.49}$$

$$\approx G_\theta \tag{6.50}$$

again confirming Chapter 4's assertion that the extended analysis converges to the phase-front analysis when the arguments of the trigonometric functions are small.

6.3 Results and Comparison

The same parameters typical of a missile threat against an aircraft or ship given in Section 4.3 will be used to examine the results derived in Section 6.2 and are repeated below for reference.

- 10° radar antenna beamwidth ($d_r = 2.54$ wavelengths, and each radar antenna element is a uniformly-excited aperture 2.54 wavelengths long),
- the jammer antenna elements are uniformly-excited apertures 2.54 wavelengths long,
- 1 km jammer range ($r = 1$ km),
- 10 m jammer antenna element separation ($d_c = 10$ m), and
- 30° jammer rotation ($\theta_c = 30°$).

The total angular separation of the cross-eye jammer antenna elements as seen by the radar for the parameters above is 0.4962° ($\theta_e = 0.2481°$), which is 5.0% of the radar

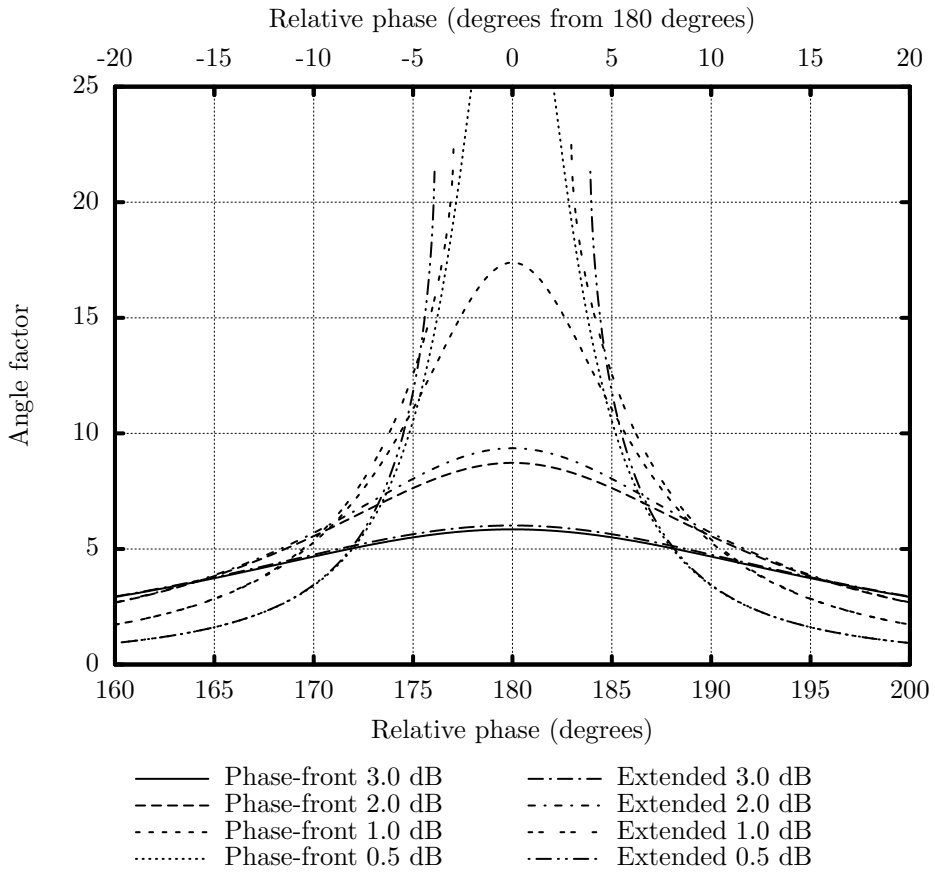

Figure 6.1: The angle factor for the scenario described in the text. The relative amplitude and phase shift of the two directions through the cross-eye jammer for each curve are indicated, and the jammer antenna element spacing is 5.0% of the radar antenna beamwidth.

antenna's 3-dB beamwidth. In all cases the relative amplitude and phase shift of the two directions through the cross-eye jammer are provided on the figures.

The relationship between a and ϕ is generally represented using a plot of the angle factor as a function of ϕ for a number of values of a (e.g. $[9, 12, 13, 18, 20, 25]$) as shown in Figure 6.1. Similar graphs are found in the glint literature (e.g. $[17, 30, 31, 38, 43, 48]$) reflecting cross-eye jamming's origin.

From Figure 6.1, the agreement between the results using the two analyses is seen to be excellent when the relative phase shift of the two directions through the jammer is far from 180° giving low cross-eye gain. However, significant differences between the phase-front and extended analyses emerge when the relative phase shift is close to 180° because the cross-eye gain becomes large. These conclusions agree well with the results in Chapters 4 and 5.

The plot of the results using the extended analysis with relative amplitudes of 1 dB and 0.5 dB end abruptly when the relative phase shifts are 2.95° and 3.90° away from 180° respectively because the settling angle does not exist in these cases.[2] These results

[2]Note that the phase-front results for a relative amplitude of 0.5 dB are defined for all angles and reach a maximum value of 34.75 at 180°.

agree well with the values of 2.97° and 3.91° obtained by determining ϕ_0 from (6.22) using the minimum cross-eye gain from (6.45).

While plots of the angle factor like Figure 6.1 are valuable, contour plots based on (6.17), (6.19), (6.22) and (6.48) as shown in Figure 6.2 are believed to be more useful. The specified angle factor will be achieved whenever the combination of a and ϕ is on a constant angle-factor contour and exceeded whenever the combination of a and ϕ is inside the contour. Figure 6.1 is effectively a number of horizontal cuts through the contour plots in Figure 6.2.

The contours in Figure 6.2 are plotted assuming that $|a| \leq 1$, so all the decibel values are negative. As mentioned in Section 6.2.1, $a = x$ and $a = 1/x$ represent equivalent cross-eye jammers, so the decibel values in Figure 6.2 can be interpreted as being either positive or negative.

The fact that improving the amplitude match between the two directions through a cross-eye jammer can lead to a lower angle factor as discussed in Section 6.2.1 is clearly demonstrated in Figure 6.2. This leads to the interesting conclusion that designing for a surprisingly large amplitude mismatch is actually the best way to achieve a specified angle factor. This characteristic of cross-eye jammers has been known for some time [16, 34], but the results in Section 6.2 and the contour plots in Figure 6.2 give clear quantitative and qualitative descriptions of this effect.

The amplitude and phase matching required to achieve a specified cross-eye gain for a given phase or amplitude match is considered in (6.17), (6.19) and (6.22) in Section 6.2.1. However, optimum tolerances to both amplitude and phase variations for a specified cross-eye gain can be achieved by designing the system for the parameters at the centre of the relevant contour in Figure 6.2. From (6.17), (6.19) and (6.22), this requires a relative phase shift of 180° and a relative amplitude of

$$a = \frac{G_S}{G_S + 1} \tag{6.51}$$

where G_S is determined either directly or from (6.48) depending on whether the phase-front or extended analysis is considered. As before, the inverse of the amplitude in (6.51) represents an equivalent solution.

The main difference between the results in Figures 6.2(a) and 6.2(b) is that the extended analysis shows that the tolerance requirements for the scenario considered are less strict than the phase-front analysis suggests. This can be seen by the fact that the contours in Figure 6.2(b) are larger than the equivalent contours in Figure 6.2(a). Furthermore, Figure 6.2(b) has a contour that gives an infinite error because the settling angle does not exist for the cross-eye jammer parameters bounded by this contour. These conclusions mirror those of Chapters 4 and 5.

Chapter 4 shows that the extended analysis converges to the phase-front analysis at longer ranges where the angular separation of the jammer antennas is small. This is explored by plotting constant angle-factor contours for the same scenario as Figure 6.2, but at a range of 10 km in Figure 6.3. As expected, the agreement between the results for the extended analysis in Figure 6.3 and those for the phase-front analysis in Figure 6.2(a) is extremely good because the angular separation of the jammer antenna elements is very small in Figure 6.3.

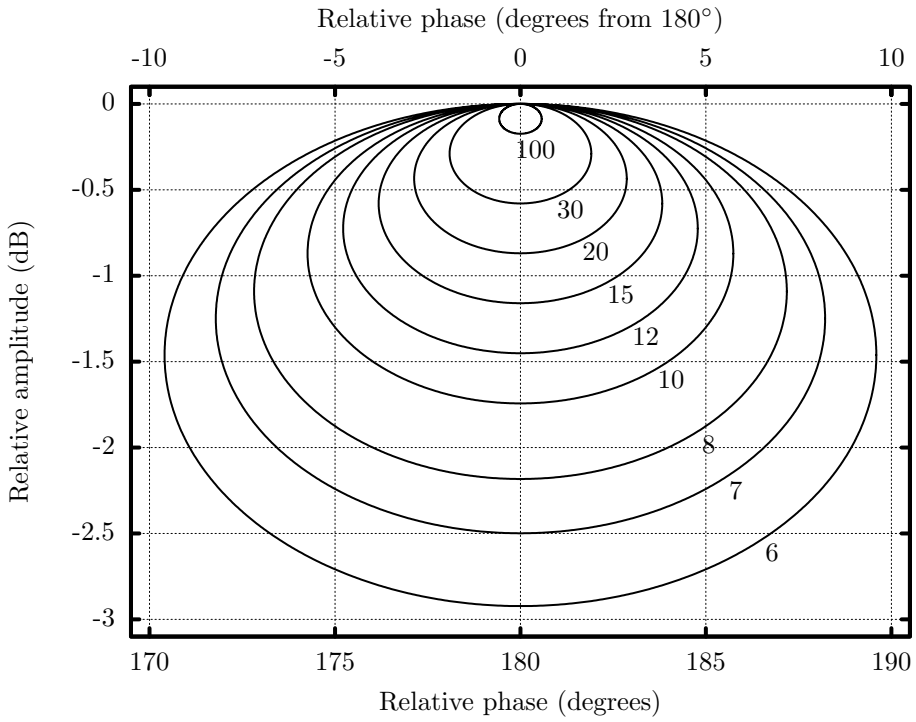

(a) Phase-front analysis.

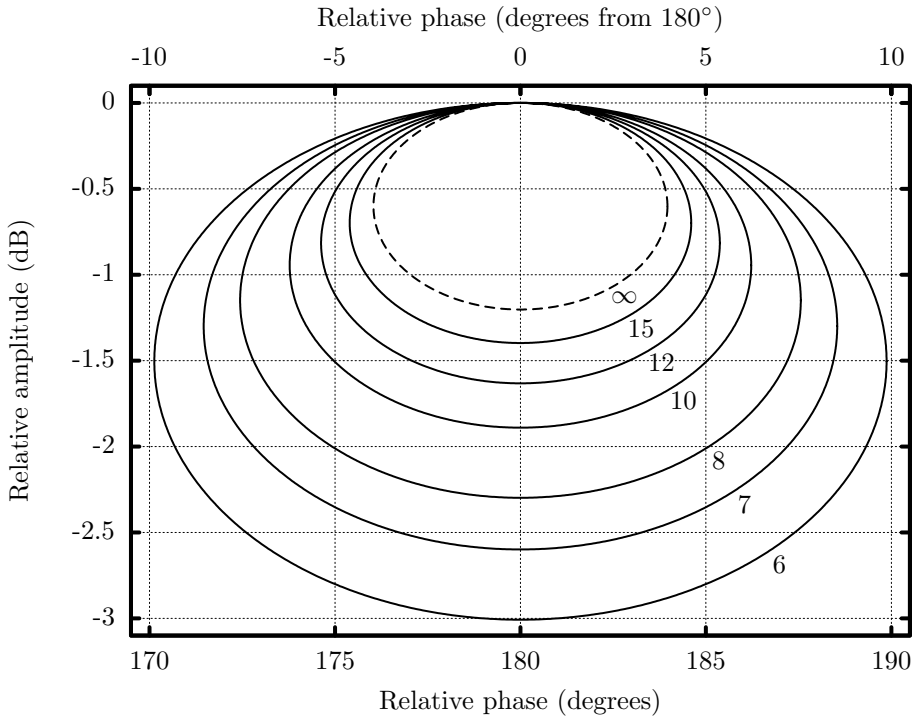

(b) Extended analysis.

Figure 6.2: Contours of constant angle factor for the engagement described in the text. The relative amplitude and phase shift of the two directions through the cross-eye jammer for each curve are indicated, and the jammer antenna element spacing is 5.0% of the radar antenna beamwidth. (Reprinted, with permission, from [4]. ©2009 IEEE.)

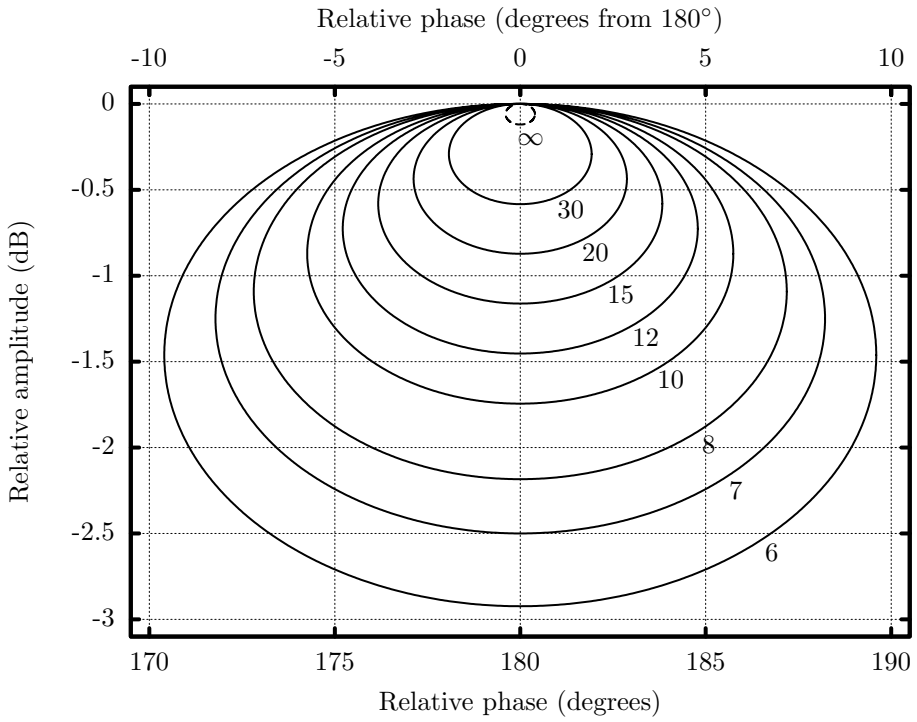

Figure 6.3: Contours of constant angle factor according to the extended analysis for the engagement described in the text, but at range of 10 km. The relative amplitude and phase shift of the two directions through the cross-eye jammer for each curve are indicated, and the jammer antenna element spacing is 0.50% of the radar antenna beamwidth. (Reprinted, with permission, from [4]. ©2009 IEEE.)

6.4 Concluding Remarks

Closed-form solutions for the amplitude and phase matching between the two directions through a retrodirective cross-eye jammer required to achieve a specified angular error are presented. The results were derived for both the phase-front and extended analyses. Contour plots that give a clear graphical representation of the relationship between the matching and angular error are provided. Lastly, the combination of jammer parameters that achieves a specified angular error with the optimum tolerance to both amplitude and phase variations is proposed.

The main conclusion from these results is that the tolerance requirements on a cross-eye jammer system are not as strict as the phase-front analysis suggests. Another important conclusion is that the angular error induced in the radar being jammed can decrease as the amplitude matching of the two directions through a cross-eye jammer improves.

Cross-eye jamming is analysed using a model applicable to any monopulse radar in Chapter 4, and the results are confirmed through the experiments described in Chapter 5. This chapter addresses the remaining objectives of this study listed in Section 1.3.2 by investigating the tolerances required from a cross-eye jammer system.

CHAPTER 7

CONCLUSIONS AND FUTURE RESEARCH

7.1 General Conclusions

Cross-eye jamming is an EA technique that seeks to induce an angular error in the radar being jammed with the aim of protecting platforms against radar-guided missiles. The main benefit of cross-eye jamming is that it is effective against monopulse radars. Despite the fact that the concept of cross-eye jamming has existed since the 1950s, only recently have practical cross-eye jammers been implemented.

The objective of this work was to obtain a comprehensive theoretical understanding of cross-eye jamming as a prelude to the construction of practical cross-eye jammers. This is essential to ensure that future cross-eye jammers are correctly specified and that the main engineering challenges associated with the realisation of practical cross-eye jammers are understood.

This objective has been addressed by performing a comprehensive, rigorous mathematical analysis of a single-loop, isolated, retrodirective cross-eye jammer scenario as described in Chapter 4. This analysis was validated by the laboratory experiments outlined in Chapter 5, which are representative of a retrodirective cross-eye jamming scenario because the radar is used for both transmission and reception, and a retrodirective cross-eye jammer is correctly simulated. These results were shown to be applicable to any type of monopulse radar by proving that a generalised phase-comparison monopulse antenna can be used to model any monopulse antenna in Chapter 3. Lastly, the relationship between the matching required from the two directions through a retrodirective cross-eye jammer and the angular error induced in the radar being jammed was investigated in Chapter 6.

The main results of this study are summarised below.

Monopulse antenna model: It has been proved that a generalised phase-comparison monopulse antenna will accurately represent any monopulse antenna near boresight. This phase-comparison monopulse antenna model is accurate over a significantly wider range of angles than the existing linear-fit model.

Sum-channel effects: No angular error is induced in the sum channel of a monopulse radar because of the retrodirective implementation of cross-eye jamming considered. By extension this means that a retrodirective cross-eye jammer will have no effect on any radar that uses the same antenna beam for both transmission and reception (e.g. some types of conical-scan radar). This contradicts the current theory that cross-eye jamming affects all types of radar because glint affects all types of radar.

Phase-front analysis limitations: The analyses of glint used to motivate cross-eye

jamming are inaccurate when the relative phase shift of the two directions through a cross-eye jammer approaches 180°, particularly when the jammer antenna element angular separation as seen by the radar being jammed is large. The angular error achieved by a retrodirective cross-eye jammer will be larger than predicted by the conventional analyses.

Settling angle existence: There are conditions under which the monopulse error never becomes zero within the sum-channel main beam. This suggests that a cross-eye jammer can be used to break a monopulse radar's lock. This is in stark contrast to the view that the error induced by a cross-eye jammer will be smaller than the sum-channel antenna's 3-dB beamwidth.

Sensitivity to tolerances: The parameters required to induce a specified angular error in the radar being jammed are derived. The amplitude and phase mismatches between the two directions through a retrodirective cross-eye jammer that give the optimum design are quantified and graphically described. A surprisingly large amplitude mismatch between the two directions through a cross-eye jammer is shown to give the lowest sensitivity to system tolerances. While this fact has been known for some time, this is the first time detailed qualitative and quantitative analyses have been presented.

Antenna element patterns: The patterns of the antenna elements used to form the phase-comparison monopulse radar and the cross-eye jammer have no effect on the induced angular error. The gains of the antenna elements do however affect the strengths of the signals received in the sum and difference channels of the radar being jammed. This result agrees with existing cross-eye jammer theory.

The main implications of this work for the construction of a practical retrodirective cross-eye jammer are outlined below.

Effect on different types of radar: Retrodirective cross-eye jamming does not affect radars that use the same antenna beam for both transmission and reception (e.g. some types of conical-scan radar). Alternative means of jamming such radars will thus have to be used, but this is not a significant problem because effective countermeasures exist for these radars.

Error magnitude: The error induced by a retrodirective cross-eye jammer is larger than suggested by the conventional phase-front analysis, particularly when the jammer antenna element separation as seen by the radar being jammed is large. Under certain conditions, it is even theoretically possible to break a monopulse radar's lock on a target using only a retrodirective cross-eye jammer.

Required matching: A retrodirective cross-eye jammer should be designed for a small amplitude mismatch on the order of 0.5 dB and a relative phase shift between the two directions through the jammer of 180° to achieve optimum tolerance to system parameter variations.

7.2 Future Research

From the outset of this work, the scope was limited as discussed in Section 1.3.1. The limitations in the scope of this study are critically re-evaluated below.

Retrodirective implementation: As shown in Section 2.5, the challenges associated with implementing a non-retrodirective cross-eye jammer are extreme. It is thus unlikely that analysing other implementations of cross-eye jamming will be useful.

Isolated case: Difficulties and delays associated with ensuring a successful pull off mean that it will not always be possible to isolate a cross-eye jammer's return from the skin return of the platform mounting the jammer. This suggests that a consideration of the case where the jammer return competes with platform skin return will be useful.

Single jammer loop: The case of multiple cross-eye jammer loops has been considered in the open literature [20,63], and there are indications that this approach reduces the system tolerance requirements associated with a cross-eye jammer. However, these analyses are based on the phase-front analysis, so it is possible that the results obtained have limited accuracy. An analysis of multiple retrodirective cross-eye jammer loops is thus likely to be valuable.

Analyses of the effect of skin return and multiple retrodirective cross-eye jammer loops have already been initiated.

Other possible applications of the results of this study are considered below.

Glint analysis: The analyses of glint have been shown to be inaccurate under certain conditions relevant to cross-eye jamming. The application of the results of this thesis to glint should be investigated to determine whether similar inaccuracies exist in the analysis of glint.

Multipath mitigation: Multipath is a major problem that affects the tracking accuracy of radar systems. Glint analyses are often used as a basis for investigating multipath effects (e.g. [15, 17, 30, 31, 40]), so it is possible that the results of this thesis can be usefully applied to multipath mitigation.

Countermeasures: The possibility of developing countermeasures to cross-eye jamming based on the results presented here should be considered. While there are suggestions [22, 77] that such countermeasures exist, no details are given due to military security restrictions.

References

[1] W. P. du Plessis, J. W. Odendaal, and J. Joubert, "A generic model of monopulse antennas," *IEEE Transactions on Aerospace and Electronic Systems*, submitted for publication.

[2] ——, "Extended analysis of retrodirective cross-eye jamming," *IEEE Transactions on Antennas and Propagation*, vol. 57, no. 9, pp. 2803–2806, September 2009.

[3] ——, "Experimental validation of retrodirective cross-eye jamming," *IEEE Transactions on Aerospace and Electronic Systems*, submitted for publication.

[4] ——, "Tolerance analysis of cross-eye jamming systems," *IEEE Transactions on Aerospace and Electronic Systems*, submitted for publication.

[5] J. Clifford, "Maneuver in the electromagnetic domain - you've got to be in it to win it!" *Journal of Electronic Defence*, vol. 33, no. 1, pp. 33–36, January 2010.

[6] D. C. Schleher, *Introduction to electronic warfare.* Artech House, 1986.

[7] A. Farina, "Electronic counter-countremeasures," in *Radar Handbook*, 2nd ed., M. I. Skolnik, Ed. McGraw-Hill, 1990, ch. 9.

[8] R. N. Lothes, M. B. Szymanski, and R. G. Wiley, *Radar vulnerability to jamming.* Artech House, 1990.

[9] F. Neri, *Introduction to electronic defense systems.* Artech House, 1991.

[10] D. C. Schleher, *Electronic warfare in the information age.* Artech House, 1999.

[11] D. L. Adamy, *EW 101: A first course in electronic warfare.* Artech House, 2001.

[12] S. A. Vakin and L. N. Shustov, "Principles of jamming and electronic reconnaissance - volume I," U.S. Air Force, Tech. Rep. FTD-MT-24-115-69, AD692642, 1969.

[13] A. I. Leonov and K. I. Fomichev, "Monopulse radar," U.S. Air Force, Tech. Rep. FTD-MT-24-982-71, AD742696, 1972.

[14] B. L. Lewis and D. D. Howard, "Security device," U.S.A. Patent 4 006 478, February 1, 1977.

[15] A. I. Leonov and K. I. Fomichev, *Monopulse radar.* Artech House, 1986.

[16] A. Golden, *Radar Electronic Warfare*. AIAA Inc., 1987.

[17] D. K. Barton, *Modern radar system analysis*. Artech House, 1988.

[18] F. Neri, "Anti-monopulse jamming techniques," in *Proc. 2001 SBMO/IEEE MTT-S Microwave and Optoelectronics Conf.*, vol. 2, 2001, pp. 45–50.

[19] L. Falk, C. Arvidsson, S. Berglund, and A. Eneroth, "Simple derivation of crosseye jamming principles," in *MilTech 2 Conf.*, 25–26 October 2005, pp. 93–100.

[20] N. M. Harwood, W. N. Dawber, V. A. Kluckers, and G. E. James, "Multiple-element crosseye," *IET Radar Sonar Navigation*, vol. 1, no. 1, pp. 67–73, February 2007.

[21] L. Falk, "Cross-eye jamming of monopulse radar," in *IEEE Waveform Diversity & Design Conf.*, 4–8 June 2007, pp. 209–213.

[22] G. W. Stimson, *Introduction to airborne radar*, 2nd ed. SciTech Publishing, 1998.

[23] D. C. Jenn. (2004) Microwave devices & radar lecture notes volume iv. Naval Postgraduate School. Ver. 4.7.2. [Online]. Available: http://www.dcjenn.com/EC4610/VolIV(v4.7.2).pdf

[24] T. W. Tucker and B. Vidger, "Cross-eye jamming effectiveness," Tactical Technologies Inc., Ottawa, ON K2A 3V6, Tech. Rep., 2009.

[25] L. B. Van Brunt, *Applied ECM*. EW Engineering, Inc., 1978, vol. 1.

[26] G. J. Meyer, "Using cross-eye techniques to counter the frequency agile monopulse processing," Master's thesis, Air Force Institute of Technology, Air University, December 1997.

[27] M. J. Sparrow, N. J. Wayne, and J. Cikalo, "High precision range measurement technique," U.S.A. Patent 6 492 937, December 10, 2002.

[28] F. Neri, "Experimental testing on cross-eye jamming," in *AOC Conference*, 2000.

[29] (2009, September) Excellence in electronic warfare. Elettronica S.p.a. [Online]. Available: http://www.elettronica-roma.com/en/company/history_90-00.html

[30] S. M. Sherman, *Monopulse principles and techniques*. Artech House, 1984.

[31] D. D. Howard, "Tracking radar," in *Radar Handbook*, 2nd ed., M. I. Skolnik, Ed. McGraw-Hill, 1990, ch. 18.

[32] A. Ivanov, "Radar guidance of missiles," in *Radar Handbook*, 2nd ed., M. I. Skolnik, Ed. McGraw-Hill, 1990, ch. 19.

[33] D. L. Adamy, *EW 102: A second course in electronic warfare*. Artech House, 2004.

[34] P. E. Redmill, "The principles of artificial glint jamming ("cross eye")," Royal Aircraft Establishment (Farnborough), Tech. note RAD. 831, March 1963.

[35] G. E. Johnson, "Jamming passive lobing radars," *Electronic Warfare*, vol. 9, pp. 75–85, April 1977.

[36] J. W. Wright, "Radar glint – a survey," *Electromagnetics*, vol. 4, no. 2, pp. 205–227, January 1984.

[37] R. H. Delano, "A theory of target glint or angular scintillation in radar tracking," *Proceedings of the IRE*, vol. 41, no. 12, pp. 1778–1784, December 1953.

[38] J. E. Meade, "Target considerations," in *Guidance*, A. S. Locke, *et al.*, Ed. D. Van Nostrand Co., Inc., 1955, ch. 11, pp. 435–444.

[39] Y. Stratakos, G. Geroulis, and N. Uzunoglu, "Analysis of glint phenomenon in a monopulse radar in the presence of skin echo and non-ideal interferometer echo signals," *Journal of Electromagnetic Waves and Applications*, vol. 19, no. 5, pp. 697–711, 2005.

[40] S. M. Sherman, "Complex indicated angles applied to unresolved radar targets and multipath," *IEEE Transactions on Aerospace and Electronic Systems*, vol. 7, no. 1, pp. 160–170, January 1971.

[41] D. D. Howard, "Radar target angular scintillation in tracking and guidance systems based on echo signal phase front distortion," in *Proc. Nat. Eng. Conf.*, vol. 15, 1959, reprinted in Radars, Vol. 4, Radar Resolution & Multipath Effects, David K. Barton, Ed., Artech House, 1975.

[42] J. E. Lindsay, "Angular glint and the moving, rotating, complex radar target," *IEEE Transactions on Aerospace and Electronic Systems*, vol. 4, no. 2, pp. 164–173, March 1968.

[43] J. H. Dunn and D. D. Howard, "Radar target amplitude, angle, and doppler scintillation from analysis of the echo signal propagating in space," *IEEE Transactions on Microwave Theory and Techniques*, vol. 9, no. 9, pp. 715–728, September 1968.

[44] C. A. Balanis, *Antenna theory: analysis and design*, 2nd ed. John Wiley & Sons, Inc., 1997.

[45] W. L. Stutzman and G. A. Thiele, *Antenna theory and design*, 2nd ed. John Wiley & Sons, Inc., 1998.

[46] H. Yin and P. Huang, "Unification and comparison between two concepts of radar target angular glint," *IEEE Transactions on Aerospace and Electronic Systems*, vol. 31, no. 2, pp. 778–783, April 1995.

[47] P. J. Kajenski, "Comparison of two theories of angle glint: polarization considerations," *IEEE Transactions on Aerospace and Electronic Systems*, vol. 42, no. 1, pp. 206–210, January 2006.

[48] R. V. Ostrovityanov, "Angular noise," *Radio engineering and electronic physics (Russia)*, vol. 11, pp. 507–515, 1966.

[49] P. T. Bryant, J. F. Weller, and L. Goldberg, "Bi-directional optical transmission system for RF electrical energy," U.S.A. Patent 5 066 148, November 19, 1991.

[50] W. K. Huggett, "Method and system of producing phase front distortion," U.S.A. Patent 5 583 504, December 10, 1996.

[51] B. H. Labitt, "Electronic countermeasures system," U.S.A. Patent 6 297 762, October 2, 2001.

[52] L. A. Gross, S. Amoroso Jr, R. W. Conklin, and J. Gessaroli, "Dual common channel cross-track system (U)," U.S.A. Patent 6 614 381, September 2, 2003.

[53] W. K. Huggett, "Electric signalling system," U.S.A. Patent 6 633 251, October 14, 2003.

[54] M. J. Sparrow, N. J. Wayne, and J. Cikalo, "Cross-eye technique implementation," U.S.A. Patent 6 885 333, April 26, 2005.

[55] W. V. Moffat, "Electronic counter-measure system for aircraft," U.S.A. Patent 5 153 594, October 6, 1992.

[56] L. C. Van Atta, "Electromagnetic reflector," U.S.A. Patent 2 908 002, Oct. 6, 1959.

[57] E. Sharp and M. Diab, "Van Atta reflector array," *IEEE Transactions on Antennas and Propagation*, vol. 8, no. 4, pp. 436–438, July 1960.

[58] T. Larsen, "Reflector arrays," *IEEE Transactions on Antennas and Propagation*, vol. 14, no. 6, pp. 689–693, November 1966.

[59] J. Appel-Hansen, "A Van Atta reflector consisting of half-wave dipoles," *IEEE Transactions on Antennas and Propagation*, vol. 14, no. 6, pp. 694–700, November 1966.

[60] E. Nielsen, "Square Van Atta reflector with conducting mounting plane," *IEEE Transactions on Antennas and Propagation*, vol. 18, no. 1, pp. 48–54, January 1970.

[61] S. J. Chung and K. Chang, "A retrodirective microstrip antenna array," *IEEE Transactions on Antennas and Propagation*, vol. 46, no. 12, pp. 1802–1809, December 1998.

[62] S. Drabowitch, A. Papiernik, H. D. Griffiths, J. Encinas, and B. L. Smith, *Modern antennas*, 2nd ed. Springer, 2005.

[63] C. Musso and C. Curt, "Robustness of a new angular counter-measure," in *Radar 97*, 14–16 October 1997, pp. 415–419.

[64] F. Neri, "Considering cross-eye," Letter to the Journal of Electronic Defence, June 2007.

[65] A. Eneroth, S. Berglund, A. D. Johansson, A. Ouacha, and R. Gunnarsson, "Novel miniaturized radar CM system," in *7th International Symposium and Exhibition*. AOC Australian Chapter, May 2008.

[66] C. Kopp. (2008, March) The Russian philosophy of beyond visual range air combat. [Online]. Available: http://www.ausairpower.net/APA-Rus-BVR-AAM.html

[67] (2009, May) Eurofighter technology and performance: defences. [Online]. Available: http://typhoon.starstreak.net/Eurofighter/defences.html

[68] (2009, February) Sorbtsiya radar jammer (Russian Federation), airborne electronic warfare (EW) systems. Jane's. Extract from Jane's Avionics. [Online]. Available: http://www.janes.com/articles/Janes-Avionics/Sorbtsiya-radar-jammer-Russian-Federation.html

[69] R. J. Mailloux, *Phased Array Antenna Handbook*. Artech House, 1994.

[70] J. R. Moore, "Unified S-band 30-foot antenna side lobe radiation," NASA Goddard Space Flight Centre, Greenbelt, Maryland, Tech. Rep. NASA-TM-X-55436, X-513-65-43, February 1965.

[71] K. Goodman, 22 October 2009, private communication. [Online]. Available: http://www.q-par.com/products/reflector-antennas/1-2-m-monopulse-cassegrain-reflector-antenna

[72] J. A. Nelder and R. Mead, "A simplex method for function minimization," *Computer Journal*, vol. 7, no. 4, pp. 308–313, January 1965.

[73] M. R. Spiegel and J. Liu, *Mathematical Handbook of Formulas and Tables*, 2nd ed., ser. Schaum's Outline Series. McGraw-Hill, 1999.

[74] D. M. Pozar, *Microwave Engineering*, 2nd ed. John Wiley & Sons, Inc., 1998.

[75] F. J. Harris, "On the use of windows for harmonic analysis with the discrete Fourier transform," *Proceedings of the IEEE*, vol. 66, no. 1, pp. 51–83, January 1978.

[76] M. H. Hayes, *Schaum's outline of theory and problems of digital signal processing*, ser. Schaum's outline series. McGraw-Hill, 1999.

[77] S. N. Vodopia, "Electronically roll stabilized and reconfigurable active array system," U.S.A. Patent 4 882 587, November 21, 1989.

APPENDIX A

TERMINOLOGY

While a significant body of literature exists on cross-eye jamming, no complete analysis of cross-eye jamming has been published. This means that no standard terminology has been established for a number of important cross-eye jamming concepts. An additional complication is that the extensive use of antenna array theory in this work could lead to confusion about the exact meaning of a number of terms. For example, the term "antenna" could refer to a complete monopulse antenna or the elements of the array comprising the complete monopulse antenna.

To rectify this deficiency, the meanings of a number of terms used throughout this thesis are summarised below.

antenna: A complete antenna. This term will usually be used in the context of a complete monopulse antenna or cross-eye jammer system that utilises a number of antenna elements.

antenna beam: A portion of a complete antenna. This term will usually be used to refer to the sum- and difference-channel beams of a monopulse antenna and the squinted antenna beams of an amplitude-comparison monopulse antenna.

antenna element: An antenna that forms part of a larger antenna system.

antenna pattern: The variation in the gain of an antenna with angle.

angle factor: The magnitude of the ratio of the settling angle to half the jammer antenna element spacing from the perspective of the radar being jammed.

boresight: The direction where the angular error of a tracking radar is zero for a single point target (the difference-channel return is zero for a monopulse radar).

broadside: The spacings of the elements of an array of antennas will be greatest when the array is viewed from the broadside direction.

cross-eye gain: The factor that determines the performance of a cross-eye jammer given in (2.10) on page 13.

jammer: The complete system used to implement jamming. This includes all antennas, cables and circuitry for all the jammer subsystems that are employed together.

indicated angle: The output of a monopulse processor given in the form of the angle from boresight to the target being tracked. The indicated angle is formed from the monopulse error.

jammer loop: The connection of two antenna elements, cables and circuitry necessary to create the simplest retrodirective cross-eye jammer.

monopulse error: The real or imaginary part of the ratio of the difference-channel return to the sum-channel return (the output of an exact monopulse processor [15,30]). Whether the real or imaginary part of the ratio is used depends on which portion of the ratio describes the position of a single point target. The monopulse literature more regularly considers the indicated angle, but the algorithm used to calculate the indicated angle from the monopulse error is not always known.

phase-front analysis: Any analysis of cross-eye jamming that gives the same result as the phase-front analysis (linear-fit, phase-front, Poynting-vector and phase-comparison monopulse analyses). This convention is used because cross-eye jamming is almost exclusively considered in terms of phase-front distortion in the literature.

platform: The craft or system mounting a cross-eye jammer. A platform will typically be an aircraft or a ship that needs to be protected against radar-guided missiles.

retrodirective: A system configuration that retransmits signals received on each side of a system from the opposite sides of the system.

settling angle: The angle where the monopulse error (and thus the indicated angle) becomes zero at a stable zero crossing (see Section 4.3).

APPENDIX B

APPROXIMATIONS

The far-field approximation that is widely used to calculate the patterns of array antennas relies on an approximation to the distance from each element to a target in a given direction [45]. This approximation is generally very accurate when the antenna is very small compared to the target distance. While this assumption is true for the radar antenna, it is unfortunately invalid for a cross-eye jammer [19, 21].

The geometry that will be used in this Appendix is given in Figure B.1, which is based on the geometry of the full cross-eye jammer system in Figure 4.1 on page 38 with extraneous information removed.

The angle from the x axis to the target (θ_e in Figure B.1) and the trigonometric relationships of this angle are extremely important in the analysis of cross-eye jamming. The value of this angle and its trigonometric values will be investigated in this section.

From inspection of Figure B.1, it can be seen that the horizonal and vertical distances to the top and bottom crosses are given by

$$\Delta x = r \pm \frac{d_c}{2} \sin(\theta_c) \tag{B.1}$$

and

$$\Delta y = \pm \frac{d_c}{2} \cos(\theta_c) \tag{B.2}$$

where the upper and lower signs give the results for the upper and lower crosses respectively.

The range to the top and bottom crosses in Figure B.1 are given by

$$r_t = \sqrt{\left[r \pm \frac{d_c}{2} \sin(\theta_c)\right]^2 + \left[\frac{d_c}{2} \cos(\theta_c)\right]^2} \tag{B.3}$$

$$= \sqrt{r^2 \pm r d_c \sin(\theta_c) + \left(\frac{d_c}{2}\right)^2} \tag{B.4}$$

and the conventional far-field range approximation is given by

$$r_t \approx \Delta x \tag{B.5}$$

$$\approx r \pm \frac{d_c}{2} \sin(\theta_c) \tag{B.6}$$

when $r \gg d_c$. In extreme cases, the range to the crosses can be approximated by the range to the point between the crosses giving

$$r_t \approx r. \tag{B.7}$$

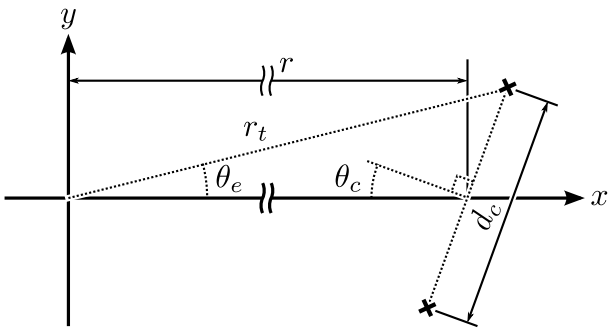

Figure B.1: The geometry used to evaluate far-field approximations.

While the relative errors caused by using the approximations in (B.6) and (B.7) are generally small compared to the true range, they can still be significant in absolute terms, particularly at short ranges. Using the conservative values of $r = 1$ km, $d_c = 20$ m and $\theta_c = 60°$, the range to the top cross displays errors of 12.4 mm and 8.67 m for (B.6) and (B.7) respectively. While these errors are less than 0.0013% and 0.9% of the true range respectively (implying a small relative error), the distance errors correspond to more than 0.4 and 289 wavelengths at X-Band respectively (large absolute error).

The value of θ_e can be calculated from

$$\tan(\theta_e) = \frac{\Delta y}{\Delta x} \tag{B.8}$$

$$= \frac{\pm\frac{d_c}{2}\cos(\theta_c)}{r \pm \frac{d_c}{2}\sin(\theta_c)} \tag{B.9}$$

for the top and bottom crosses. This can be simplified by noting that $r \gg d_c$ to give

$$\tan(\theta_e) \approx \frac{d_c}{2r}\cos(\theta_c) \tag{B.10}$$

to a high degree of accuracy at all but very short ranges. For example, (B.10) gives an error of less than 0.9% for the conservative values of $r = 1$ km, $d_c = 20$ m and $\theta_c = 60°$.

Given that r is much larger than d_c, the approximation $\tan(x) \approx x$ can be used to simplify (B.9) and (B.10) to

$$\theta_e \approx \frac{\frac{d_c}{2}\cos(\theta_c)}{r \pm \frac{d_c}{2}\sin(\theta_c)} \tag{B.11}$$

and

$$\theta_e \approx \frac{d_c}{2r}\cos(\theta_c) \tag{B.12}$$

respectively. The difference between (B.9) and (B.12) for the conservative values of $r = 1$ km, $d_c = 20$ m and $\theta_c = 60°$ is again less than 0.9%, so the accuracies of (B.10) and (B.12) are comparable.

The cosine of θ_e can be computed from

$$\cos(\theta_e) = \frac{\Delta x}{r_t} \tag{B.13}$$

$$= \frac{r + \frac{d_c}{2}\sin(\theta_c)}{\sqrt{r^2 + 2r\frac{d_c}{2}\sin(\theta_c) + \left(\frac{d_c}{2}\right)^2}} \tag{B.14}$$

$$\approx 1 \tag{B.15}$$

and the sine of θ_e is given by

$$\sin(\theta_e) = \frac{\Delta y}{r_t} \tag{B.16}$$

$$= \frac{\frac{d_c}{2}\cos(\theta_c)}{\sqrt{r^2 + 2r\frac{d_c}{2}\sin(\theta_c) + \left(\frac{d_c}{2}\right)^2}} \tag{B.17}$$

$$= \frac{\frac{d_c}{2}\cos(\theta_c)}{r + \frac{d_c}{2}\sin(\theta_c)} \times \frac{r + \frac{d_c}{2}\sin(\theta_c)}{\sqrt{r^2 + 2r\frac{d_c}{2}\sin(\theta_c) + \left(\frac{d_c}{2}\right)^2}} \tag{B.18}$$

$$= \tan(\theta_e) \times \cos(\theta_e) \tag{B.19}$$

$$\approx \frac{d_c}{2r}\cos(\theta_c)\,. \tag{B.20}$$

The errors that arise from using the approximations in (B.15) and (B.20) are less than 0.0013% and 0.9% respectively.

The above trigonometric approximations can be summarised as

$$\tan(\theta_e) \approx \sin(\theta_e) \approx \theta_e \approx \frac{d_c}{2r}\cos(\theta_c) \tag{B.21}$$

and

$$\cos(\theta_e) \approx 1 \tag{B.22}$$

as long as $r \gg d_c$ making θ_e small.

APPENDIX C

DERIVATIVES OF MONOPULSE PATTERN

The general form of the monopulse error for the general and phase-comparison cases is given by (3.15) on page 31 which is repeated below for reference.

$$M_X = \frac{\sum_{m=0}^{M} \gamma_m \sin(\epsilon_m x)}{\sum_{n=0}^{N} \zeta_n \cos(\kappa_n x)} \tag{C.1}$$

This appendix proves that all even-order derivatives of (C.1) are zero when x is zero.

The general monopulse error in (C.1) can be rewritten as

$$M_X = M_{XS} M_{XC} \tag{C.2}$$

where M_{XS} and M_{XC} are given by

$$M_{XS} = \sum_{m=0}^{M} \gamma_m \sin(\epsilon_m x) \tag{C.3}$$

and

$$M_{XC} = \left[\sum_{n=0}^{N} \zeta_n \cos(\kappa_n x) \right]^{-1}. \tag{C.4}$$

The Nth-order derivatives of M_X can be determined from Leibniz's rule for higher-order derivatives of products [73] and are given by

$$\begin{aligned} \frac{\partial^N}{\partial x^N} M_X = &\left[\frac{\partial^N}{\partial x^N} M_{XS} \right] M_{XC} + \binom{N}{1} \left[\frac{\partial^{N-1}}{\partial x^{N-1}} M_{XS} \right] \left[\frac{\partial}{\partial x} M_{XC} \right] + \\ &\binom{N}{2} \left[\frac{\partial^{N-2}}{\partial x^{N-2}} M_{XS} \right] \left[\frac{\partial^2}{\partial x^2} M_{XC} \right] + \cdots + \left[\frac{\partial}{\partial x} M_{XS} \right] \left[\frac{\partial^N}{\partial x^N} M_{XC} \right] \qquad \text{(C.5)} \\ = &\sum_{n=0}^{N} \binom{N}{n} \left[\frac{\partial^{N-n}}{\partial x^{N-n}} M_{XS} \right] \left[\frac{\partial^n}{\partial x^n} M_{XC} \right]. \qquad \text{(C.6)} \end{aligned}$$

The most important point to note about (C.6) is that the sum of the order of the derivatives of M_{XS} and M_{XC} is equal to N in all the terms. This means that all terms of (C.6) where N is even will thus have either odd-order derivatives of both M_{XS} and M_{XC} or even-order derivatives of both M_{XS} and M_{XC}.

The Pth-order derivatives of M_{XS} are given by

$$\frac{\partial^P}{\partial x^P} M_{XS} = \sum_{m=0}^{M} \gamma_m \frac{\partial^P}{\partial x^P} \sin(\epsilon_m x). \tag{C.7}$$

From (C.7), it is clear that all even-order derivatives of M_{XS} are zero when x is zero because all the terms of the derivative contain sine functions. This means that all the even-order derivatives of M_X will all be zero when x is zero if all the odd-order derivatives of M_{XC} can be shown to be zero when x is zero.

The derivatives of M_{XC} are more complicated because the function of x is in the denominator, so the chain rule is required [73]. The first three derivatives of M_{XC} are given by

$$\frac{\partial}{\partial x}M_{XC} = -\left[\sum_{n=0}^{N}\zeta_n\cos\left(\kappa_n x\right)\right]^{-2}\left[\sum_{n=0}^{N}\zeta_n\frac{\partial}{\partial x}\cos\left(\kappa_n x\right)\right] \tag{C.8}$$

$$\frac{\partial^2}{\partial x^2}M_{XC} = \frac{\partial}{\partial x}\left[\frac{\partial}{\partial x}M_{XC}\right] \tag{C.9}$$

$$= 2\left[\sum_{n=0}^{N}\zeta_n\cos\left(\kappa_n x\right)\right]^{-3}\left[\sum_{n=0}^{N}\zeta_n\frac{\partial}{\partial x}\cos\left(\kappa_n x\right)\right]^{2} - \left[\sum_{n=0}^{N}\zeta_n\cos\left(\kappa_n x\right)\right]^{-2}\left[\sum_{n=0}^{N}\zeta_n\frac{\partial^2}{\partial x^2}\cos\left(\kappa_n x\right)\right] \tag{C.10}$$

$$\frac{\partial^3}{\partial x^3}M_{XC} = \frac{\partial}{\partial x}\left[\frac{\partial^2}{\partial x^2}M_{XC}\right] \tag{C.11}$$

$$= -6\left[\sum_{n=0}^{N}\zeta_n\cos\left(\kappa_n x\right)\right]^{-4}\left[\sum_{n=0}^{N}\zeta_n\frac{\partial}{\partial x}\cos\left(\kappa_n x\right)\right]^{3} + 6\left[\sum_{n=0}^{N}\zeta_n\cos\left(\kappa_n x\right)\right]^{-3}\left[\sum_{n=0}^{N}\zeta_n\frac{\partial}{\partial x}\cos\left(\kappa_n x\right)\right]\left[\sum_{n=0}^{N}\zeta_n\frac{\partial^2}{\partial x^2}\cos\left(\kappa_n x\right)\right] + \left[\sum_{n=0}^{N}\zeta_n\cos\left(\kappa_n x\right)\right]^{-2}\left[\sum_{n=0}^{N}\zeta_n\frac{\partial^3}{\partial x^3}\cos\left(\kappa_n x\right)\right] \tag{C.12}$$

where the details of the derivations are suppressed in the interests of brevity. The first- and third-order derivatives of M_{XC} in (C.8) and (C.12) both contain odd-order derivatives of cosine in every term, so these derivatives of M_{XC} are zero when x is zero.

Every term of the Pth-order derivative of M_{XC} can be represented by

$$K\left[\sum_{n=0}^{N}\zeta_n\cos\left(\kappa_n x\right)\right]^{-k_d}\prod_{p=1}^{P}K_p\left[\sum_{n=0}^{N}\zeta_n\frac{\partial^p}{\partial x^p}\cos\left(\kappa_n x\right)\right]^{k_p} \tag{C.13}$$

where K and K_P are arbitrary integer constants, k_d is a positive integer and k_p are arbitrary integers greater than or equal to zero. From (C.6), the total number of differentiations of each term in (C.13) must equal the order of the derivative, so the following relationship must hold

$$P = \sum_{n=1}^{P} nk_p \tag{C.14}$$

as seen in (C.8), (C.10) and (C.12). This means that there must be at least one odd-order derivative of a sum of cosines in every term of the derivative of M_{XC} whenever P is odd. These odd-order derivatives will be sums of sines which are zero when their argument is zero.

All that remains to prove that all even-order derivatives of (C.1) are zero is to prove that (C.13) is indeed the general form of any term of the Pth-order derivative of (C.1). Mathematical induction is used to prove this statement.

The form of M_{XC} in (C.4) can be represented by (C.13) by setting $K = 1$, $k_d = 1$ and $M = 0$. The base case for mathematical induction is thus proved.

The inductive step can be proved by taking the derivative of (C.13) and noting that all the terms in the result can also be represented by (C.13).

$$\frac{\partial}{\partial x}\left\{K\left[\sum_{n=0}^{N}\zeta_n\cos\left(\kappa_n x\right)\right]^{-k_d}\prod_{p=1}^{P}K_p\left[\sum_{n=0}^{N}\zeta_n\frac{\partial^p}{\partial x^p}\cos\left(\kappa_n x\right)\right]^{k_p}\right\} \tag{C.15}$$

$$= K\frac{\partial}{\partial x}\left\{\left[\sum_{n=0}^{N}\zeta_n\cos\left(\kappa_n x\right)\right]^{-k_d}\right\}\prod_{p=1}^{P}K_p\left[\sum_{n=0}^{N}\zeta_n\frac{\partial^p}{\partial x^p}\cos\left(\kappa_n x\right)\right]^{k_p} +$$
$$K\left[\sum_{n=0}^{N}\zeta_n\cos\left(\kappa_n x\right)\right]^{-k_d}\frac{\partial}{\partial x}\left\{\prod_{p=1}^{P}K_p\left[\sum_{n=0}^{N}\zeta_n\frac{\partial^p}{\partial x^p}\cos\left(\kappa_n x\right)\right]^{k_p}\right\} \tag{C.16}$$

$$= -Kk_d\left[\sum_{n=0}^{N}\zeta_n\cos\left(\kappa_n x\right)\right]^{-k_d-1}\sum_{n=0}^{N}\zeta_n\frac{\partial}{\partial x}\cos\left(\kappa_n x\right)\prod_{p=1}^{P}K_p\left[\sum_{n=0}^{N}\zeta_n\frac{\partial^p}{\partial x^p}\cos\left(\kappa_n x\right)\right]^{k_p} +$$
$$K\left[\sum_{n=0}^{N}\zeta_n\cos\left(\kappa_n x\right)\right]^{-k_d}\sum_{m=1}^{P}\left[\frac{\partial}{\partial x}\left\{K_m\left[\sum_{n=0}^{N}\zeta_n\frac{\partial^m}{\partial x^m}\cos\left(\kappa_n x\right)\right]^{k_m}\right\}\times\right.$$
$$\left.\prod_{\substack{p=1\\p\neq m}}^{P}K_p\left[\sum_{n=0}^{N}\zeta_n\frac{\partial^p}{\partial x^p}\cos\left(\kappa_n x\right)\right]^{k_p}\right] \tag{C.17}$$

$$= -Kk_d\left[\sum_{n=0}^{N}\zeta_n\cos\left(\kappa_n x\right)\right]^{-k_d-1}\sum_{n=0}^{N}\zeta_n\frac{\partial}{\partial x}\cos\left(\kappa_n x\right)\prod_{p=1}^{P}K_p\left[\sum_{n=0}^{N}\zeta_n\frac{\partial^p}{\partial x^p}\cos\left(\kappa_n x\right)\right]^{k_p} +$$
$$K\left[\sum_{n=0}^{N}\zeta_n\cos\left(\kappa_n x\right)\right]^{-k_d}\sum_{m=1}^{P}\left[K_m k_m\left[\sum_{n=0}^{N}\zeta_n\frac{\partial^m}{\partial x^m}\cos\left(\kappa_n x\right)\right]^{k_m-1}\times\right.$$
$$\left.\sum_{n=0}^{N}\zeta_n\frac{\partial^{m+1}}{\partial x^{m+1}}\cos\left(\kappa_n x\right)\prod_{\substack{p=1\\p\neq m}}^{P}K_p\left[\sum_{n=0}^{N}\zeta_n\frac{\partial^p}{\partial x^p}\cos\left(\kappa_n x\right)\right]^{k_p}\right] \tag{C.18}$$

Careful examination of (C.18) shows that each term has the form given in (C.13) thereby proving the inductive step and completing the proof.

All the even-order derivatives of (C.1) are thus equal to zero when x is zero.